

INFORMATION TO USERS

The most advanced technology has been used to photograph and reproduce this manuscript from the microfilm master. UMI films the text directly from the original or copy submitted. Thus, some thesis and dissertation copies are in typewriter face, while others may be from any type of computer printer.

The quality of this reproduction is dependent upon the quality of the copy submitted. Broken or indistinct print, colored or poor quality illustrations and photographs, print bleedthrough, substandard margins, and improper alignment can adversely affect reproduction.

In the unlikely event that the author did not send UMI a complete manuscript and there are missing pages, these will be noted. Also, if unauthorized copyright material had to be removed, a note will indicate the deletion.

Oversize materials (e.g., maps, drawings, charts) are reproduced by sectioning the original, beginning at the upper left-hand corner and continuing from left to right in equal sections with small overlaps. Each original is also photographed in one exposure and is included in reduced form at the back of the book.

Photographs included in the original manuscript have been reproduced xerographically in this copy. Higher quality 6" x 9" black and white photographic prints are available for any photographs or illustrations appearing in this copy for an additional charge. Contact UMI directly to order.

U·M·I

University Microfilms International
A Bell & Howell Information Company
300 North Zeeb Road, Ann Arbor, MI 48106-1346 USA
313/761-4700 800/521-0600



Order Number 1341497

Experimental effectiveness of rock fracture grouting

Sharpe, Colin James, M.S.

The University of Arizona, 1990

U·M·I

300 N. Zeeb Rd.
Ann Arbor, MI 48106



NOTE TO USERS

**THE ORIGINAL DOCUMENT RECEIVED BY U.M.I. CONTAINED PAGES WITH
PHOTOGRAPHS WHICH MAY NOT REPRODUCE PROPERLY.**

THIS REPRODUCTION IS THE BEST AVAILABLE COPY.



EXPERIMENTAL EFFECTIVENESS OF ROCK FRACTURE GROUTING

by

Colin James Sharpe

A Thesis Submitted to the Faculty of the
DEPARTMENT OF MINING AND GEOLOGICAL ENGINEERING

In Partial Fulfillment of the Requirements
For the Degree of

MASTERS OF SCIENCE
WITH A MAJOR IN MINING ENGINEERING

In the Graduate College
THE UNIVERSITY OF ARIZONA

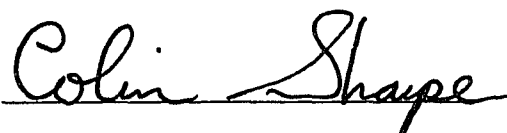
1 9 9 0

STATEMENT BY AUTHOR

This thesis has been submitted in partial fulfillment of requirements for an advanced degree at the University of Arizona and is deposited in the University Library to be made available to borrowers under rules of the Library.

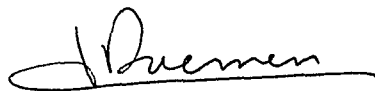
Brief quotations from this thesis are allowable without special permission, provided that accurate acknowledgment of source is made. Requests for permission for extended quotation from or reproduction of this manuscript in whole or in part may be granted by the head of the major department or the Dean of the Graduate College when in his or her judgment the proposed use of the material is in the interests of scholarship. In all other instances, however, permission must be obtained from the author.

SIGNED:



APPROVAL BY THESIS DIRECTOR

This thesis has been approved on the date shown below:



Jaak J. K. Daemen
Associate Professor
Mining and Geological Engineering

7-16-90

Date

IN MEMORY OF JACOB PAUL

ACKNOWLEDGMENTS

The author would like to express thanks to his parents for their continued love and support, and to his advisor, Dr. J.J.K. Daemen for his supervision and motivation.

The author also wishes to thank those who contributed to this research. Special thanks goes to Janice Seger who typed this thesis.

This research program, "Sealing of Boreholes and Shafts in Tuff", was sponsored by the U.S. Nuclear Regulatory Commission, Office of Nuclear Regulatory Research, Division of Engineering.

TABLE OF CONTENTS

	PAGE
LIST OF ILLUSTRATIONS	6
LIST OF TABLES	9
NOMENCLATURE	12
ABSTRACT	14
1.0 INTRODUCTION	15
2.0 FLUID FLOW IN FRACTURED ROCK	19
2.1 Introduction	19
2.2 Theory of Fluid Flow Within a Single Fracture	20
2.3 Rock Mass Permeability	28
2.4 Method of Permeability Calculation	29
3.0 FRACTURE GROUTING	34
3.1 Introduction	34
3.2 Pressure Grouting	34
3.3 Grout Mix Design	36
4.0 EXPERIMENTAL PROCEDURE	50
4.1 Sample Preparation	50
4.2 Permeability Testing	59
4.3 Surface Characterization	66
4.4 Grout Preparation	69
4.5 Grout Characterization	74
4.6 Fracture Grouting	79
4.7 Fracture Compression Behavior	82
5.0 EXPERIMENTAL RESULTS	86
5.1 Permeability of Intact Tuff	86
5.2 Fracture Permeability	91
5.3 Fracture Compression	132
5.4 Surface Characterization	134
5.5 Grout Characterization	140
5.6 Grouting Effectiveness	140
6.0 CONCLUSIONS AND RECOMMENDATIONS	168
REFERENCES	171

LIST OF ILLUSTRATIONS

FIGURE		PAGE
2.1	RANGE OF VALIDITY FOR FLOW LAWS	25
2.2	RELATIVE ROUGHNESS OF A FRACTURE'S SURFACE	26
2.3	PARAMETERS INVOLVED IN A FALLING HEAD TEST	31
3.1	MAXIMUM ALLOWABLE GROUTING PRESSURES	37
3.2	EFFECT OF WATER TO CEMENT RATIO ON GROUT PROPERTIES	39
3.3	EFFECT OF BENTONITE AND WATER-CEMENT RATIO ON MARSH FUNNEL VISCOSITY	44
3.4	FLOW BEHAVIOR OF NEWTONIAN AND BINGHAM FLUIDS	45
3.5	FLOW VELOCITY CROSS SECTION	46
3.6	MAXIMUM RADIUS OF PENETRATION	49
4.1	NOMINAL SAMPLE DIMENSIONS	51
4.2	SAMPLE MEASUREMENT SCHEME	52
4.3a,b	3hp ACKER AND 2hp CENTURY CORING DRILLS	53
4.4	KENT AUTOMATIC SURFACE GRINDING MACHINE	54
4.5	INTACT SAMPLE OF APACHE LEAP TUFF	55
4.6	COVINGTON DIAMOND SAW	56
4.7	SAWCUT SURFACES	57
4.8a,b	S.B.E.L LOAD FRAME AND SERVO CONTROLLER	58
4.9	FRACTURE SURFACES PRODUCED BY MODIFIED POINT LOAD TEST .	60
4.10	CORING OF BLOCKS CONTAINING A SINGLE NATURAL FRACTURE ..	61
4.11a,b	CORED SAMPLES CONTAINING NATURAL FRACTURES	62
4.12	LABORATORY ARRANGMENT FOR FLOW TESTING AND GROUTING	64
4.13a,b	GUIDE PLATE AND NEEDLE PROBE USED TO CHARACTERIZE FRACTURE SURFACE	68
4.14	GRAIN SIZE DISTRIBUTION OF O.P.C, COLLOID, AND MC-500 CEMENTS	71
4.15	FANN VISCOMETER	77
4.16	MARSH FUNNEL AND CUP	78
4.17	SIMPLE SINGLE PISTON GROUT PUMP WITH GAUGE SAVER	81
4.18	FRACTURE COMPRESSION MONITORING SYSTEM	83

5.1	THREE TYPES OF WELDED TUFF	87
5.2	HYDRAULIC CONDUCTIVITY OF INTACT TUFF	88
5.3	EFFECT OF NORMAL STRESS ON HYDRAULIC CONDUCTIVITY OF INTACT APACHE LEAP TUFF	89
5.4	EFFECT OF NORMAL STRESS ON THE PERMEABILITY OF INTACT SAMPLE AP7-1-6-FG4	90
5.5	HYDRAULIC CONDUCTIVITY AS A FUNCTION OF NORMAL STRESS FOR SAMPLE AP21-3-6-FG1	97
5.6	EQUIVALENT FRACTURE APERTURE AS A FUNCTION OF NORMAL STRESS FOR SAMPLE AP21-3-6-FG1	98
5.7	HYDRAULIC CONDUCTIVITY AS A FUNCTION OF NORMAL STRESS FOR SAMPLE AP30-2-6-FG10	99
5.8	EQUIVALENT FRACTURE APERTURE AS A FUNCTION OF NORMAL STRESS FOR SAMPLE AP30-2-6-FG10	100
5.9	HYDRAULIC CONDUCTIVITY AS A FUNCTION OF NORMAL STRESS FOR SAMPLE AP30-1-6-FG11	101
5.10	EQUIVALENT FRACTURE APERTURE AS A FUNCTION OF NORMAL STRESS FOR SAMPLE AP30-1-6-FG11	102
5.11	HYDRAULIC CONDUCTIVITY AS A FUNCTION OF NORMAL STRESS FOR SAMPLE AP36-1-6-FG13	103
5.12	EQUIVALENT FRACTURE APERTURE AS A FUNCTION OF NORMAL STRESS FOR SAMPLE AP36-1-6-FG13	104
5.13	HYDRAULIC CONDUCTIVITY AS A FUNCTION OF NORMAL STRESS FOR SAMPLE AP4-1-6-FG2	105
5.14	EQUIVALENT FRACTURE APERTURE AS A FUNCTION OF NORMAL STRESS FOR SAMPLE AP4-1-6-FG2	106
5.15	HYDRAULIC CONDUCTIVITY AS A FUNCTION OF NORMAL STRESS FOR SAMPLE AP7-2-6-FG5	107
5.16	EQUIVALENT FRACTURE APERTURE AS A FUNCTION OF NORMAL STRESS FOR SAMPLE AP7-2-6-FG5	108
5.17	HYDRAULIC CONDUCTIVITY AS A FUNCTION OF NORMAL STRESS FOR SAMPLE AP3-1-6-FG6	109
5.18	EQUIVALENT FRACTURE APERTURE AS A FUNCTION OF NORMAL STRESS FOR SAMPLE AP3-1-6FG6	110
5.19	HYDRAULIC CONDUCTIVITY AS A FUNCTION OF NORMAL STRESS FOR SAMPLE AP2-1-6-FG7	111
5.20	EQUIVALENT FRACTURE APERTURE AS A FUNCTION OF NORMAL STRESS FOR SAMPLE AP2-1-6-FG7	112
5.21	HYDRAULIC CONDUCTIVITY AS A FUNCTION OF NORMAL STRESS FOR SAMPLE AP56-5-6-FG12	113

5.22	EQUIVALENT FRACTURE APERTURE AS A FUNCTION OF NORMAL STRESS FOR SAMPLE AP56-5-6-FG12	114
5.23	HYDRAULIC CONDUCTIVITY AS A FUNCTION OF NORMAL STRESS FOR SAMPLE AP56-2-6-FG14	115
5.24	EQUIVALENT FRACTURE APERTURE AS A FUNCTION OF NORMAL STRESS FOR SAMPLE AP56-2-6-FG14	116
5.25	HYDRAULIC CONDUCTIVITY AS A FUNCTION OF NORMAL STRESS FOR SAMPLE AP56-3-6-FG15	117
5.26	EQUIVALENT FRACTURE APERTURE AS A FUNCTION OF NORMAL STRESS FOR SAMPLE AP56-3-6-FG15	118
5.27	EFFECT OF NORMAL STRESS ON FRACTURE CLOSURE	133
5.28	COMPARISON BETWEEN FRACTURE COMPRESSION AND EQUIVALENT FRACTURE APERTURE	135
5.29	THREE-DIMENSIONAL IMAGE OF FRACTURE SURFACE ROUGHNESS ..	136
5.30	THREE-DIMENSIONAL IMAGE OF FRACTURE SURFACE ROUGHNESS ..	137
5.31	TOPOGRAPHIC PLOT OF FRACTURE SURFACE ROUGHNESS	138
5.32	TOPOGRAPHIC PLOT OF FRACTURE SURFACE ROUGHNESS	139
5.33	FANN VISCOSITY AS A FUNCTION OF ROTOR SPEED	143
5.34	REDUCTION IN HYDRAULIC CONDUCTIVITY RESULTING FROM GROUTING SAMPLE AP21-3-6-FG1 (TEST 1)	145
5.35	FILTER BLOCKAGE OF SAMPLE AP21-3-6-FG1 (TEST 1)	146
5.36	HYDRAULIC CONDUCTIVITY OF SAMPLE AP21-3-6-FG1 BEFORE AND AFTER GROUTING (TEST 2)	147
5.37	MC-500 GROUT FLOWING FROM THE FRACTURE OF SAMPLE AP21-3-6-FG1 (TEST 2)	148
5.38	SURFACES OF SAMPLE AP21-3-6-FG1 AFTER GROUTING (TEST 2) .	149
5.39	FILTER BLOCKAGE OF SAMPLE AP30-2-6-FG10 (TESTS 1 AND 2) .	151
5.40	FILTER BLOCKAGE OF SHIMMED SAMPLE AP30-2-FG10 (TEST 3) ..	152
5.41	DECREASE IN HYDRAULIC CONDUCTIVITY OF SAMPLE AP30-2-6-FG10 DUE TO FILTER BLOCKAGE (TEST 3)	153
5.42	FILTER BLOCKAGE OF SAWCUT SAMPLE AP4-1-6-FG2	155
5.43	RING OF CEMENT CAUSING FILTER BLOCKAGE OF SAMPLE AP3-1-6-FG6	156
5.44a,b	GROUTING OF SAMPLE AP3-11-6-FG6	157
5.45	SHIMS USED TO PROP OPEN THE APERTURE OF SAMPLE AP-SHAFT6-FG16	159

5.46	GROUTED SURFACES OF SHIMMED SAMPLE AP-SHAFT6-FG16	160
5.47	PERMEABILITY OF GROUTED SAMPLE AP-SHAFT6-FG16	161
5.48	PERMEABILITY OF SAMPLE AP56-2-6-FG14 AFTER GROUTING	162
5.49a,b	FILTER BLOCKAGE OF SAMPLE AP56-2-6-FG14	164
5.50	POCKETS OF EMPLACED GROUT IN SAMPLE AP56-3-6-FG15	165
5.51	PERMEABILITY OF GROUTED SAMPLE AP56-3-6-FG15	166

LIST OF TABLES

	PAGE
4.1	GROUT MIX PROPORTIONS 72
4.2	ROTOR SPEED VERSUS TIME INTERVAL FOR FANN VISCOMETER 75
4.3	MIX PROPORTIONS FOR MARSH FUNNEL VISCOSITY 76
5.1	FALLING HEAD RESULTS FOR INTACT SAMPLE AP21-3-6-FG1 92
5.2	FALLING HEAD RESULTS FOR INTACT SAMPLE AP4-1-6-FG2 92
5.3	FALLING HEAD RESULTS FOR INTACT SAMPLE AP10-8-6-FG3 92
5.4	RESULTS OF FLOW TESTING INTACT SAMPLE AP7-1-6-FG4 93
5.5	FALLING HEAD RESULTS FOR INTACT SAMPLE AP7-2-G-FG5 93
5.6	FALLING HEAD RESULTS FOR INTACT SAMPLE AP3-1-6-FG6 94
5.7	FALLING HEAD RESULTS FOR INTACT SAMPLE TPS-6-FG8 94
5.8	FALLING HEAD RESULTS FOR INTACT SAMPLE T-1-6-FG9 94
5.9	PARAMETERS INVOLVED IN DETERMINING FRACTURE PERMEABILITY AND EQUIVALENT FRACTURE APERTURE FOR SAMPLE AP21-3-6-FG1 119
5.10	PARAMETERS INVOLVED IN DETERMINING FRACTURE PERMEABILITY AND EQUIVALENT FRACTURE APERTURE FOR SAMPLE AP30-2-6-FG10 120
5.11	PARAMETERS INVOLVED IN DETERMINING FRACTURE PERMEABILITY AND EQUIVALENT FRACTURE APERTURE FOR SAMPLE AP30-1-6-FG11 121
5.12	PARAMETERS INVOLVED IN DETERMINING FRACTURE PERMEABILITY AND EQUIVALENT FRACTURE APERTURE FOR SAMPLE AP36-1-6-FG13 122
5.13	PARAMETERS INVOLVED IN DETERMINING FRACTURE PERMEABILITY AND EQUIVALENT FRACTURE APERTURE FOR SAMPLE AP4-1-6-FG2 123
5.14	PARAMETERS INVOLVED IN DETERMINING FRACTURE PERMEABILITY AND EQUIVALENT FRACTURE APERTURE FOR SAMPLE AP7-2-6-FG5 124
5.15	PARAMETERS INVOLVED IN DETERMINING FRACTURE PERMEABILITY AND EQUIVALENT FRACTURE APERTURE FOR SAMPLE AP1-6-FG6 .. 125
5.16	PARAMETERS INVOLVED IN DETERMINING FRACTURE PERMEABILITY AND EQUIVALENT FRACTURE APERTURE FOR SAMPLE AP2-1-6-FG7 126
5.17	PARAMETERS INVOLVED IN DETERMINING FRACTURE PERMEABILITY AND EQUIVALENT FRACTURE APERTURE FOR SAMPLE AP56-5-6-FG12 127
5.18	PARAMETERS INVOLVED IN DETERMINING FRACTURE PERMEABILITY AND EQUIVALENT FRACTURE APERTURE FOR SAMPLE AP56-2-6-FG14 128
5.19	PARAMETERS INVOLVED IN DETERMINING FRACTURE PERMEABILITY AND EQUIVALENT FRACTURE APERTURE FOR SAMPLE AP56-3-6-FG15 129
5.20	UNIAXIAL COMPRESSIVE STRENGTH OF CURED GROUT 141

5.21	FANN VISCOSITIES OF GROUT FORMULATIONS	142
5.22	PLASTIC VISCOSITIES AND YIELD VALUES OF GROUT FORMULATIONS	142
5.23	MARSH FUNNEL VISCOSITIES OF GROUT FORMULATIONS	142
5.24	GROUTABILITY RATIOS CORRESPONDING TO GROUT PENETRATION ..	167

NOMENCLATURE

GREEK SYMBOLS

μ	dynamic viscosity
ρ	fluid density
ν	kinematic viscosity
α	degree of non-linearity
ψ	friction factor
$\frac{\epsilon}{D}$	relative roughness
σ_N	normal stress
γ	unit weight of water
τ	shear stress
τ_0	shear strength
∇	gradient operator
ΔW	weight difference
ΔS	piston travel length
Δh	water head difference
θ	angle

ROMAN SYMBOLS

a	diameter of pipette
2b	parallel plate aperture
c	cohesion or yield value
d	representative pore length
e	equivalent fracture aperture
f	correction factor
g	gravitational constant
h	water head
i	hydraulic gradient
k	matrix permeability

NOMENCLATURE (Continued)

k_f	fracture permeability
q	flow rate
t	1/2 the joint aperture
t_o	initial time
t_1	final time
x, y, z	cartesian coordinates
A	area
B	body force
C	constant representing fluid properties and system geometry
D_h	hydraulic diameter
$D_{fissure}$	fracture aperture
D_{MAX}	maximum particle diameter
E	Young's modulus
K	absolute roughness
L	length of flow path
L_H	length of borehole
P	pressure
Q	volumetric flow
R_e	Reynold's number
R_h	hydraulic radius
R_i	inner radius of cylinder
R_o	outer radius of cylinder
V	fluid velocity

ABSTRACT

The objective of this investigation is to experimentally determine the effectiveness of fracture sealing in welded tuff using ordinary portland cement and microfine cement grouts.

Fracture grouting will most likely be used to seal fractures intersecting high level nuclear waste repositories. Fractures are potential pathways for the migration of radionuclides.

Laboratory experiments have been performed on seventeen tuff cylinders. 1) tension induced cracks, 2) natural and 3) sawcut surfaces serve as fractures. Prior to grouting, the hydraulic conductivity of the intact rock and that of the fractures themselves are measured under a range of normal stresses.

Grouts are injected through axial boreholes at pressures of 0.3 to 4.1 MPa while holding fractures under a constant normal stress. Five grout formulations have been selected. Minor amounts of bentonite (0 to 5 percent by weight) have been added to these grouts to increase stability. Water to cement ratios range from 0.45 to 1.0. Permeameter testing of grouted fractures is used to evaluate the effectiveness of fracture grouting.

CHAPTER 1
INTRODUCTION

The great volume of high level nuclear waste (HLW) produced in the past, some not yet dealt with in interim storage (Lutze and Ewing, 1988), and yet greater amounts to be produced in our future (>50,000 tonnes by year 2000), requires that an effective means of isolating it from the biosphere for many thousands of years be developed (Chapman and McKinley, 1987).

The Nuclear Waste Policy Act of 1982 requires the Federal Government, who has given the Department of Energy the responsibility, to develop the technology to ensure safe and permanent disposal of HLW (Fitzsimmons, 1987).

Proposed HLW repository designs must be economically feasible with current technology while inspiring a high degree of confidence with all people involved. This man made barrier must remain intact and not be breached as long as its contents are dangerous to the environment or until new technology can be developed to better handle this waste.

The Department of Energy's (DOE) principal design goals for seals in an unsaturated medium, such as at the proposed Yucca Mountain site should be (1) prevent significant amounts of surface or groundwater from reaching emplaced waste, and, (2) prevent significant amounts of gaseous radionuclides from escaping through shafts, ramps, and boreholes to the accessible environment (Gupta and Buckley, 1989).

Grouting, the emplacement of a cementitious or chemical slurry, is one of the proposed means of forming a water tight barrier between the waste and its surrounding environment. This technology may be used to create or augment one of the proposed barriers in the multibarrier system that will most likely be needed. Other candidate sealing materials include earthen materials such as clay, sand, aggregate and crushed host rock, ceramics, and metals. Admixtures will most probably

be added to the grout slurries to enhance material properties and improve flow characteristics to aid in their emplacement. Such additives include expansive agents used to reduce syneresis, plasticizers, accelerators, and pozzolans used to reduce porosity while increasing strength and durability.

Cement based grouts are considered most appropriate for sealing due to their known material properties and well documented longevity and durability. The use of chemical grouts are still in question due to their toxicity, cost and unknown stability over long periods of time. Chemical grouts however, possess other desirable characteristics such as high strength and bonding properties, impermeability, and low viscosity needed for grout emplacement.

Anticipated performance characteristics of emplaced grout should be (Gyenge, 1980):

- That they be a dense, impermeable solid,
- Have low wetting, drying and thermal shrinkage,
- Have sufficient deformability to allow for rock movement without developing cracks,
- That the coefficient of thermal expansion has an order of magnitude similar to that of the surrounding rock material,
- Be inert to sulfate, H^+ , chloride ions, and other sulfates in the groundwater of the disposal site,
- Have a low leach rate in the presence of groundwater,
- Have good bonding strength,
- Have the ability to immobilize radionuclides by sorption or other means,
- Have exceptionally long-term durability.

Grouting will be needed to seal connecting fracture or fissure networks around the waste repository to deter or slow down groundwater inflow while eliminating preferential flowpaths that may potentially carry gaseous radionuclides and allow their migration. Grouting can also be used to improve rock mass strength and stability in the repository itself.

Two other obvious applications for grouting involve the sealing of access routes needed for repository construction and waste emplacement as well as seals for exploratory boreholes used to characterize the host rock mass and evaluate its suitability. Desired performance characteristics of seals include low hydraulic conductivity, physical properties that will retain sealing effectiveness under natural and thermally induced states of rock stress, chemical compatibility with groundwater and host rock as well as resistance to erosion under hydraulic heads up to several MPa. (Gnirk, 1988).

Nuclear waste repository sealing is just one application of grouting. Common uses of grouting include civil engineering projects such as the construction of underground containment caverns and tunnels. In the case of dam construction and their remedial repair, grout curtains are used to reduce destabilizing uplift pressures while reducing water losses. Grouting is used in foundation control to stabilize and consolidate soil masses as well as to lift and level building foundations. Mining applications include rock mass stabilization to increase strength and standup time, the backfilling of drift liners (contact grouting), and the control of dangerous groundwater inflow.

The scope of this report involves the study of cementitious grouts used to seal single horizontal fractures in welded tuff (a proposed nuclear waste repository host rock). The objective of grouting is to reduce fracture permeability.

Experimental work includes the measurement of permeability in intact rock and of fractures under ranges of normal stresses and injection pressures, the determination and characterization of fracture roughness, and the injection of grout into the fractures. The effectiveness of grouting is evaluated in terms of the permeability reduction as well as by visual inspection of bond quality and grout

penetration. Results are analyzed to study the effects of normal stress, injection pressure, fracture roughness and grout formulations on sealing effectiveness.

Chapter two contains a review of the basic concepts of fluid flow and factors effecting permeability such as aperture, contact area, and surface roughness. Equations used in this study to calculate permeability are presented.

Chapter Three contains a state-of-the-art review of fracture grouting practices. Fundamental concepts such as grout mix design and fracture characterization are discussed.

Chapter Four presents the experimental procedures followed such as sample preparation, permeability testing, grout preparation and characterization as well as fracture characterization and fracture compression behavior.

Chapter Five includes the results. Chapter Six presents conclusions drawn as well as future work suggestions.

CHAPTER 2

FLUID FLOW IN FRACTURE ROCK

2.1 Introduction

Accurate estimates of permeability in quantitative and directional terms is of prime importance in the design, construction and upkeep of many engineering projects.

Knowledge of the flow characteristics in soil and rock masses define water transport systems. The potential for these systems to carry water or other fluids dictate the need and extent of grouting to reach some targeted permeability value. In the case of radioactive or toxic waste confinement, permeability must be kept very low (water and/or gas being the main agent of transport for radionuclides), while water inflow or outflow from underground excavations as well as seepage under and around dams requires only that permeability be reduced to a point where structural integrity is maintained. In the case of oil well production high permeabilities are desirable.

Recently the topic of fluid flow through porous and discontinuous media has brought about a lot of research by workers trying to describe and model the flow of fluids through rock and soil. This is a difficult task due to the inability to easily and accurately define the flow system. This problem is even more compounded in the field or in situ where direct visualization of flow conduits and their arrangement in space is denied, requiring complex analytical models to describe the flow system behavior.

It is not proposed nor in the scope of this report to review all the relevant work performed on this subject, which is voluminous, but only to briefly describe important aspects of this combined work needed to characterize permeability so as to define sealing and grouting requirements.

2.2 Theory of Fluid Flow Within a Single Fracture

The flow of an incompressible viscous fluid through rock fractures is generally modeled as flow between open, smooth parallel plates (Snow, 1965; Louis, 1969, 1974; Maini, 1971; Zeigler, 1976, Iwai, 1976; Witherspoon et al, 1980). Gale et al (1985) provides an excellent review of the literature on this subject.

A common approach to the flow analysis starts by considering the Navier-Stokes equations. The basic assumptions are that flow is governed only by mechanical and thermal energy within the system, the flow is isothermal, the flow is newtonian and homogeneous, and Stokes' equation is valid (Bawden and Roegiers, 1979). The Navier-Stokes equations are:

$$\rho \frac{DV_x}{Dt} = \rho B_x + \left(-\frac{\partial P}{\partial x} + \mu \nabla^2 V_x \right) \quad (2.1)$$

$$\rho \frac{DV_y}{Dt} = \rho B_y + \left(-\frac{\partial P}{\partial y} + \mu \nabla^2 V_y \right) \quad (2.2)$$

$$\rho \frac{DV_z}{Dt} = \rho B_z + \left(-\frac{\partial P}{\partial z} + \mu \nabla^2 V_z \right) \quad (2.3)$$

or in vector notation -

$$\rho \frac{D\vec{v}}{Dt} = \rho \vec{B} + \left(\nabla P + \mu \nabla^2 \vec{v} \right) \quad (2.4)$$

The equation of continuity:

$$\nabla \cdot \vec{V} = 0 \quad (2.5)$$

Equations 2.4 and 2.5 form four simultaneous differential equations from which the four unknowns (V_x , V_y , V_z , P) can be solved given simple boundary conditions.

In the case of a difficult set of boundary condition the Navier-Stokes analysis of flow behavior becomes cumbersome and difficult to handle making a Darcy parallel plate model analysis more attractive.

Darcy's law describes flow of a viscous incompressible fluid in a porous medium. Darcy over a hundred years ago showed experimentally that the rate of water (q) flowing through clean sand of cross sectional area (A) was proportional to the imposed hydraulic gradient (i) or (Holtz and Kovacs, 1981):

$$\frac{q}{A} \sim i \quad q = kiA \quad (2.6)$$

The coefficient of proportionality k has been called the permeability.

Permeability enters all problems involving the fluid flow through a porous medium. Permeability depends on the size of the soil grains, the void ratio, shape and distribution of pores, the degree of saturation, and the properties of the fluid (Lambe, 1951).

Darcy's relationship can be expressed for fracture flow as (Louis, 1974):

$$\text{Laminar or steady flow: } V = k_f i_f \quad (2.7)$$

$$\text{Turbulent flow: } V = k'_f i_f^\alpha \quad (2.8)$$

In these expressions, V stands for the mean velocity, k_f for the fracture permeability, k'_f for the turbulent fracture permeability, i_f for the perpendicular projection of the hydraulic gradient on the plane of the fracture, and α for the degree of non-linearity.

According to Darcy (Equation 2.6), the volumetric flow is given as:

$$Q = KA \frac{\Delta h}{L} \quad (2.9)$$

As previously implied this relation is valid if the fracture behaves similarly to a porous medium. This empirical flow relation can be derived directly from the Navier-Stokes equation by taking an average velocity of flow instead of velocities for each fluid particle, provided the inertia forces are negligible and the flow is steady state (Iwai,

1976). Mongan (1985) verified the validity of this equation through application of Hankel transforms to linearized Navier-Stokes equations for transient flow conditions.

If the flow is steady and isothermal, the flux per unit drop in head can be developed from Darcy's law and may be written in simplified form as (Witherspoon et al, 1980):

$$Q = C(2b)^3 \Delta h \quad (2.10)$$

This is the familiar cubic law with C representing the geometry of the system and the fluid properties.

In the case of radial flow:

$$C = \left(\frac{2\pi}{\ln\left(\frac{R_o}{R_i}\right)} \right) \left(\frac{\rho g}{12\mu} \right) \quad (2.11)$$

and in the case of straight flow:

$$C = \left(\frac{W}{L} \right) \left(\frac{\rho g}{12\mu} \right) \quad (2.12)$$

The flow rate of a newtonian fluid through an open fracture is a function of the aperture, the hydraulic gradient and the roughness of the fracture surfaces. Iwai (1976) showed that fracture permeability is a unique function of the fracture aperture independent of the loading path or how the loading is repeated. Conversely, no two different apertures will result in the same permeability given identical hydraulic gradients and surface roughness.

In actual rock fractures, the surfaces are far from smooth, and the validity of the cubic law is in question.

For flow in open fractures, the transition from laminar to turbulent takes place at very low values of the Reynold's number (Down to 100 or even 10), decreasing as the relative roughness of the fracture increases (Louis, 1974).

The Reynold's number as defined by Louis (1976) is:

$$Re = \frac{uD_h}{\nu} \quad (2.13)$$

where V = mean fluid velocity, u = dynamic viscosity, and D_h = the hydraulic diameter. This number is difficult to determine since it can vary from point to point along the fracture surface for a given type of flow.

In the case of flow through a porous media the Reynold's number is defined as:

$$R_e = \frac{qd}{\nu}$$

where q = specific discharge

d = representative length of the porous media

ν = kinematic viscosity

Darcy's law is valid as long as the Reynold's number does not exceed some value between 1 and 10 (Bear, 1979).

Lomize (1951 as referenced by Gale, 1985) introduced the concept of relative roughness (ϵ) which he defined as the ratio of the absolute height of the surface asperities to the fracture opening or aperture (2b). The aperture was calculated by dividing the volume of fluid contained in the fracture plane by the length and width of the fracture plane. He demonstrated the validity of the cubic law as long as the flow remained laminar and presented the empirically derived roughness equation:

$$\psi = \frac{96}{Re'} \left[1 + 6.0 \left(\frac{\epsilon}{2b} \right)^{1.5} \right] \quad (2.14)$$

which is valid for $\frac{\epsilon}{2b} > 0.065$

and relates the friction factor (ψ) to the Reynold's number (Re).

Louis (1976) contributes to Lomize's concept of relative roughness while defining different flow regimes corresponding to the Reynold's number. He then provides empirical equations to describe the flow in each regime. Figure 2.1 shows the range of validity for flow laws and there characteristic equations. The relative roughness is defined (by Louis):

$$R.R. = \frac{K}{D_h} \quad (2.15)$$

where K is the height of the asperities or absolute roughness
and

D_h = hydraulic diameter
= 4 times the hydraulic radius (R_h)
= 2 times the aperture (2b)

Figure 2.2 depicts Louis's representation for relative roughness.

Other workers have performed flow experiments to establish the laws of flow in similar flow regimens. The existing flow laws for parallel plate models including Lomize's are summarized below (from Iwai, 1976).

(a) Laminar flow

$$(i) \quad \epsilon/D < 0.033 \quad \psi = \frac{96}{Re} \quad (\text{Poiseville}) \quad (2.16)$$

$$(ii) \quad \epsilon/D > 0.033 \quad \psi = \frac{96}{Re} \left\{ 1 + 8.8 \left(\frac{\epsilon}{D} \right)^{1.5} \right\} \quad (\text{Louis}) \quad (2.17)$$

$$\psi' = \frac{6}{Re'} \left\{ 1 + 6.0 \left(\frac{\epsilon}{2R_h} \right)^{1.5} \right\} \quad (\text{Lomize}) \quad (2.18)$$

(b) Transition flow

$$\frac{1}{\sqrt{\psi}} = -2 \log \left(\frac{2.51}{Re \sqrt{\psi}} + \frac{\epsilon}{3.7D} \right) \quad (\text{Colebrook \& White}) \quad (2.19)$$

(c) Turbulent flow

$$(i) \quad \epsilon/D < 0.033 \quad \psi = 0.316 Re^{-\frac{1}{4}} \quad (\text{Blasius}) \quad (2.20)$$

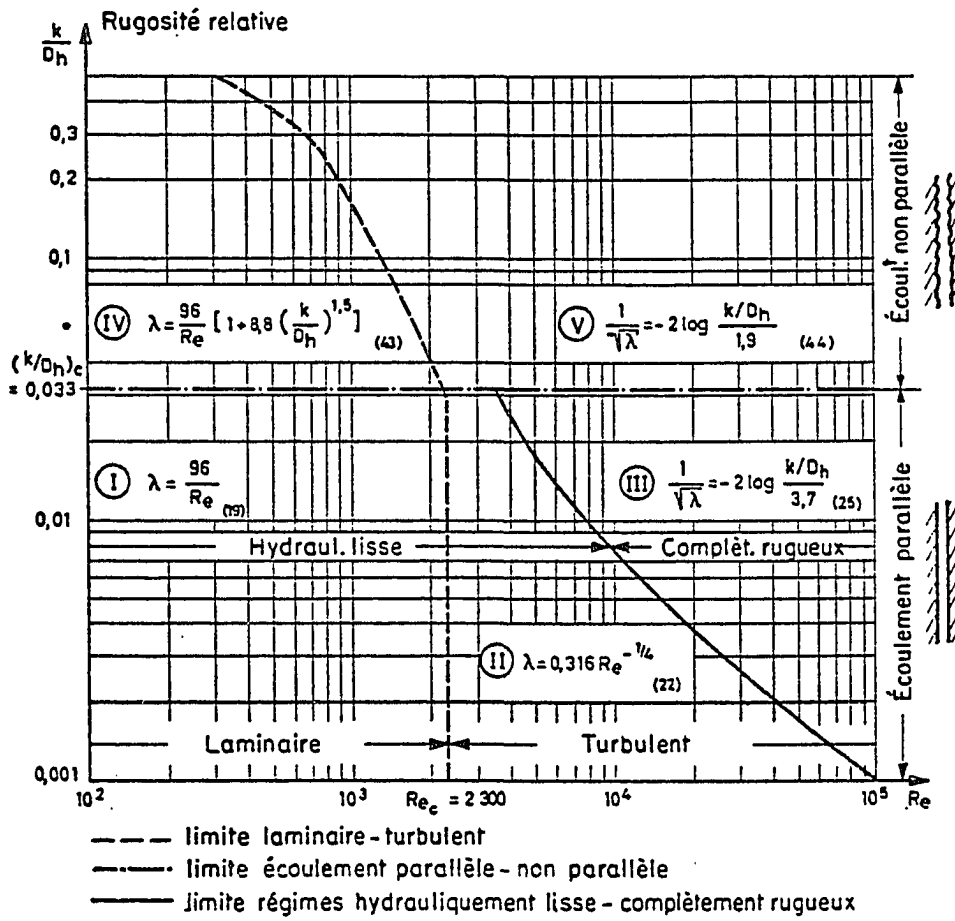


Figure 2.1 Range of validity for flow laws and their characteristic equations (From Louis, 1976 p. 66).

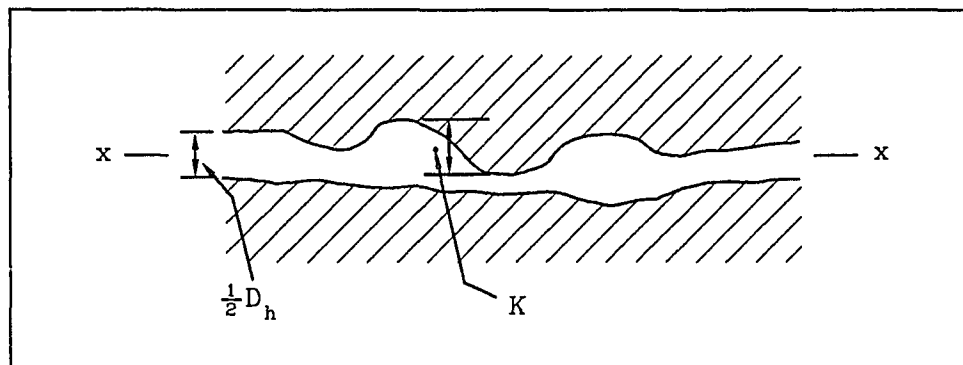


Figure 2.2 Relative roughness of a fracture's surface (After Louis, 1976, p. 49).

$$\frac{1}{\sqrt{\psi}} = -2 \log \frac{2.51}{Re \sqrt{\psi}} \quad (\text{Karman}) \quad (2.21)$$

$$(ii) \quad \epsilon/D > 0.033 \quad \frac{1}{\sqrt{\psi}} = -2 \log \frac{\epsilon}{3.7 D} \quad (\text{Nikuradse}) \quad (2.22)$$

$$\frac{1}{\sqrt{\psi}} = -2 \log \frac{\epsilon}{1.9 D} \quad (\text{Louis}) \quad (2.23)$$

$$\frac{1}{\sqrt{\psi}} = 2.6 - 5.11 \log \frac{\epsilon}{R_h} \quad (\text{Lomize}) \quad (2.24)$$

where $\psi' = \frac{\psi}{4}, \quad Re' = \frac{Re}{4}$

Contact area is of great importance in defining apertures and the area available for flow. Under compression as the fracture surfaces come in contact and the surface asperities begin to mesh the flow is effectively halted at these points.

Londe (1971) and Sharp and Maini (1972) describe contact area as dead water areas, which divide the fracture into discrete flow channels, such that the flow is effectively concentrated within a limited area of the joint. This resulting flow area is termed effective flow area.

The geometry of the effective flow area dictates the paths or channels available for fluid movement. The surface roughness along these paths induces numerous changes in flow direction. These changes account for the increase in travel distance required for the fluids tortuous path and the associated pressure drop away from the initial flow potential.

The cubic law has been derived for an open fracture where the surfaces remain parallel and not in contact at any point. In light of this what is the validity of the cubic law in real fractures that are closed at some points and have some varying degree of contact?

Detournay (1980) carried out a regression analysis on calculated conductivity coefficients and joint closure data under straight flow conditions and found the parallel-plate cubic law to be valid provided that one introduces an initial aperture, which is computed from the conductivity-closure data.

Witherspoon et al (1980) analyzed Iwai's data and concluded that the cubic law was valid (down to apertures of 4um) whether the fracture surfaces were held open or were closed under stress. The effect of deviating from the ideal parallel plate concept only caused an apparent reduction in flow and could be accounted for by incorporating into the cubic law a factor f , which varied from 1.04 to 1.65 or:

$$\frac{Q}{\Delta h} = \left(\frac{C}{f}\right)e^3 \quad (2.25)$$

2.3 Rock Mass Permeability

In fractured rock masses flow occurs through an arrangement of discontinuities with the intact rock often considered impermeable.

Traditionally two accepted methods are used to analyze the hydraulic response of the rock mass. These analyses use either a continuum (representative porous media) or a discontinuum (discrete flow path) model. For further information see: Snow, 1965; Banks, 1972; Louis, 1974; Zeigler, 1976; Sagar and Runchal, 1982; Englman et al, 1983.

Continuum Model

This first model considers the rock mass to be continuous. Based on Darcy's law (Equation 2.6), a linear relationship exists between flow velocity and hydraulic gradient,

$$V = ki$$

It is assumed that the rock mass is so fractured that it resembles a porous medium.

Discontinuum Model

This second approach is used when fractures or discontinuities are so independent that they may be analyzed as separate channels, each representing a parallel plate with flow behavior assumed linear, incompressible, and viscous. These flow conductors vary in frequency, orientation and fracture characteristics (aperture, contact area, and roughness). The flow rate in each discrete path is proportional to the cube of its aperture and the projection of the field gradient generally parallel to no fluid conductor (Snow, 1965). The total flow is then the sum of the individual flows.

Hsieh and Neuman (1985) found that single hole pressure tests yield results that are only good in the vicinity of the borehole. They propose the "cross hole test" for investigating the relationship between fracturing and anisotropy. The test consists of first mapping the fractures in a single borehole by sectioned pressure tests and by looking at core orientations. Next the primary hole is sealed or "packed" off and injected with water at constant pressure. Nearby holes, previously pack off are then monitored for their hydraulic-head response.

2.4 Method of Permeability Calculation

In this investigation permeability of a single horizontal fracture is calculated by assuming that the intact rock permeability is low and negligible, the fracture plane is a smooth parallel plate, and that the radial flow normal to the borehole is laminar. The method of calculation is as follows.

1. Normal Stress on Sample

The normal stress σ_n is calculated from the oil pressure in the hydraulic load cell.

$$\sigma_N = (P \cdot A_p) / A_s \quad \text{Pa}$$

where P = oil injection pressure in Pa

A_p = cross-sectional area of the piston inside the
load cell in square meters

A_s = area of the sample in square meters.

2. Permeability of Intact Rock

The rock permeability is calculated by assuming that the flow is laminar, all connective voids are filled with water, and the Darcy's law is valid. For falling head tests, the hydraulic conductivity (k) of the rock sample is calculated from an equation derived from Bear (1979, pp. 305-306) and Freeze and Cherry (1979, p. 336):

$$k = \frac{\alpha \ln(R_o/R_i) \ln(h_o/h_i)}{2\pi L_H (t_1 - t_o)} \quad \text{cm/second}$$

where a = cross-sectional area of the pipette in cm^2

R_o, R_i = outer and inner radii of the hollow cylinder in cm

L_H = length of the center hole in cm

t_1, t_o = time in seconds

h_o = initial height of water in the pipette measured from the midsection of the cylinder at time t_o (in cm)

h_1 = height of water in the pipette at time t_1 (in cm) (Figure 2.3)

For steady-state flow tests, the hydraulic conductivity of the rock cylinder is calculated using an equation modified from Bear (1979, pp. 305-306):

$$k = \frac{Q \ln(R_o/R_i)}{2\pi L_H \Delta h} \quad \text{cm/second}$$

where Q = flow rate in $\text{cm}^3/\text{second}$

R_o, R_i = outer and inner radii of the hollow cylinder in cm

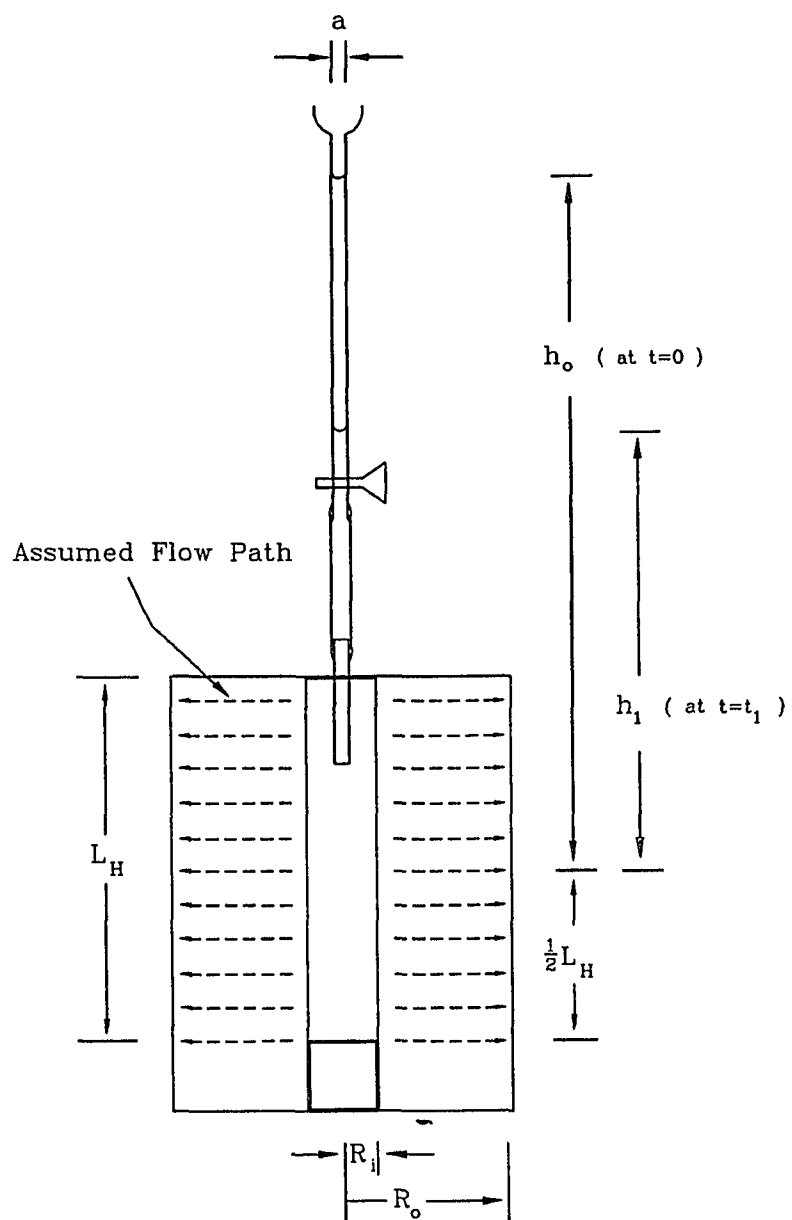


Figure 2.3 Parameters involved in a falling head test.

L_B = length of the borehole in cm
 Δh = difference of water head between inner hole and cylinder
 outer surface

The inflow rate, Q , is calculated from equation

$$Q = A_I(\Delta S/\Delta t) \quad \text{cc/second}$$

where A_I = cross-sectional area of the piston in the
 intensifier, in cm^2

ΔS = travel distance of the push-rod in cm

Δt = travel time in seconds

The water head difference (Δh) is calculated from the injection
 pressure (P_i),

$$\Delta h = (P_i/\gamma) - h_o \quad \text{cm}$$

3. Permeability of Fracture

The permeability of the fracture is calculated by assuming that the
 rock permeability is low and negligible, flow is radial from the
 borehole and Darcy's law applies. The equivalent fracture aperture (e)
 can be calculated using an equation given by Witherspoon, et al. (1980):

$$e = [Q/(\Delta h C)]^{\frac{1}{3}}$$

where Q = flow rate in cc/second

Δh = head difference in cm

C = constant representing flow geometry and
 fluid properties.

For the case of radial flow, the constant C is

$$C = \frac{2\pi \gamma}{\ln(R_o/R_i) 12\mu}$$

where R_o, R_i = outer and inner radii of the hollow
cylinder in cm

γ = unit weight of water in g/cm^3

μ = viscosity of water in $g \cdot sec/cm^2$

The permeability of the fracture (k_f) is calculated using an equation (modified from Zeigler, 1976, p. 10, as cited by Schaffer and Daemen, 1987, p. 18):

$$k_f = (\gamma/12\mu)e^2 \quad \text{cm/second}$$

For the falling head test, the equivalent fracture aperture is given by (Schaffer and Daemen, 1987, p. 64):

$$e = \left[\frac{\ln(h_o/h_i) \alpha \ln(R_o/R_i) 6\mu}{\pi(t_i - t_o)\gamma} \right]^{1/3} \quad \text{cm}$$

For the steady-state flow test, the fracture aperture is calculated using equation:

$$e = \left[\frac{Q \ln(R_o/R_i) 6\mu}{\Delta h \pi \gamma} \right]^{1/3} \quad \text{cm}$$

where Q = inflow rate in $cm^3/second$

Δh = difference of water head between the

inner hole and cylinder outer surface in cm

CHAPTER 3

FRACTURE GROUTING

3.1 Introduction

The scope of this chapter deals with cement based grouts due to their well documented material behavior and longevity, which are important to satisfy design criteria for the development of deep underground nuclear waste repositories. Chemical grouts are largely ignored in this report due to their present high cost, toxicity, and unknown longevity performance (Gnirk, 1988) but offer advantageous properties such as low viscosity, low permeability and good surface bonding (Karol, 1983).

Grouting is typically practiced, based on a rational and "seat of the pants" approach rather than a theoretical one due to the complexity of fracture systems and a grout's fluid properties changing with time.

For successful grouting of fractured rock, grout slurries must be fluid enough to be efficiently pumped at limited pressures, while possessing a maximum grain size that will allow admission into the fractures without premature clogging. The hardened grout must possess the performance characteristics such as, complete void filling, impermeability, bond strength, longevity, etc., needed to accomplish or satisfy the engineering purpose.

3.2 Pressure Grouting

SITE INVESTIGATION

As with all engineering projects a complete description of the problem at hand is essential. In grouting, to reduce rock mass permeability, this description starts with a thorough site investigation. The site investigation should include the geologic nature of the fracture system, locations of large voids, zones of weakness, and permeability values.

Spatial descriptions of the fracture system and voids includes surface mapping and borehole drill logs. Permeability values are obtained by flow tests performed at designed grouting pressures. The most common test for obtaining fluid takes along the length of a borehole is the Lugeon. This test is defined as the flow in liters per minute per meter of borehole at a pressure of 10 Kgf/cm² (0.1 MPa). One Lugeon is equivalent to the permeability of 1×10^{-5} cm/s (Consulting Engineer, 1969).

From the information gained from the site investigation, such as permeability values and major flow conduits, a general grouting plan may be implemented along with a targeted permeability value (i.e. when to stop grouting).

HOLE LAYOUT

Once the zones of rock to be grouted are identified, hole spacing and depth can be selected based on approximate equations predicting the radial extent or penetration of the grout front. These equations depend on such things as injection pressure and the grout slurries rheological properties (see Section 3.3).

In the case of severely or uniformly fractured rock a regular grid pattern or curtain of grout holes should be used to shut off flow. These curtains are generally oriented perpendicular to groundwater flow lines. Hole spacings are decreased with grouting continuing until the targeted permeability values are reached.

Large voids and major flow conduits such as faults need special attention and should be grouted separately.

INJECTION PRESSURES

Grout under pressure produces great stresses in the rock mass. Injection pressures if not under control at all times can quickly get

the grouter into trouble. Particular attention must be paid to ground movement when grouting in the vicinity of the surface, near surface structures or near underground excavations.

Rules of thumb can be used to select appropriate injection pressures, but must first be site tested to confirm their suitability. Figure 3.1 shows the maximum allowable grouting pressures which are dictated by rock mass strength and hole depth.

The use of high injection pressures are condoned by European grouting experts (approximately four times greater than U.S. engineers) (Shannon and Wilson, 1987). Pressures of up to 4.4 psi (30.3 kPa) per foot of depth (refusal pressure) are deemed necessary to dilate fractures so they will accept grout. High pressures are assumed to squeeze out and drive off excess bleed water so as to achieve better grout filling in the fractures. In addition to this, lower water to cement ratios can be used with higher injection pressures.

Confidence can be placed in using higher injection pressures since this process requires grout flow and pressure meters to be watch diligently so any hydrofracturing can be identified in its early stages (Deere, 1982). At any sudden increase in flow or drop in pressure, the pumping pressure can be immediately lowered avoiding fracture propagation and ground movement.

3.3 Grout Mix Design

WATER TO CEMENT RATIO

Water is the main ingredient in a grout that gives the slurry mobility. After the water's transportation role has ended and the grout is positioned where it will stay, the remaining water not needed for further cement hydration and curing becomes a bother, affecting the

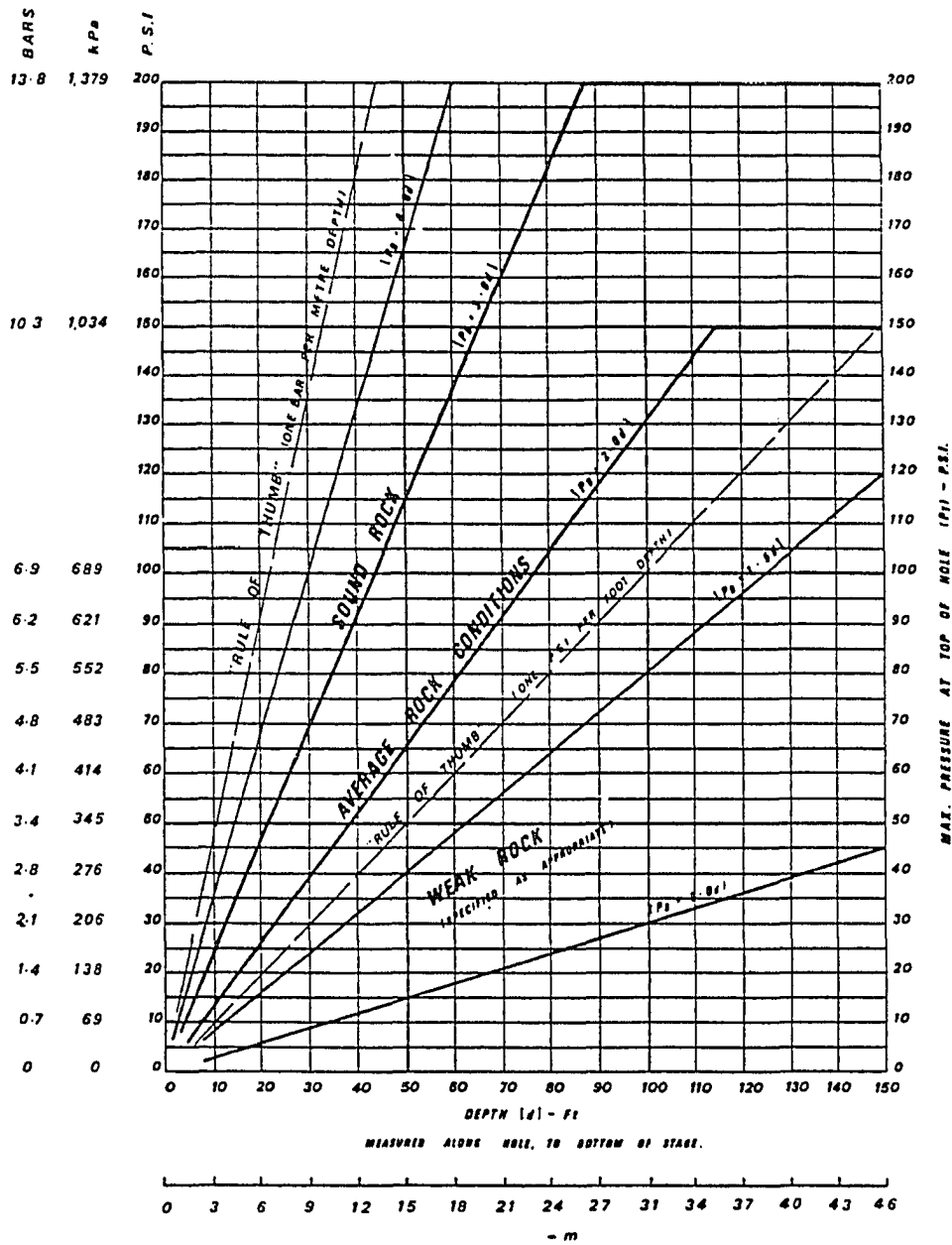


Figure 3.1 Maximum allowable grouting pressures (After Houlby, 1977, p. 41).

grout films bonding, strength, shrinkage, durability, and permeability. The greater the amount of water used the greater these problems become (Houlsby, 1985).

The effect of the water to cement (W/C) ratio on compressive strength, viscosity, and bleed capacity of cement slurries are well documented (Farmer, 1970, Littlejohn, 1982) figure 3.2. W/C ratios are defined as a volume or weight ratio. Thin grouts with W/C ratios greater than 1:1 and up to 9:1 by weight are not uncommon and allow considerable grout travel. When grouting pressures are reduced fracture dilation is reduced and excess or bleed water is presumably squeezed out. Thick grout advocates question this line of thought and try to avoid excess fracture dilation and potentially dangerous hydrofracturing that can actually increase rock mass permeability by fracture propagation.

Thick grouts are usually defined with water to cement ratios of 0.5:1 to 1:1. Without high grouting pressure and large fracture dilation thick grout penetration and fracture admittance are basically limited by the grout's maximum grain size (Karol, 1985).

Too thick a grout can cause inadequate penetration and premature fracture blockage requiring additional holes to be drilled and grouted. Too thin a grout can cause excessive penetration which wastes grout and increases the possibility of rock movement.

Based on examination of grout films obtained in the U.S. Army Corps of Engineers work and research in regard to durability and sealing effectiveness, the use of a final W/C ratio greater than 1:1 is not desirable due to the bleed water from these grouts becoming trapped in the grout film and reducing the amount of area available for complete cement filling (Kennedy, 1958).

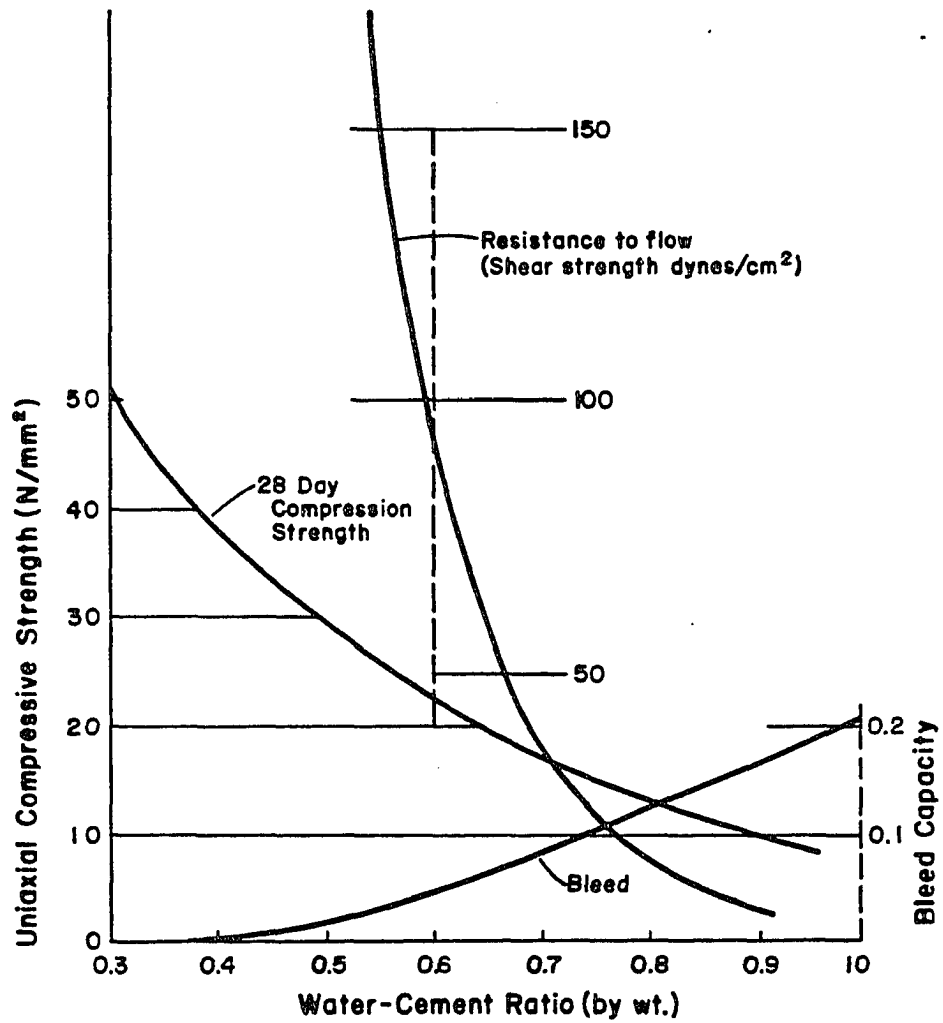


Figure 3.2 Effect of water-cement ratio on grout properties. (After Farmer, 1970, p. 5).

Houlsby (1982a) references numerous case histories where large W/C ratios used in dam grouting produced grout films that had completely leached away. The view that bleed water is driven off during grouting was not supported.

It is worthwhile to note that numerous case histories record the success of both (W/C ratio) methods and no one method can be singled out as being superior, however it would be desirable to use the lowest W/C ratio and injection pressure that will get the job done (Houlsby, 1982b; Deere and Lombardi, 1985).

In the field, pressure tests, fracture openings and grout takes on previous grout holes help determine the lowest W/C ratio that can be started with to ensure that filter blockage and possible loss of the grout hole does not take place. As the rate of grout take increases and pressures decrease the grout mix is slowly thickened to grout refusal.

CEMENT TYPE

Selection of appropriate cement types are site dependent and must be chosen on the basis of maximum grain size versus fracture opening, depth at which grouting will take place, intended admixtures used to improve flow properties, geochemical and thermal compatibility with the country rock in regard to nuclear waste storage, and finally appropriate resistance to leaching and chemical attack such as in the presents of salts and sulfides.

Once an approximation of the fracture's average aperture has been made then the performance of a selected cement type can be evaluated in terms of its ability to penetrate the fracture. This designation is defined by Mitchell (1970) as the groutability ratio:

$$G.R. = \frac{D_{fissure}}{(D_{max})_{grout}} > 3$$

For successful penetration this ratio of fissure aperture to maximum particle size must be greater than about 3 and corresponds to a lower limit of penetration into apertures less than 0.3 mm for ordinary portland cements. Shannon and Wilson (1987) also set this limit at 0.3 mm for grouts without a lubricating additive. The Consulting Engineer (1969) sets this lower limit at 0.1 mm which would correspond to a groutability ratio of 1.0. In the case of ultra fine grouting materials the groutability ratio would predict a lower limit of penetration into apertures of 0.03 mm (Shimoda and Ohmori, 1982).

In theory, when the groutability ratio is less than 3 the entrance to the fracture becomes clogged with cement. This phenomenon is known as filter blockage. Karol (1985) defines this no flow situation as "blinding" where a few larger particles in the slurry try to enter the fracture at the same location at the same time causing the crack to become clogged resulting in premature refusal of cement by the fracture.

ADMIXTURES

Admixtures are used to improve the flow properties of the grout. Bentonite, a colloidal material prepared from montmorillonite clays transforms sedimentation unstable grouts to sedimentation stable grouts (Cambeford, 1977). Stable grouts are desirable since they do not settle out and clog grout lines, as well as help in the complete filling of voids. Lombardi (1985) states that bentonite increases viscosity and cohesion thereby limiting the extent of grout travel.

Other commonly used admixtures include accelerators that speed up set time by increasing the rate at which chemical reactions would otherwise occur, dispersants and inhibitors that reduce interparticle attraction thereby slowing down set, emulsifiers and wetting agents that modify surface tension of the grout particles to reduce sedimentation and facilitate penetration, fluidifiers which improve flowability

without changing the water to cement ratio, expansive agents that reduce shrinkage and cracking, and fillers that increase grout volume while reducing total grout cost.

After a grout has been selected that is felt will function adequately given the site conditions, estimates of the penetration and extent of grout propagation can be made. This knowledge aids the grouter in selecting appropriate grout pumps, injection pressures and the grout hole layout.

GROUT RHEOLOGY

Probably the most important rheological properties of a cementitious grout slurry in regard to penetration and grout travel are viscosity and cohesion. As the water to cement ratio of a cementitious grout slurry is increased the viscosity and cohesion are decreased.

In the field the Marsh funnel is used to find the apparent viscosity of a grout slurry. The term apparent is used to define the viscosity because what is actually being measured is a combination of the slurry rheological properties (viscosity, rigidity, and specific weight) including the roughness of the flow cone (Cambefort 1977). Lombardi (1985) found that cohesion, which is analogous to rigidity is generally low and that the flow time through the Marsh funnel is approximately a function of the viscosity only and no information on the cohesion value results from the Marsh test. Many different types of flow cones are used in industry and results are hardly comparable. A rotary or coaxial viscometer is used to obtain the actual viscosity and cohesion in the laboratory.

Bentonite markedly increases the viscosity of grouts and must be accounted for in all measurements (Consulting Engineer, 1969). Deere (1982) also found that bentonite does increase appreciably the funnel viscosity of a grout slurry and is an important index property for

quality control of field mixes, particularly of the bentonite content. Figure 3.3 shows the effect of bentonite and water to cement ratio on the Marsh funnel viscosity. In this figure 1000 ml of slurry was allowed to pass through the funnel instead of 946 ml.

According to Deere and Lombardi (1985) and others, the radial penetration and rate of penetration of a grout mix is governed by the yield stress, τ_0 and viscosity, μ . A stable grout slurry is characterized as a visco-plastic or Bingham fluid with rheological properties controlled by viscosity and cohesion. It is well established that under conditions of Laminar flow that cementitious grouts behave in a similar manner to Bingham fluids (Deere & Lombardi, 1985; Farmer, 1970; Nonveiller, 1989). Figure 3.4 shows the flow behavior of Newtonian and Bingham fluids. The shear stress (τ) needed to overcome the cohesion of the grout slurry and cause flow at a constant rate of strain (Figure 3.5) is given by:

$$\tau = \tau_0 + \mu \frac{dv}{dz}$$

where τ_0 = threshold resistance (cohesion)

μ = plastic viscosity coefficient

$\frac{dv}{dz}$ = velocity gradient (rate of strain)

The viscosity component determines the flow rate at which a grout travels away from the grout hole under a given pressure and aperture, while the cohesion component determines the final distance of penetration. Therefore the cohesion limits the extent of grout travel while the viscosity component influences the time needed for the grout to travel a finite distance. Lombardi (1985), Wallner (1974), and Ruiz (1970) develop equations which allow an approximation of the maximum radius of penetration (R_{max}), the maximum volume of injected grout (V_{max}), and the maximum total uplift force (F_{max}), to be computed.

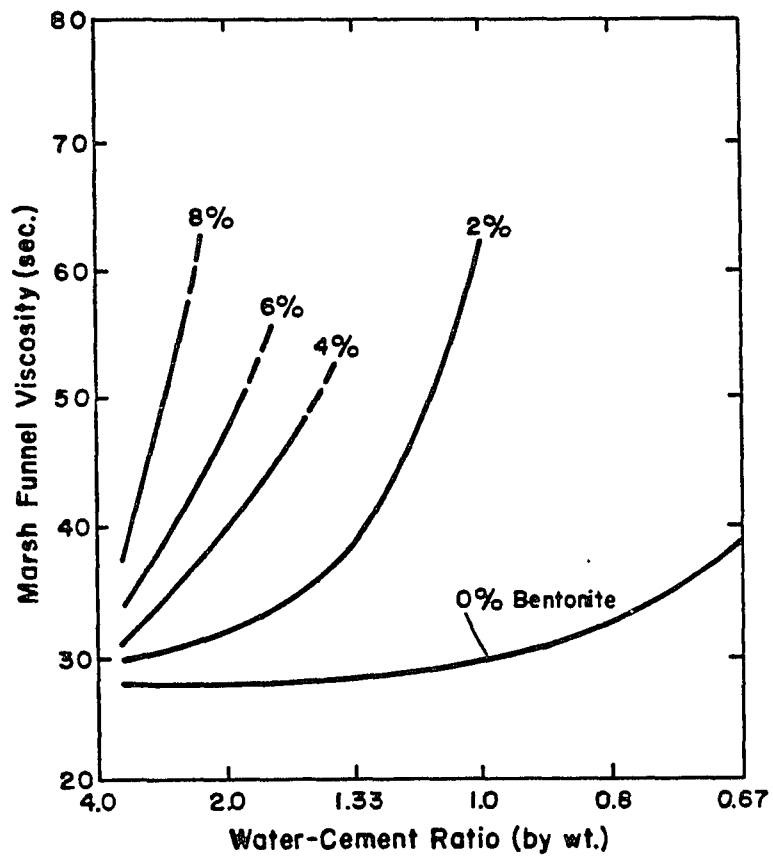


Figure 3.3 The effect of bentonite and water to cement ratio on Marsh funnel viscosity. (After Burgin, as referenced by Deere, 1982).

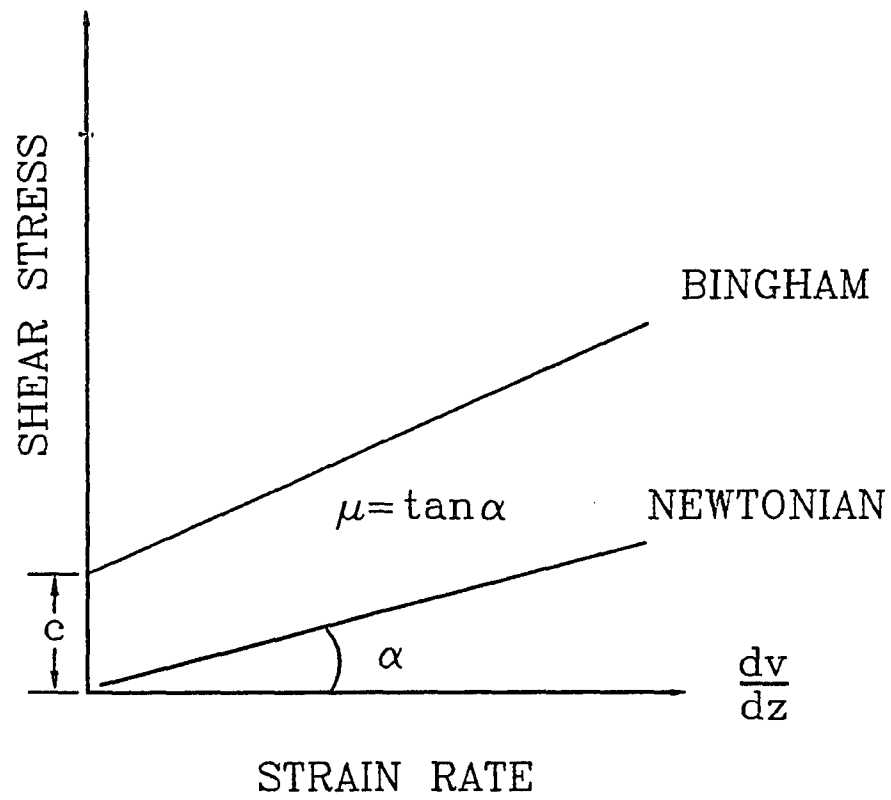


Figure 3.4 Flow behavior of Newtonian and Bingham fluids.

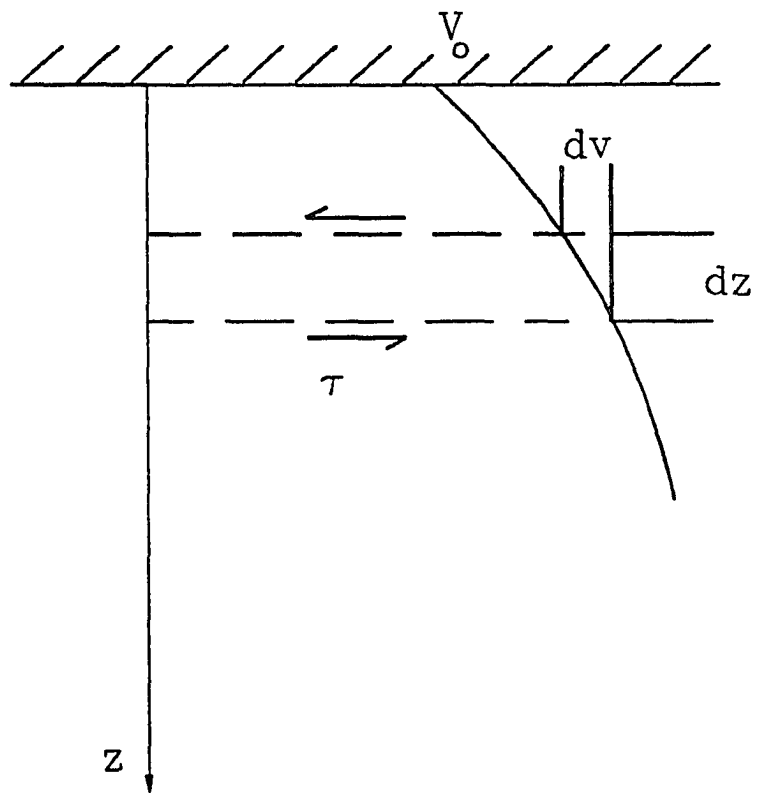


Figure 3.5 Flow velocity cross section.

$$R_{\max} = \frac{P_{\max} t}{c}$$

$$V_{\max} = \frac{2\pi P_{\max}^2 t^3}{c^2}$$

$$F_{\max} = \frac{\pi P_{\max}^3 t^2}{3c^2}$$

Where, P_{\max} = final injection pressure

t = 1/2 the joint thickness (aperture)

c = cohesion (yield value)

These equations are developed from an equilibrium of forces and correspond to empirical findings on grouting jobs (Lombardi 1985). Assumptions include the use of stable grout on a single dry rough horizontal open planer joint with laminar flow. These equations are valid for fractures that are wider than the maximum grain size in the grout. Figure 3.6 shows the maximum radius of penetration as a function of grout consistency. Thin, medium, and thick grouts correspond to Marsh flow times of 30, 40, and 50 seconds respectively.

As can be seen the only rheological property of the grout slurry that is needed to use the above equations is the cohesion or yield value. This value may be obtained from a rotary viscometer or a plate cohesion meter developed by Lombardi. This simple test is readily used in the field and is comprised of a rough metal plate of 15x15 cm that is submerged in grout slurry. The weight of the slurry left adhering to the plate after removal from the slurry container is recorded. From the weight difference ΔW between the dry plate and the plate with the adhering suspension allows the cohesion or shear strength, τ_o , to be obtained (Nonveiller 1989).

$$\tau_o = \frac{\Delta W}{2A} (kN/m^2)$$

where A is the area of the metal plate.

The resulting cohesion value corresponds to the thickness of a layer adhering to the roughened plate (Lombardi 1985).

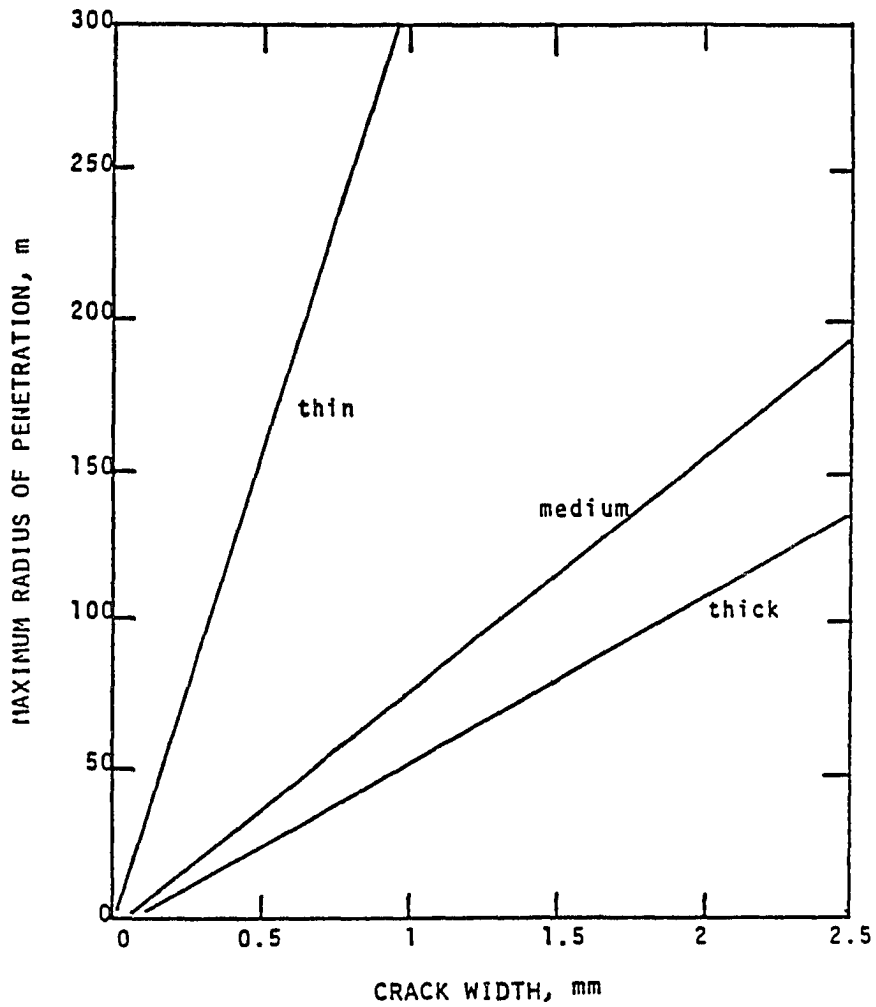


Figure 3.6 Maximum radius of penetration as function of crack width and grout consistency (After Deere and Lombardi, 1982, p. 11).

CHAPTER 4

EXPERIMENTAL PROCEDURE

4.1 Sample Preparation

1. Intact Samples

Cylindrical tuff specimens are obtained by coring tuff blocks parallel to the ash flow layering using a 15 cm inside diameter diamond coring bit. Samples have a nominal length of 20 cm (Figure 4.1). Figure 4.2 shows the measurement scheme. Figures 4.3a and b show the 3 hp Acker and 2 hp Century drills used to core samples.

A 2.54 cm diameter borehole cored through the axis of the sample provides access to the interior of the sample. Boreholes are closed off at the bottom of each sample using a tuff and epoxy adhesive plug.

To ensure even loading of sample during testing the ends of each cylinder are ground parallel and flat using a Kent automatic surface grinding machine (Figure 4.4). Figure 4.5 shows a prepared sample of Apache Leap tuff.

2. Fracture Creation

Three types of fracture surfaces are used in this study: sawcut, tension induced and natural fractures. Even though sawcuts are not true fractures, they still will be referred to as such. Fractures are oriented normal to the longitudinal axis of each cylinder.

Sawcuts are made using a Covington diamond saw (Figure 4.6). Alignment marks are placed on each sample prior to cutting to ensure correct orientation during testing. Figure 4.7 shows the resulting sample halves with smooth sawcut surfaces.

Artificially produced tension fractures are created using a modified point load test. Figures 4.8a and b show the equipment used to create such fractures. Two 5 mm diameter holes 3 mm in depth are drilled diametrically apart at the midsection of each sample. These holes hold the tips of the #316 stainless steel loading points and ensure proper alignment as well as to direct the load. An SBEL servo

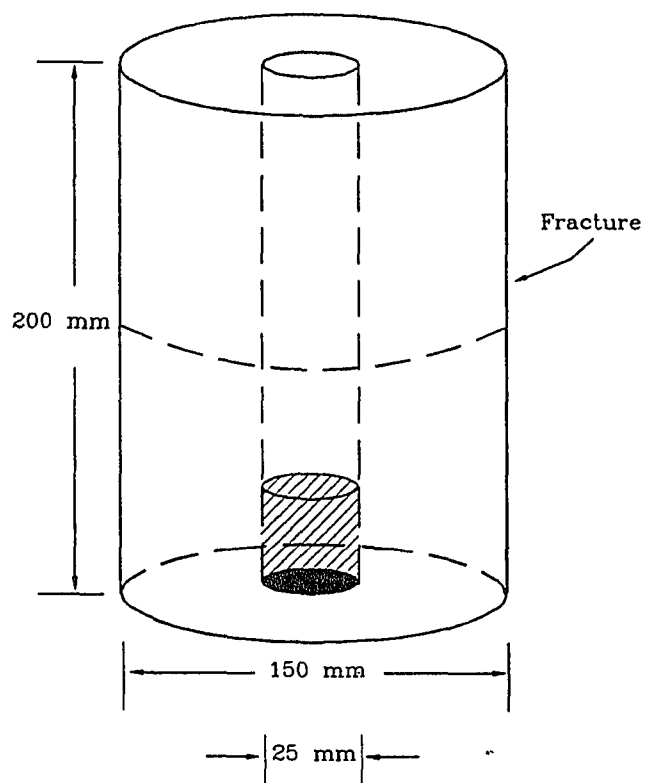


Figure 4.1 Nominal sample dimensions.

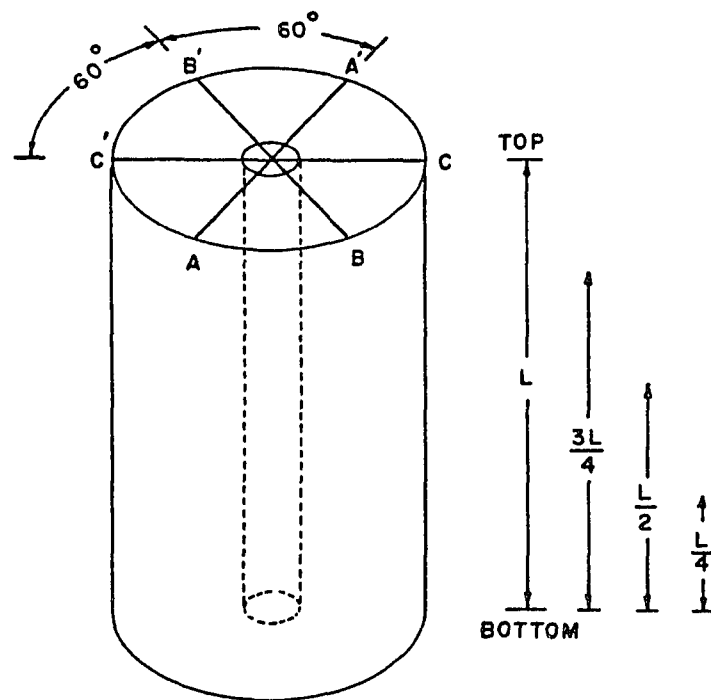


Figure 4.2 Sample measurement scheme.

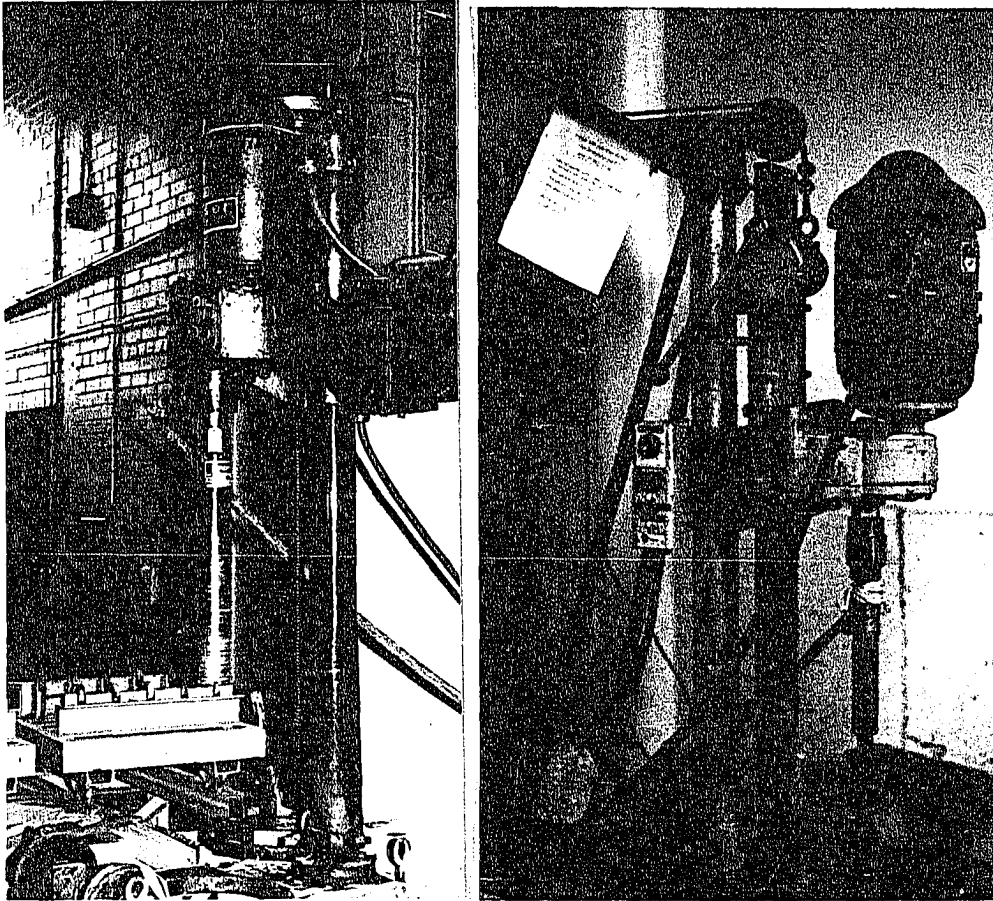


Figure 4.3a (left) and b (right) 3hp Acker and 2hp Century drills used to core samples.

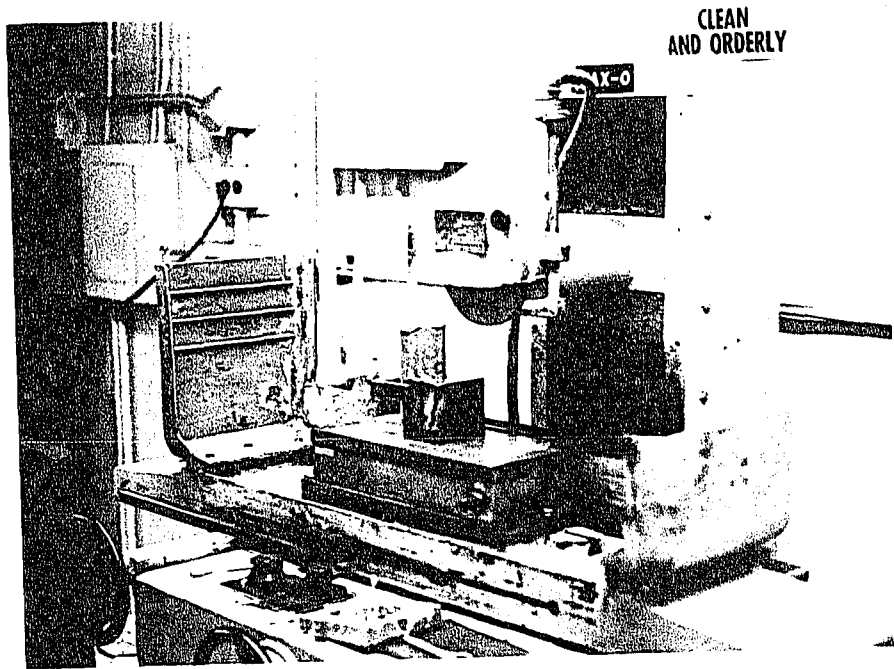


Figure 4.4 Kent automatic surface grinding machine.

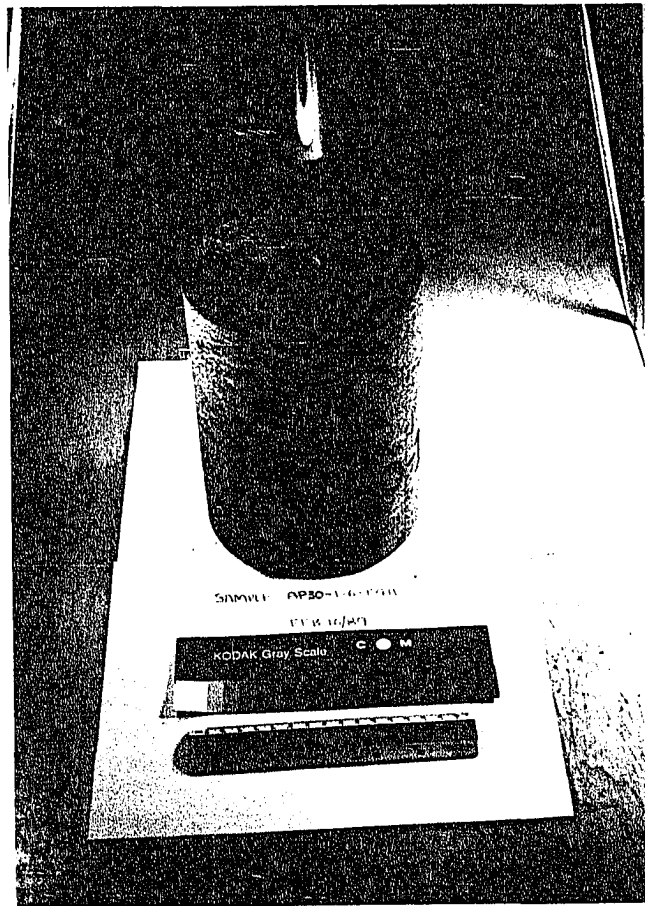


Figure 4.5 Intact sample of Apache Leap tuff.

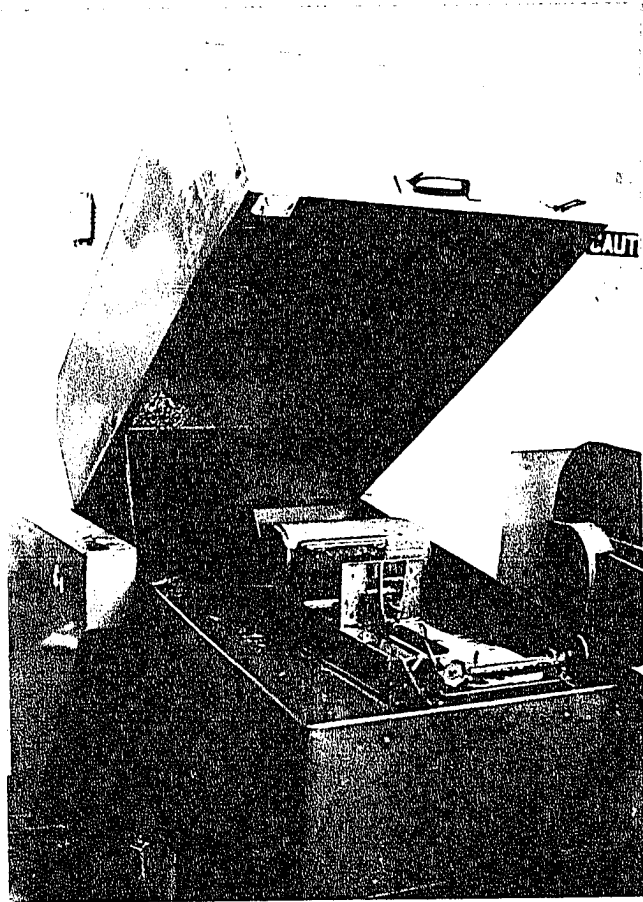


Figure 4.6 Covington diamond saw used to cut sawcut surfaces.

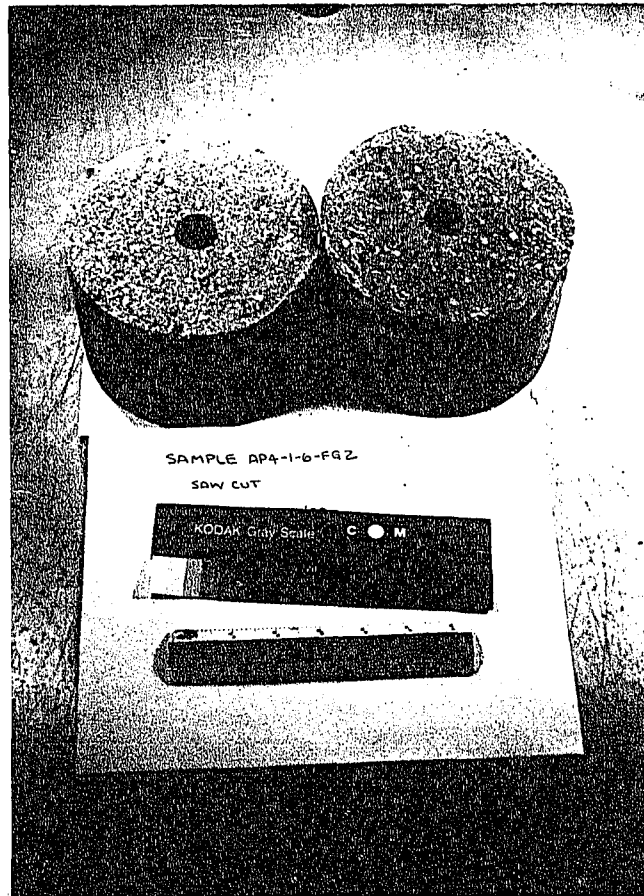


Figure 4.7 Sawcut surfaces of sample AP4-1-6-FG2.

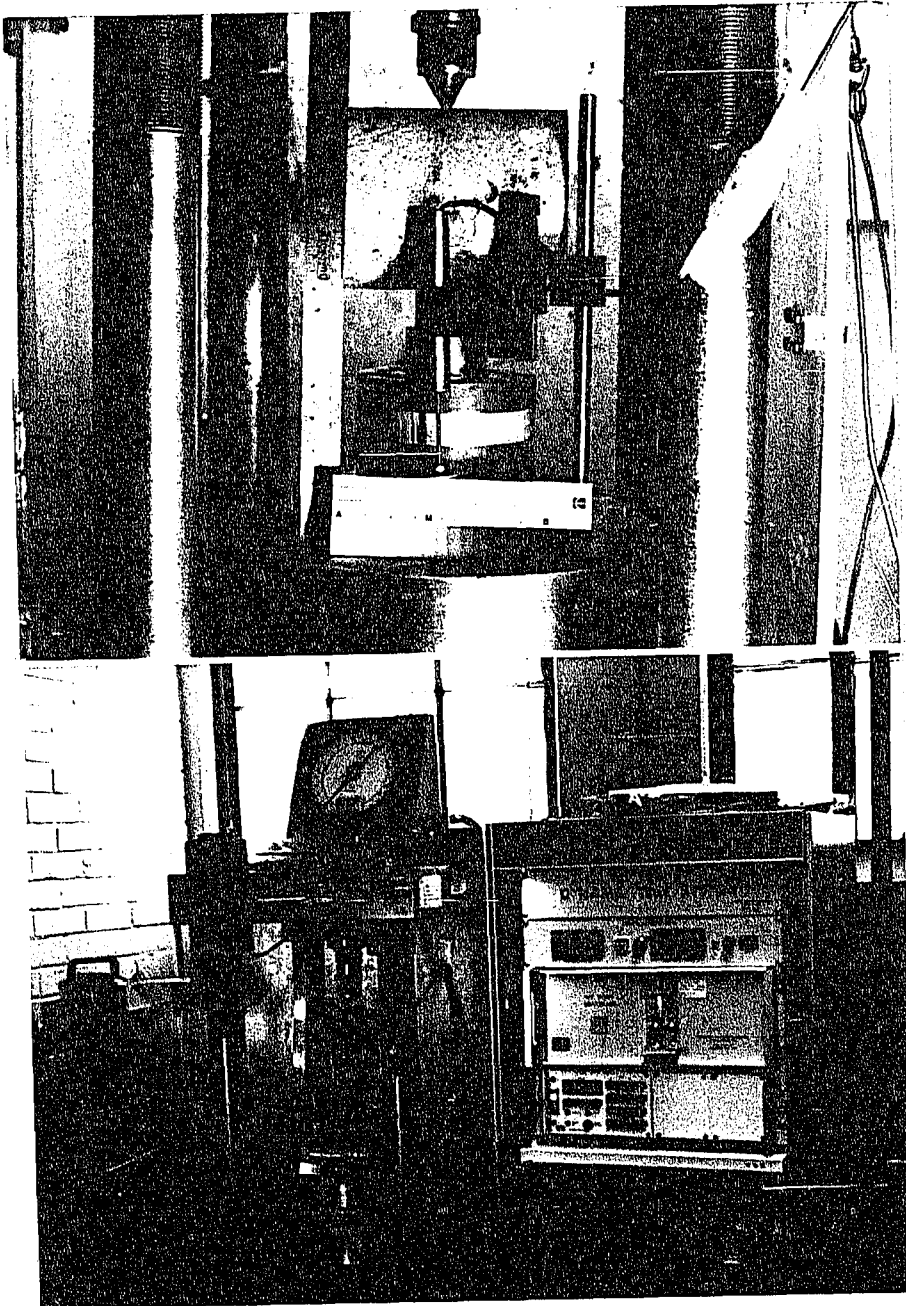


Figure 4.8a (top), b (bottom) S.B.E.L. load frame and Servo controller used for modified point load test.

controller is used to load the sample to failure. The failure load and time as well as the angle between the fracture surface and core axis are recorded. Figure 4.9 shows the resulting fracture surfaces.

Blocks containing single natural fractures are collected in the field. Due to the great weight of these blocks, their fractures are pried apart in the field to facilitate transportation and then put back together prior to coring.

In the laboratory these naturally fractured blocks are aligned and positioned to have their natural fractures positioned perpendicular to the proposed coring orientation. The fractured blocks are tightly clamped together to prevent overcoring. Figure 4.10 shows such a block being cored. As the coring bit first reaches the natural fracture the top portion of the core is removed to prevent damage to the fracture surface due to rotation.

During surface grinding and the drilling of the 2.54 cm center borehole the resulting sample halves of the natural fracture must be tightly clamped together. Figure 4.11a shows the resulting core containing a single natural fracture.

The only exception in the preparation of naturally fractured samples was sample AP2-1-6-FG7 which was left intact and contains a complex nonplanar fracture geometry (Figure 4.11b). Black lines trace the fractures as they appear on the sample's surfaces.

4.2 Permeability Testing

1. Objective

The objective of this test procedure is to determine the permeability of intact, fractured, and grouted rock under uniaxial compression. Permeability is measured as a function of normal stress and injection pressure.



Figure 4.9 Fracture surfaces produced by modified point load test.



Figure 4.10 Coring of blocks containing a single natural fracture.

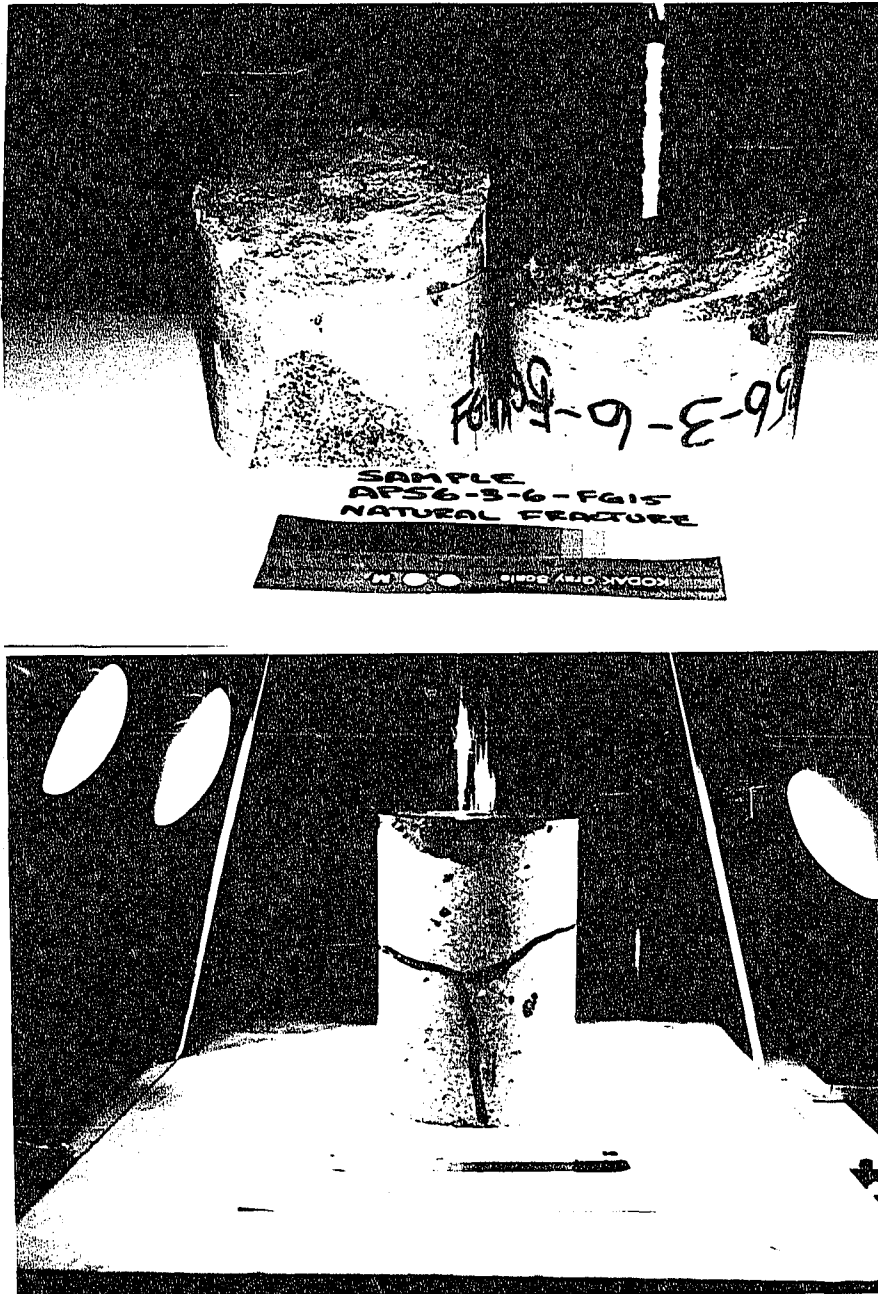


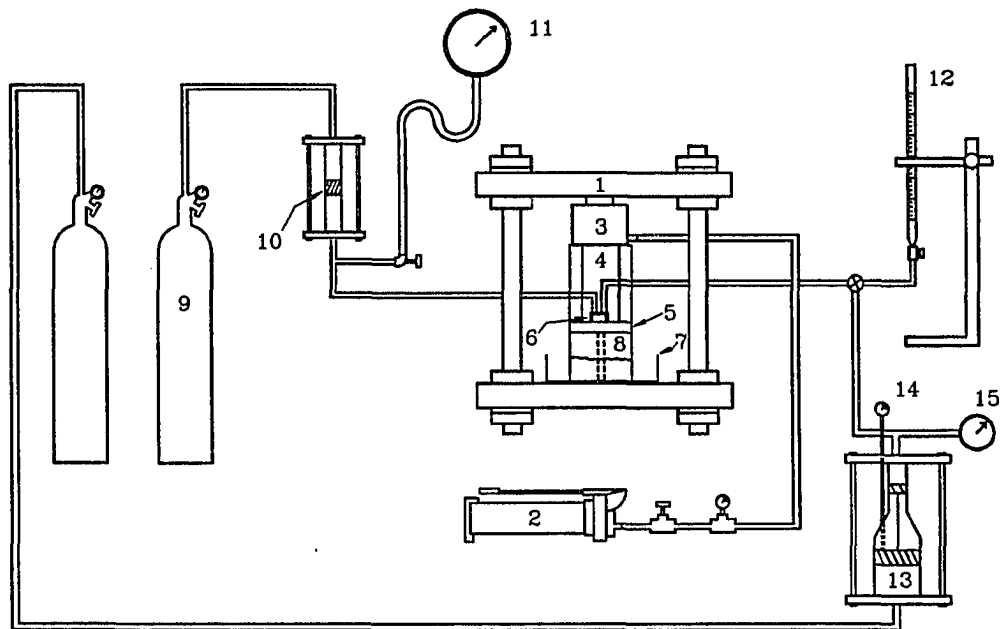
Figure 4.11a (top) and b (bottom) a) Cored sample (AP56-3-6-FG15) containing a single natural fracture, b) complex nonplanar fracture geometry of sample AP2-1-6-FG7.

2. Apparatus

- load frame (1 MN capacity) (Cobb and Daemen, 1982, pp. 35-36)
- hydraulic load cell (Enerpac JSL-1002)
- hydraulic hand pump (Enerpac EH-80)
- shut-off valve
- pressure gauge (Heise; 7 MPa range, 10kPa accuracy)
- cut-away loading platens (Schaffer and Daemen, 1987, p. 59)
- falling head permeameter (2 and 50 ml high-precision pipette)
- nitrogen gas tank
- regulating valve (Victor model VTS-250D)
- pressure intensifier (Fuenkajorn and Daemen, 1986, pp. 257-260)
- water-tight plexi-glass pan (300 mm diameter and 200 mm height)
- Micronta stop watch (1/100 second accuracy)
- Omega digital thermometer (Model HH22)
- displacement dial gauge (Starrett; 25.4 cm displacement, 0.025 mm accuracy)

3. Test set-up

Figure 4.12 gives the laboratory arrangement for grouting and permeability testing. A hydraulic load cell, cutaway loading platens, rock sample and water-tight plastic pan are placed in a 1 MN capacity load frame. The rock sample is submerged in the water pan. A teflon gasket is placed between the lower platen and the rock sample. The hydraulic load cell is connected to a hydraulic hand pump via a pressure gauge and a shut-off valve. A vertical force (normal load on the sample) is applied to the sample by pumping hydraulic oil into the load cell. The shut-off valve is used to maintain the cell pressure constant during permeability testing. The loading platens transmit the force from the cell to the sample. The vertical load on the sample is



- | | |
|-------------------------------|-------------------------------------|
| 1) Load frame | 9) Nitrogen tank |
| 2) Hydraulic hand pump | 10) Grout pump |
| 3) Hydraulic lifting cylinder | 11) Pressure gauge with Gauge Saver |
| 4) Cut-away loading platens | 12) Falling head permeameter |
| 5) Quick connect platen | 13) Pressure intensifier |
| 6) Injection nozzle | 14) Displacement dial gauge |
| 7) Plastic pan | 15) Water injection pressure gauge |
| 8) Rock sample | |

Figure 4.12 Laboratory arrangement for flow testing and grouting.

calculated from the oil pressure. The lower loading platen is connected to a falling head permeameter or pressure intensifier for permeability testing. The temperature of the testing room is monitored and is expected to remain constant at $22 \pm 2^\circ\text{C}$. Distilled water is allowed to pass through the rock sample for 24 hours prior to testing. Prior to testing the rock sample is visually inspected to see whether the flow is radial from the cylinder hole, not leaking from connections, and uniformly damp on the sample's surface.

4. Flow Testing

This section describes the methods used to measure the permeability of a hollow rock cylinder with or without a fracture. Distilled deaired water is used as the testing fluid. The flow test is conducted after a constant vertical load is applied to the sample. The laboratory arrangement shown in Figure 4.12 allows both steady-state and falling head tests to be performed.

For steady-state flow testing, the lower loading platen is connected to the high-pressure (top) cylinder of a gas-over-water pressure intensifier. The low-pressure (bottom) cylinder is connected to a nitrogen gas tank via a regulating valve. The regulating valve is used to adjust the injection pressure. The water inflow rate is measured by monitoring the displacement of a push-rod attached to the piston inside the intensifier. The measurement is made by means of a displacement dial gauge. For each injection pressure and each normal load, steady-state flow testing is conducted as a function of time and is terminated after a constant flow rate can be established.

If the rock sample (with or without a fracture) has such high permeability that the water in the intensifier runs out before a steady-state flow rate can be established, a falling head test is conducted. For falling head testing the lower loading platen is connected to a high-precision pipette using a plastic (Tygon) tube.

Distilled deaired water is then filled into the pipette, tube and center hole of the sample. The inside diameter of the pipette can be varied from 1 to 20 mm, depending upon the permeability of the rock sample. The height of the water level is measured from the midsection of the rock cylinder (the approximate location of the fracture). The measurement is made to the nearest millimeter. A decrease of the water level in the pipette is measured as a function of time. The permeability of the intact rock or of the fracture is calculated from each reading. For each normal load, the test is terminated when the calculated permeabilities do not change with time. The flow test is repeated after the normal load is changed (increased or decreased). The permeability of the fracture after grouting is determined in accordance with the procedure given here.

4.3 Surface Characterization

1. Objective

The purpose of this procedure is to measure the roughness of a fracture surface perpendicular to the axis of a hollow rock cylinder. The method is applicable to a rock cylinder having 25.4 mm ID and a maximum of 150 mm OD.

2. Apparatus

- 1) guide plate (178 mm diameter)
- 2) displacement dial gauge (Starrett; 5.1 cm displacement, 0.025 mm accuracy, 0.0025 mm precision)
- 3) surface grinder (Rockwell Delta)
- 4) needle probe (1 mm diameter, 70 mm length)

The guide plate is made of a 3.18 mm thick plexiglass template. A 25.4 mm diameter and 176 mm long plexiglass rod is glued at the center of the plate (Figure 4.13a). Holes (1.47 mm diameter) are drilled into the plate in a square grid pattern. The template contains 100 holes per

square inch. The distance between the center of adjacent holes is 2.54 mm. The template has sufficient holes to cover a 152 mm diameter (circular) surface.

The needle probe is attached to the dial gauge probe with a straight alignment.

3. Measurement Method

- Place the guide plate on top of the rock surface to be measured, inserting the plexiglass rod into the center hole of the sample (Figure 4.13a). The distance between the plate and rock surface is approximately 4-6 cm. Be sure that the rod is tight (i.e. no rotation allowed) and that the plate is perpendicular to the hole axis.
- Mount the displacement dial gauge on a stationary point on top of the grinding table. The needle probe must be vertical (Figure 4.13b).
- Place the rock sample with the guide plate on the grinding table underneath the dial gauge.
- Stabilize the sample using a steel clamp. Be sure that there is no relative displacement between the rock sample and grinding table.

NOTE: There are three control wheels on the grinder; 2 wheels are used to slide the table in the horizontal (mutually perpendicular) directions; the third wheel is used to move the table up and down in the vertical direction.

- Adjust the grinding table (vertically) so that the needle probe can reach the highest and lowest points of the rock surface. After a desired elevation is obtained, lock the wheel and be sure that the elevation does not change until all measurements are complete.

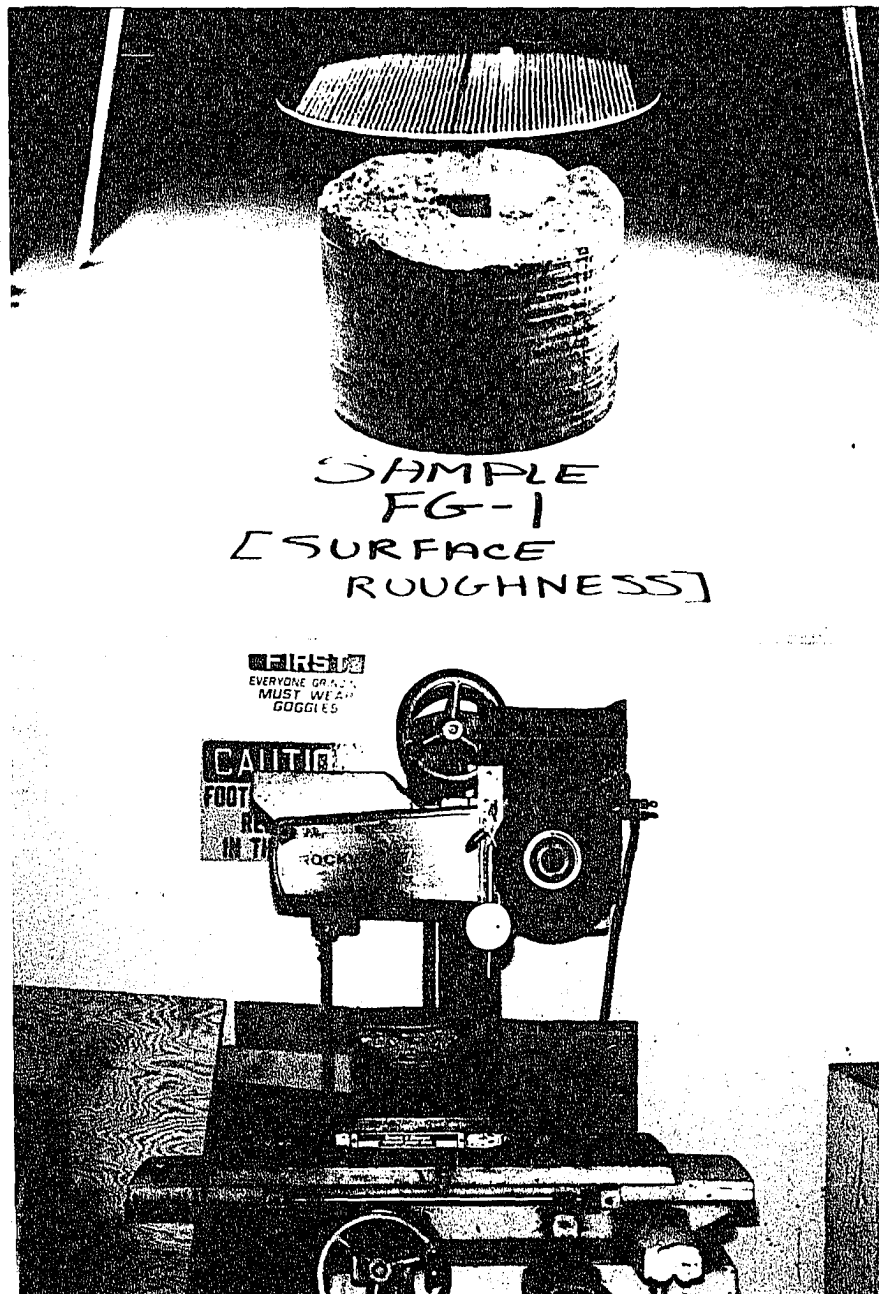


Figure 4.13a (top), b (bottom) Guide plate installed on fracture surface of 150 mm diameter cylinder of Apache Leap tuff. Plexiglass rod (25 mm diameter) glued at the center of the plate, and inserted into the center hole.

- Select a datum plane on the rock cylinder. The lowest point on the fracture surface may be selected as a datum plane. Set the dial gauge to read zero when the needle touches the datum plane.
- Use the horizontal control wheels to move the sample until the needle probe slips through the guide hole and touches the rock surface. Record the dial gauge reading to the nearest 0.0025 mm.
- Since the guide holes are drilled in a square grid pattern, the points of measurement can be made in a rectangular coordinate system (x and y axes with the origin at the center of the template). A measurement is made for every guide hole until the entire fracture area is covered.
- Make the measurements in a systematic row or column pattern in order to minimize the risk of skipping guide holes. Check the notebook records to assure that all measurements have been taken before unclamping the sample.
- If the maximum difference between the highest and the lowest points on the fracture surface is larger than 70 mm, a longer needle probe is required.
- After the measurement for the last guide hole is made, remeasure the first guide hole and compare the result with the reading previously made. The two results should be identical if no vertical movement of the table and no relative movement between the sample and the table occur during the measurement.

4.4 Grout Preparation

1. Introduction

The mixing of cementitious grouts for fracture sealing studied in this project is performed according to the API Specification No. 10 (American Petroleum Institute, 1986, pp. 14-19). The types of cement

used include Ideal Type I/II referred to as Self-Stress II and Micro Fine Cement referred to as MC-500. The type of bentonite used is C/S granular (provided by American Colloid Co. Arlington Heights, Ill.).

Self-Stress II cement (provided by Dowell Schlumberger, Tulsa, OK) is composed of Ideal Type I/II portland cement (from Tijeras Canyon, NM), mixed at the factory with 10% D53 (an expansive agent), 1% D65 (a dispersant), and prepared at a water-to-cement ratio ranging from 0.45 to 0.9. MC-500 is a cement which has an ultra fine grain diameter (Figure 4.14) with a mean grain size of 4 μ m and a maximum grain size of approximately 10 μ m. It is mixed with 1% NS-200 (Naphthalene Sulphonate) at a water to cement ratio of 1:1 by weight of cement. C/S granular bentonite from Upton, WY, is added to SSII cement in amounts ranging from 2 to 5%. All percentages are weight percent with respect to cement.

Parameters involved in grout preparation are: 1) mixing time and temperature, 2) grout viscosity, density, and bleed capacity, 3) time between grout mixing and pouring, 4) weight control of grout ingredients, and 5) curing conditions, i.e. water bath at room temperature, pressure and relative humidity, along with curing time.

2. Apparatus

- 1) plastic scoop, spatula
- 2) American Scientific balance (12 kg capacity, readable to 1g)
- 3) Oster commercial blender (Model 44006E); 2-speed; 2.3 liter volume
- 4) Fann 35A/SR 12 viscometer (part no. 30166)
- 5) plastic bags (0.25 and 2.0 liter capacity)
- 6) 1000 ml graduate cylinder
- 7) Omega digital thermometer (Model HH22)
- 8) VWR Dylatherm hot plate with container
- 9) funnel

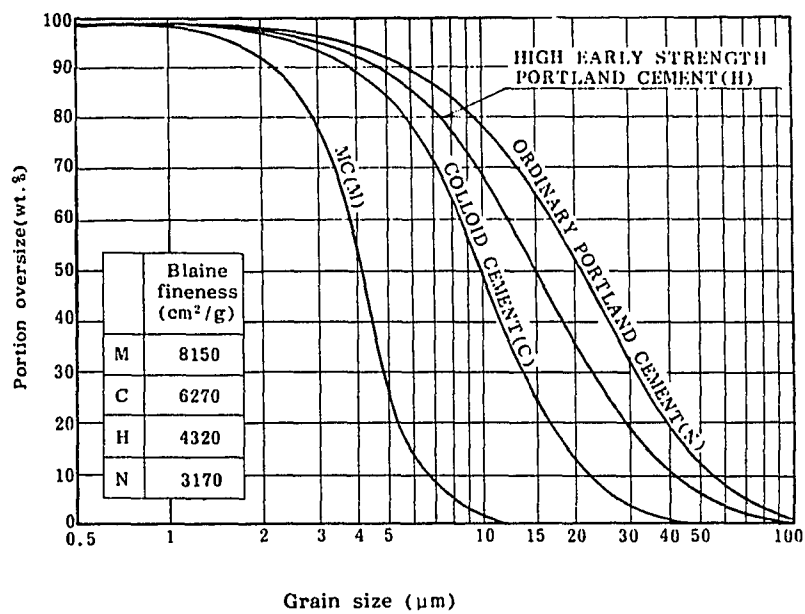


Figure 4.14 Grain size distribution of O.P.C, Colloid, and MC-500 cements. (From Shimoda and Ohmori, p.78)

- 10) plexiglass curing molds (150 mm long, 57.2 mm OD, 50.8 mm ID)
- 11) stirring rod (250 mm long, 6 mm diameter)
- 12) laboratory stirrer (Stir-pak Model R-4554-00)
- 13) Micronta stop watch (1/100 second accuracy)

3. Procedure for Preparing MC-500 and SSII Bentonite grouts

- 1) Prepare the grout slurry at ambient room temperature ($27 \pm 6^\circ\text{C}$ - API, 1986) and a relative room humidity not less than 50% (ASTM C305-82, Sect. 4). Make certain that the temperature of the distilled water prior to mixing is $27 \pm 3^\circ\text{C}$. Record the room temperature, relative humidity and atmospheric pressure. Raise the temperature of the mixing water if necessary.
- 2) Weigh out the cement, bentonite and 85% of the mix water and place in individual sealed plastic bags (2 liter capacity).

NOTE: 15% of the total mix water is added to the bentonite and allowed to prehydrate for two hours in a small (0.25 liter capacity) plastic bag prior to its mixing with other ingredients (Deere, 1982a, p. 296).

TABLE 4.1

Mix Number	Cement (g)	Bentonite (g)	Water (g)
1	772	15	463
2	772	23	540
3	772	38	695
4	772	0	348
5	666	13	885
MC-500*	746	0	746

* 1 $\frac{1}{2}$ NS-200.

- 3) After two hours have elapsed since the addition of water to the bentonite, pour the remaining mix water (85% of the total) into blender. Add bentonite. Be sure to scrape all bentonite remaining on the sides of the plastic bag into the mix. Mix 15 seconds.¹ Scrape down bentonite from sides of blender. At low speed add cement to blender in not more than 15 seconds. After all the cement has been added, mix at high speed for an additional 35 seconds.² Note: MC-500 grouts contain no bentonite component so omit procedures involving preparing bentonite. Pour mixed cement grout into curing mold, viscometer cup, or graduated cylinder. A funnel is used to direct the slurry into its respective container thus avoiding violent turbulence and possible sedimentation, layering, and/or trapped air bubbles. The curing mold is filled with slurry up to a point 13 cm above the base of the mold. The viscometer cup is filled up to the line inscribed on the cup (approximately 350 ml). The graduated cylinder is filled with 1000 ml of slurry. When pouring, submerge the bottom end of the funnel in the slurry and gradually raise the funnel as the cement slurry level increases. Record pouring time. Immediately after pouring slurry into curing mold the specimen is puddled 25 times with a stirring rod. After 20 minutes of curing in molds, pour distilled water on top of the sample to prevent cement drying. Note: For MC-500 grouts add water one hour after pouring in curing molds.

1 Personal communication with Lorra Craver, American Colloid, regarding thorough mixing of bentonite.

2 ASTM C305-82 (Section 4) differs from API Specification No. 10, 1986 (with respect to mixing cement) in the following regards: 1) Pour the distilled water into the mixing container, 2) add the cement to the water and allow 30 seconds for the adsorption of water, 3) start the mixer and mix at slow speed (140 ± 5 rpm) for 30 seconds, 4) stop the mixer for 15 seconds, and during this time scrape down into the batch any paste that may have collected on the sides of the bowl, and 5) start the mixer at medium speed (280 ± 10 rpm) and mix for 1 minute.

4.5 Grout Characterization

1. Objective

The objective of this test procedure is to characterize grouts in terms of their uniaxial compressive strength, Fann viscosity/cohesion, Marsh flow time, density, and bleed capacity.

2. Uniaxial compressive strength testing

2.1 Apparatus

- 1) Hammer
- 2) Flat head screwdriver
- 3) Kent automatic surface grinding machine
- 4) 2 and 5 inch (5.1 and 12.7 mm) micrometers
- 5) Displacement dial gauge (Starrett; 0.0025 mm precision)
- 6) Mettler balance (Model P1200-1/100 g accuracy)
- 7) Versa Tester compression machine

2.2 Sample preparation testing

Each grout specimens is cured for 7, 8 or 28 day testing. Each specimen is freed from its mold by gently cracking the mold longitudinally using a hammer and screwdriver as a chisel. Care is taken not to chip the specimen during this procedure. Each specimen is kept in contact with water accept when being freed from its mold, measuring dimensions, weighing, or during compression testing.

The ends of each specimen is ground flat and parallel using a surface grinder.

Measurement of specimen dimensions include diameter, height, side smoothness, and end perpendicularity (ASTM D2938-79, Section 4).

Just prior to compression testing the specimen is removed from its water bath, patted dry with a paper towel, and weighed to the nearest 1/100 gram.

Each specimen in turn is placed in the Versa Tester compression machine and loaded to failure at a loading rate of approximately 460 kPa/s (API Spec. No. 10, 1986, p. 18). The failure load of each specimen is recorded as well as a post-failure sketch drawn.

3. Determination of viscosity and cohesion (Fann viscometer)

3.1 Apparatus

- 1) Fann 35A/SR12 viscometer (Part No. 30166)
- 2) Stir-Pak laboratory stirrer (Model 4554)
- 3) Omega digital thermometer (Model HH22)
- 4) Micronta stop watch (1/100 second accuracy)

3.2. Test procedure

The slurry previously poured into the viscometer cup (Section 4.4.3) is stirred with the laboratory stirrer at speed 1.4 (approximately 300 rpm) for 20 minutes. Measure and record the temperature (T_1) in the cup.³ Record dial readings at the following speeds in descending order:

TABLE 4.2

Speed (rpm)	Time Interval (sec)
300	60
200	20
100	20
6	20
3	20

³ Procedure deviates from API, 1986, due to lack of an atmospheric consistometer.

Measure the temperature (T_2) in the cup after the final viscosity reading. Report the slurry's rheological properties at the average of the temperatures T_1 and T_2 . Figure 4.15 shows a Fann viscometer. Newtonian viscosities are read directly from the viscometer at a rotor speed of 300 rpm. Plastic viscosities are obtained by subtracting the 100 rpm reading from the 300 rpm reading, then multiplying by a factor of 1.5. The yield point or cohesion value are obtained by subtracting the plastic viscosity from the 300 rpm reading⁴.

4. Marsh viscosity or flow time

4.1 Apparatus

- 1) Marsh flow cone (Figure 4.16)
- 2) Marsh cup
- 3) Micronta stop watch (1/100 second accuracy)

4.2 Test procedure

Slurry preparation is performed in accordance with section 4.4.3 with, the following mix proportions (Table 4.3) to produce the 1.5 liters of slurry needed for this test:

TABLE 4.3

Mix#	Cement (g)	Water (g)	Bentonite (g)	W/C**
1	1666	1000	33	0.6
2	1544	1080	46	0.7
3	1544	1390	76	0.9
4	1000	450	0	0.45
5	666	885	2	1.33
MC-500*	1492	1492	0	1.0

⁴ Personal communication from Pat Gill of Dowell-Schlumberger, Inc.

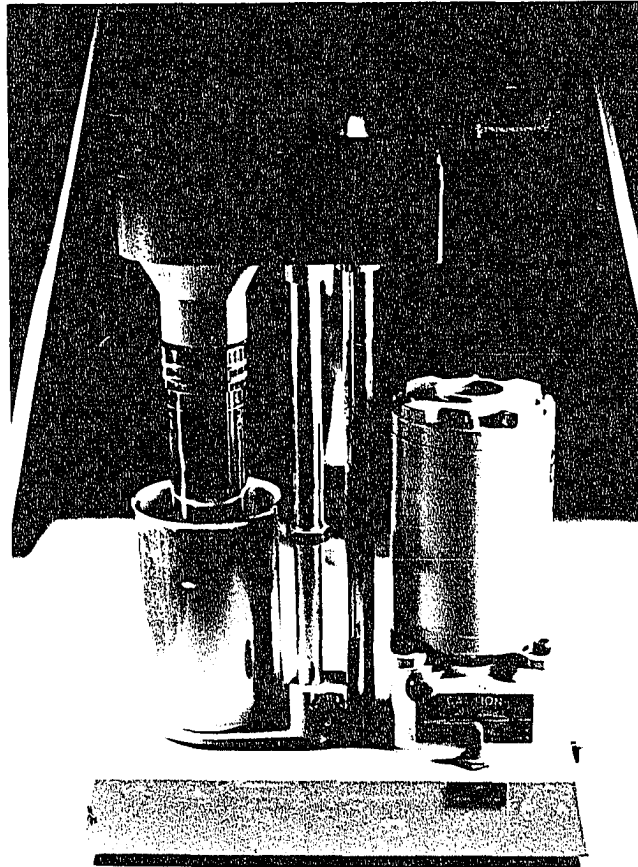


Figure 4.15 Fann viscometer used to measure viscosity and yield point.

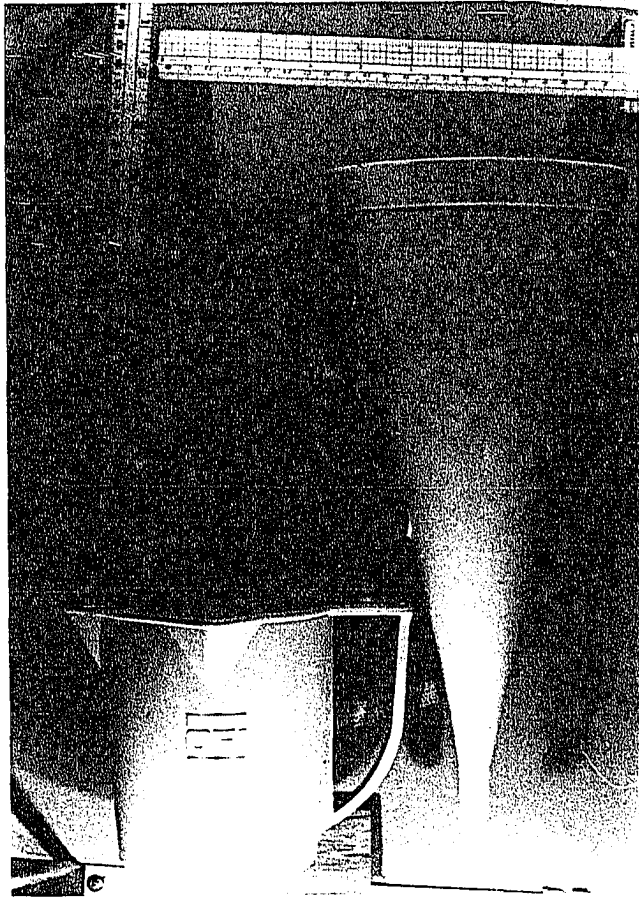


Figure 4.16 Marsh funnel and cup used to measure apparent viscosity.

- * MC-500 Microfine cement with 1% NS-200
- ** Water to cement ratio with respect to weight of cement

NOTE: Mixes 1 through 5 contain self-stress II cement.

The prepared slurry is poured into the funnel until it just touches the screen, a volume of 1.5 liters. Recorded the time for 0.946 liters of slurry to pass through the funnel into the measuring cup. Record this time. The flow time to the nearest second is the Marsh funnel viscosity.

5. Determination of Slurry Density

5.1 Apparatus

- 1) Ertco hydrometer (S.G. = 1.00-2.00)
- 2) 1000 ml graduated cylinder

5.2 Test procedure

Grout preparation is performed in accordance to section 4.4.3. Gently pour approximately 600 ml of slurry into a 1000 ml graduated cylinder. Gently lower the hydrometer into the slurry until it floats freely. Record the density. Perform this measurement as quickly as possible to avoid any possible thixotropic behavior.

6. Determination of Bleed Capacity

Grout preparation is performed in accordance to section 4.4.3. Pour 1000 ml of slurry into a 1000 ml graduated cylinder. Measure the volume of the slurry in the cylinder. Measure the free water above the slurry two hours after pouring. This is the bleed water. The volume of bleed water divided by the initial slurry volume is the bleed capacity (Shannon and Wilson, Inc., 1987, pp. 14-15).

4.6 Fracture Grouting

1. Objective

The objective of this test procedure is to inject grout into a fracture that is oriented perpendicular to the rock cylinder's axis.

2. Apparatus

- 1) Uniaxial loading system as described in the permeability testing procedure (Section 4.2.1)
- 2) Grout pump with vented piston (Schaffer and Daemen, 1987, p. 58)
- 3) Buffered pressure gauge (Ashcroft; 4 MPa range, 10 KPa accuracy)
- 4) High pressure tubing with pressure release valve
- 5) High pressure Victor regulator (L-TEC TYPE-89)
- 6) Micronta stop watch (1/100 second accuracy)

3. Test Procedure

Fracture grouting is performed using a single piston grout pump. This pump is capable of delivering 280 ml of slurry at a maximum pressure of 13 MPa (Figure 4.17).

After a constant normal load is applied to the fracture a high-pressure grout tube, equipped with a quick-fit adaptor, is attached to the lower loading platen. The other end of the high-pressure tubing is attached to the grout pump and pressure release valve. Teed into the high-pressure tubing at this point is a water buffered gauge used to monitor the grout injection pressure.

Prior to grouting, the top plate on the grout pump is removed. Grout slurry previously prepared is filled into the pump. The pump's piston, with its bleed vent open is forced down into the pump until grout free of air bubbles can be seen exiting the vent. The vent is now closed. The pump's top plate is bolted securely to the pumps housing. This is done as quickly as possible.

Nitrogen gas is used to drive the piston and pressurize the grout slurry into the rock sample. A regulating valve is used to control the grouting pressure. The grouting pressure is maintained constant during grouting and it should not exceed the normal stress applied to the fracture. The pressure is measured to the nearest 10 kPa. The test is

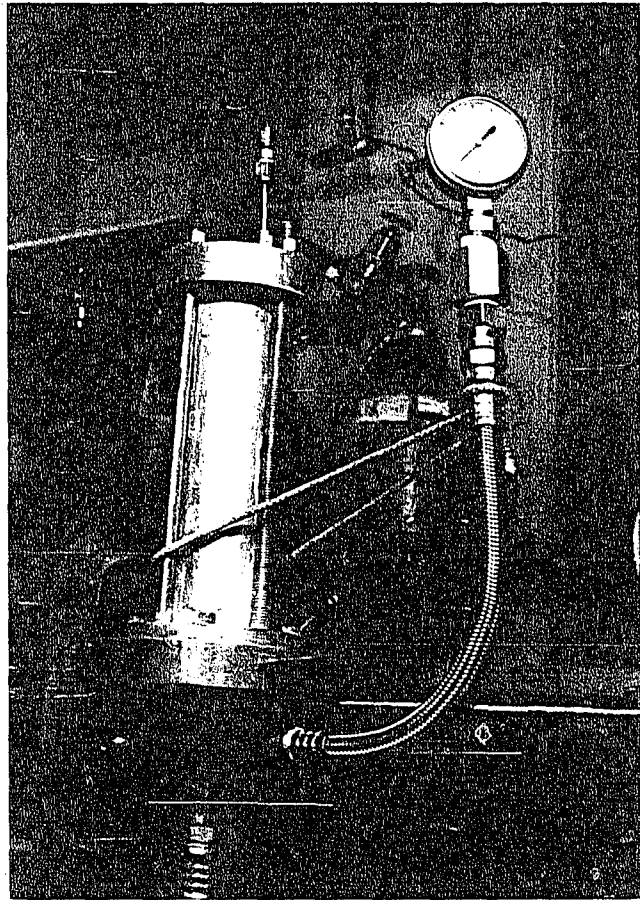


Figure 4.17 Simple single piston grout pump with gauge saver.

terminated after the grout slurry flows out of the fracture or when displacement of the piston is not detectable for 5 to 10 minutes. Immediately after grouting, the grout tube is removed from the lower loading platen. The bore hole is flushed with distilled water to remove excess grout slurry. Distilled water is then used to fill the hole during curing of the grout. Grouting, and curing times are recorded. The permeability of the fracture after grouting is determined in accordance with the procedure given in Section 4.2.1.

4.7 Fracture Compression Behavior

1. Introduction

The aperture or width of a fracture is an important parameter when dealing with the ability of a grout to enter a fracture and travel along its surfaces. To measure the actual aperture directly is difficult due to the limited access available and the unknown geometry of the fracture surfaces.

One important aspect of the compression behavior of a fracture that can be measured easily is its stiffness or opening and closing behavior under normal stress. This procedure does not give an actual value of the fracture aperture at any point but does provide information as to how the fracture width changes as a function of the axial stress applied to the sample.

This procedure assumes that the fracture compresses uniformly over its surface area. Figure 4.18 shows the monitoring system.

2. Apparatus

- 1) clamping rings (O.D. = 21.0 mm, I.D. = 16.0)
- 2) displacement dial gauge (Scherr-Tumico; 0.00254 mm precision)
- 3) caliper (0.0254 mm precision)
- 4) load frame (Cobb and Daemen, 1982, pp. 35-36)
- 5) loading platens (Schaffer and Daemen, 1987, p. 59)

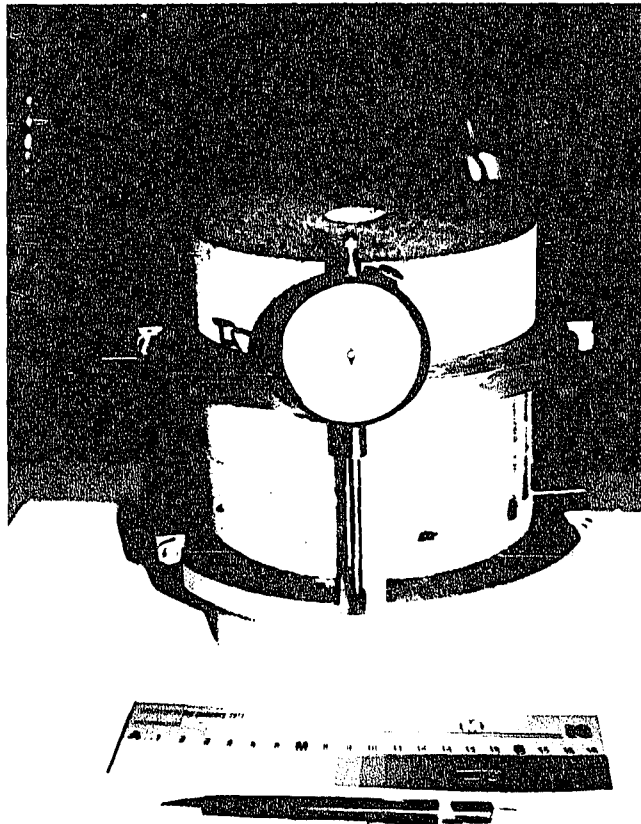


Figure 4.18 Fracture compression monitoring system.

- 6) hydraulic load cell (Enerpac JSL-1002)
- 7) hydraulic pump (Enerpac EH-80) with 41.4 MPa Acco Helicoid gauge
- 8) Micronta stop watch (1/100 second accuracy)

NOTE: The loading system is identical to the one described in the measurement of permeability procedure. (Section 4.4.2).

3. Measurement method

- Mount the dial gauge vertically on the upper clamping ring.
- Fix the top clamping ring with dial gauge attached to the top half of the tuff specimen. Bolt the ring approximately 38 mm above the fracture. Use a bubble level to ensure that the ring is secured horizontally with respect to the top and bottom of the sample.
- Fix the lower clamping ring on the bottom half of the sample and bolt approximately 38 mm below the fracture. As before, use a bubble level to ensure that the ring is secured horizontally.
- Use a caliper to measure the vertical distance between the dial gauge mounting point and the end of its probe. Record this distance.
- Place the sample with both rings attached in the loading frame with loading platens and hydraulic load cell resting on the sample. The weight of the platens and load cell correspond to a normal stress of 0.05 MPa.
- At zero gauge pressure zero out the dial gauge.
- Take readings in the following sequence of normal stresses:
0.05, 1, 2, 3, 4, 5, 6, 7, 8, 9, 10, 9, 8, 7, 6, 5, 4, 3, 2, 1,
0.05, 1, 2, 3, 4, 5, 6, 7, 8, 9, 10 MPa. Use a stop watch to time the reading interval between each stress level. Readings

are taken thirty seconds after the desired normal stress is reached to allow some immediate time dependent compression to take place.

- Run three sequential tests for each loading cycle described above. The dial gauge is zeroed prior to each test to account for surface deformation.
- The actual fracture compression is obtained by subtracting the calculated intact rock compression $\frac{\sigma_N E}{L}$ from the measured dial gauge reading.

NOTE: If the angle between the fracture surface and horizontal axis deviate appreciatively, then the stress across the fracture surface may be calculated by $\sigma_y = \sigma_N \sin^2 \theta$ (Jaeger and Cook, 1979, Pg 141).

CHAPTER 5
EXPERIMENTAL RESULTS

5.1 Permeability of Intact Tuff

Prior to determining the permeability of a fracture within the rock sample, the permeability of the intact rock itself is measured. Eight samples representing three types of densely welded tuff are tested for their intact or matrix permeability. Figure 5.1 shows three types of tuff, A-Mountain (far right), Topopah Spring (second from right), and Apache Leap (four samples on the left). The curves of Figure 5.2 compare the hydraulic conductivities of the three types of tuff as a function of the applied normal stress. The maximum load on each sample is less than 35 percent of its uniaxial compressive strength. See Fuenkajorn and Daemen (1990) for comparison of mechanical properties.

One would expect that the greater the density and degree of welding, indicating a smaller void ratio, the greater the resistance to flow. This was supported by testing and is evident in Figure 5.2, which shows sample T-1-6-FG9 (A-Mountain tuff) with the greatest permeability and sample AP3-1-6-FG6 (Apache Leap tuff) with the lowest permeability. All three samples show the same magnitude of permeability (approximately 10^{-7} cm/s). Previous work on Apache Leap Tuff and on A-Mountain Tuff shows similar intact rock permeabilities (Fuenkajorn and Daemen, 1990).

Figure 5.3 shows the effect of normal stress on the permeability of intact Apache Leap tuff. Permeability decreases as normal stress is increased. This is presumably due to the closing of microfractures, or due to a change in the geometry of the pore spaces. Permeabilities range from 10^{-7} to 10^{-9} cm/s at 0.05 MPa normal stress and 10^{-8} to 10^{-9} cm/s at 10 MPa normal stress. Sample AP7-1-6-FG4 (Figure 5.4) developed a fracture at 5 MPa normal stress, which accounts for the large increase

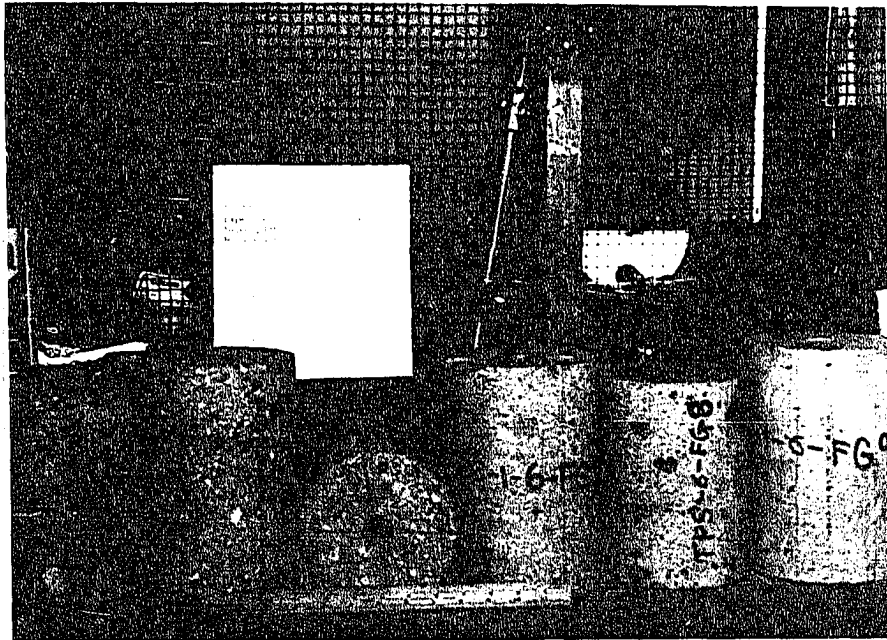


Figure 5.1 Three types of welded tuff. A-Mountain (far right), Topopah Spring (second from right), and Apache Leap (four samples on left).

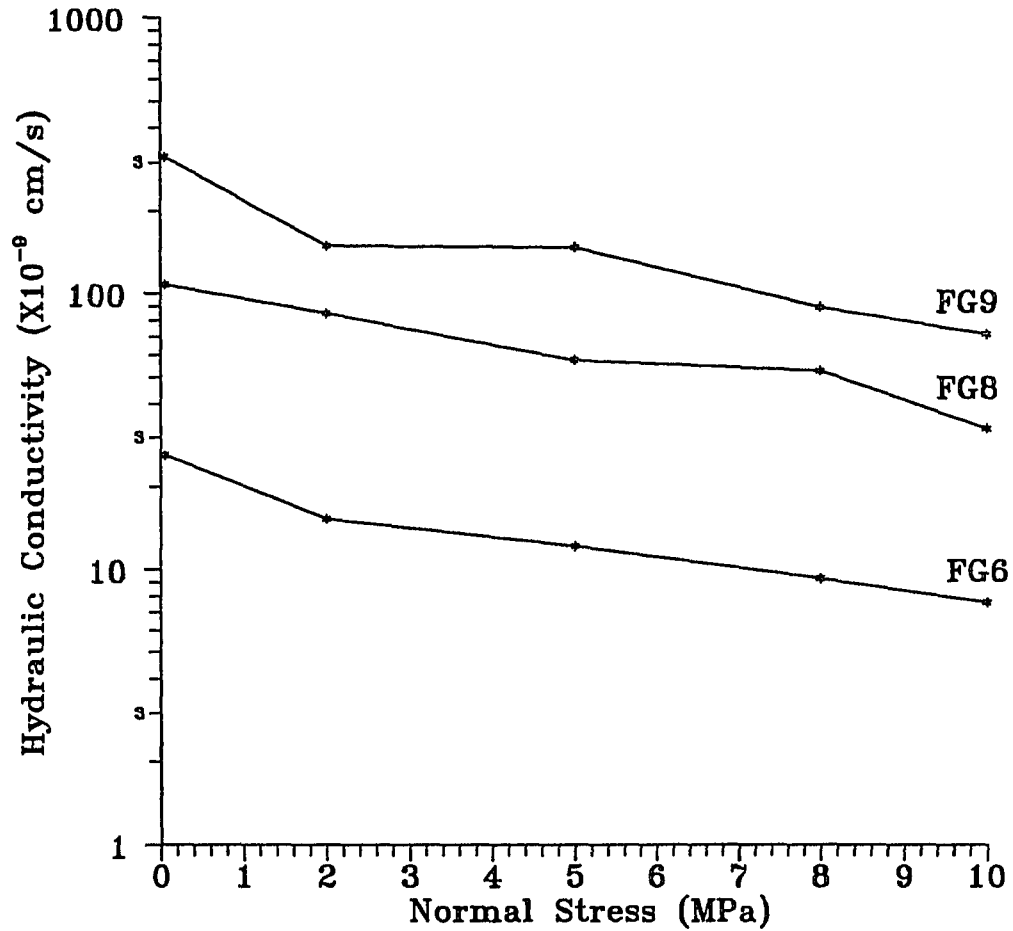


Figure 5.2 Hydraulic conductivity of intact Apache Leap tuff (FG6), Topopah Spring tuff (FG8), and A-Mountain tuff (FG9) cylinders as a function of normal stress. Each data point represents the average of all test runs for each normal stress.

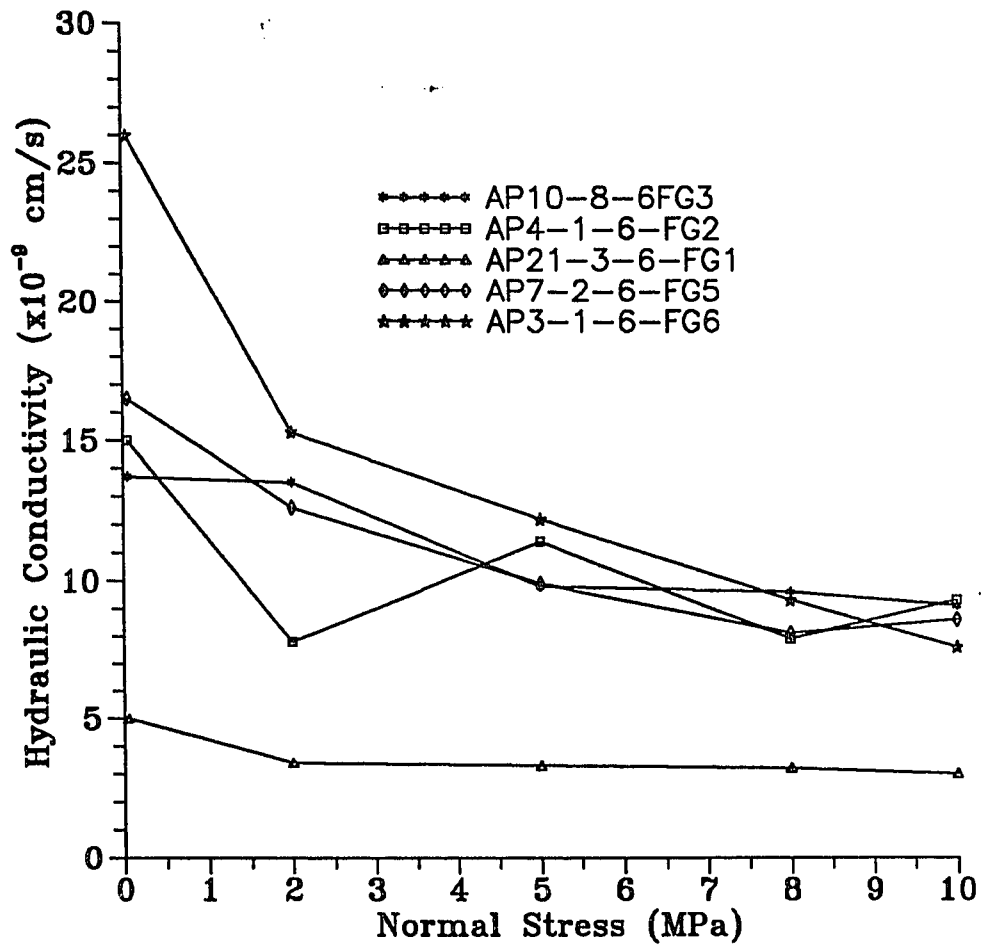


Figure 5.3 Effect of normal stress on hydraulic conductivity of intact Apache Leap tuff.

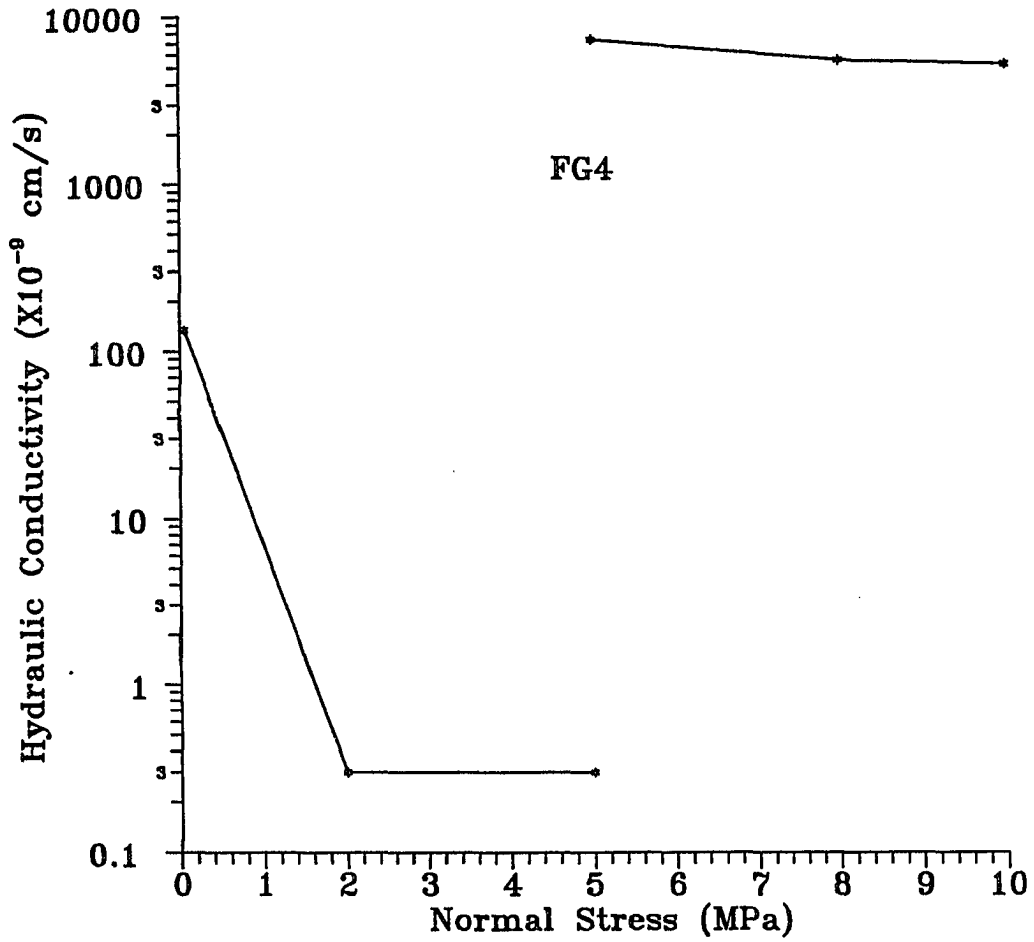


Figure 5.4 Effect of normal stress on the permeability of intact sample AP7-1-6-FG4. The break in the graph at 5 MPa normal stress is a result of the development of a vertical crack.

in flow at that point. On all samples the greatest reduction in flow occurs at low normal stress. Tables 5.1 through 5.8 contain test data. Test data is averaged at each normal stress.

5.2 Fracture Permeability

The permeability of a fracture is calculated by assuming that the intact rock permeability is low and negligible, the horizontal fracture plane is a smooth parallel plate, and that the radial flow normal to the borehole is laminar. The relation between flow and the pressure gradient will be governed by the "cubic law" using the theory of incompressible viscous flow (Snow, 65; Wilson & Witherspoon, 1970). Equations for the equivalent fracture aperture and fracture permeability are given in Section 2.4. Section 2.2 discusses the validity and restrictions using these flow laws.

At low normal stresses (<2 MPa) the relationship between permeability and stress is a non-linear one. This non-linearity manifests itself such that a small change in stress produces a corresponding large change in the slope of the curve. This effect will later be seen to be less pronounced at intermediate normal stresses ($2 < \sigma_N < 5$ MPa) and in some cases at high normal stress (> 5 MPa) to assume almost linear behavior.

The hydromechanical properties of a the fractures were found to be coupled and directly affected by the geometry of the void space between the two surfaces. The effect of joint compression was to change the area available for flow, thereby changing the permeability. The resistance to flow was caused by the viscous drag of the fluid through the resulting narrow openings.

This simplified model of the relationship between permeability and stress is used in an attempt to describe the overall flow behavior of several samples. This behavior can be affected by several factors such as the initial seating or orientation of the fracture surfaces, the

Table 5.1 Results of Falling Head Test on Intact Sample AP21-3-6-FG1.

Number of Readings	σ_N (MPa)	K ($\times 10^{-9} \text{cm/s}$)	h_o (cm)	h_f (cm)	SD ($k \times 10^{-12}$)
3	0.05	5.0	126.7	119.7	0.6
3	2	3.4	121.2	111.2	0.2
2	5	3.3	121.2	116.4	0.1
3	8	3.2	126.0	120.8	0.1
2	10	3.0	126.0	122.6	0

Table 5.2 Results of Falling Head Test on Intact Sample AP4-1-6-FG2.

Number of Readings	σ_N (MPa)	K ($\times 10^{-9} \text{cm/s}$)	h_o (cm)	h_f (cm)	SD ($k \times 10^{-9}$)
3	0.05	15	126.0	108.6	0
3	2	7.8	126.0	116.6	1.6
3	5	11.4	126.0	117.1	2.6
2	8	7.9	126.0	119.0	0.3
2	10	9.3	126.0	120.6	0.1

Table 5.3 Results of Falling Head Test on Intact Sample AP10-8-6-FG3.

Number of Readings	σ_N (MPa)	K ($\times 10^{-9} \text{cm/s}$)	h_o (cm)	h_f (cm)	SD ($k \times 10^{-9}$)
2	0.05	13.7	126.0	111.5	1.7
2	2	13.5	126.0	116.8	4.7
3	5	9.8	126.0	110.1	0.2
2	8	9.6	126.0	118.5	0.1
3	10	9.1	126.0	116.8	0.2

σ_N = normal stress.

K = intact hydraulic conductivity.

h_o = initial height of water in pipette measured from the midsection of the sample.

h_f = final height of water in pipette.

SD = standard deviation about the mean.

Table 5.4 Results of flow testing intact sample AP7-1-6-FG4.

Number of Readings	σ_N (MPa)	K ($\times 10^{-9} \text{cm/s}$)	P_i (MPa)	Δh (cm)	SD ($k \times 10^{-9}$)
3	0.05	134.3	0.15	1496	56.1
3	2	0.3	1.0	9993	0.06
3	5	0.3	2.0	20033	0.1
SAMPLE FRACTURES ALONG A PREEXISTING DISCONTINUITIY					
1	5	7500	2.0	19993	0
1	8	5700	2.0	19991	0
1	10	5400	2.0	19990	0

σ_N = normal stress.

K = intact hydraulic conductivity (mean).

e = equivalent fracture aperture (mean).

P_i = injection pressure.

Δh = water head difference used in falling head permeameter test.
($P_i/\gamma_w - h_o$)

SD(k_j) = standard deviation about the mean.

Table 5.5 Results of Falling Head Test on Intact Sample AP7-2-6-FG5.

Number of Readings	σ_N (MPa)	K ($\times 10^{-9} \text{cm/s}$)	h_o (cm)	h_f (cm)	SD ($k \times 10^{-9}$)
2	0.05	16.5	126.0	112.0	0.6
3	2	12.6	126.0	109.0	0.2
2	5	9.9	126.0	119.6	0.6
2	8	8.1	126.0	115.5	0.1
2	10	8.6	126.0	120.5	0.4

σ_N = normal stress.

K = intact hydraulic conductivity.

h_o = initial height of water in pipette measured from the midsection of the sample.

h_f = final height of water in pipette.

SD = standard deviation about the mean.

Table 5.6 Results of Falling Head Test on Intact Sample AP3-1-6-FG6.

Number of Readings	σ_N (MPa)	K ($\times 10^{-9} \text{cm/s}$)	h_o (cm)	h_f (cm)	SD ($k \times 10^{-9}$)
7	0.05	26.0	126.0	117.8	0.8
7	2	15.3	126.0	103.5	0.5
6	5	12.2	126.0	118.3	0.4
9	8	9.3	126.0	117.3	0.9
9	10	7.6	126.0	117.6	0.5

Table 5.7 Results of Falling Head Test on Intact Sample TPS-6-FG8.

Number of Readings	σ_N (MPa)	K ($\times 10^{-9} \text{cm/s}$)	h_o (cm)	h_f (cm)	SD ($k \times 10^{-9}$)
3	0.05	107.7	126.0	110.8	6.1
3	2	85.3	126.0	116.8	14.1
3	5	58.0	126.0	113.2	1.7
2	8	53.0	126.0	116.6	1.4
3	10	32.7	126.0	111.1	3.1

Table 5.8 Results of Falling Head Test on Intact Sample T-1-6-FG9.

Number of Readings	σ_N (MPa)	K ($\times 10^{-9} \text{cm/s}$)	h_o (cm)	h_f (cm)	SD ($k \times 10^{-9}$)
14	0.05	314.3	126.0	102.0	49.3
17	2	150.0	126.0	107.7	10.0
7	5	148.6	126.0	106.0	3.8
4	8	90.0	126.0	105.5	18.3
6	10	71.7	126.0	107.3	4.1

σ_N = normal stress.

K = intact hydraulic conductivity.

h_o = initial height of water in pipette measured from the midsection of the sample.

h_f = final height of water in pipette.

SD = standard deviation about the mean.

presence and resulting opening or closing of microfractures contained in the sample, the formation of new fractures resulting in new flow conduits, and/or the deformation of surface asperities making initial surface contact and therefore carry a higher percentage of the surface load.

The initial seating of the fracture surfaces or their preliminary orientation with their once perfectly mated asperities, control the equivalent fracture aperture and thereby dictates the permeability at low normal stress. Any surface misalignment, even a minuscule one, leads to the large change in the slope of the curve at low normal stress. This was found to occur in all samples tested. This change continues until the frictional components acting along the surfaces of the asperities come to equilibrium and the fracture surfaces are once again in very close proximity to their original locations. At this point fracture deformation presumably became generally uniform over of the fracture surface accounting for the more continuous slope of the permeability versus stress curves.

Determination of the aperture geometry and flow channels constitutes a limiting factor in evaluating the actual velocities in a fractures.

The fracture surface's contact area was of great importance affecting the fracture apertures and resulting area available for flow. Under compression the cross-sectional area decreased, and resistance to flow increased. As the fracture surfaces came in contact and the surface asperities began to mesh the flow was effectively halted at these points. Any resulting flow was presumably forced to find alternative pathways resulting in discrete fingers of flow. The assumption of radial flow may not be valid when these preferential flow paths are created (Tsang, 1981). If the fractures were to remain open the velocity profile would most likely take the form of a two

dimensional parabolic surface with a viscous sublayer effect at the surface boundaries (Shames, 1982). With the tight fractures studied here fluid travel probably resembled flow through a porous medium (Detournay, 1980).

The geometry of the effective flow area dictates the paths or channels available for fluid movement. The surface roughness along these paths induce numerous changes in flow direction. These changes account for the increase in travel distance required for the fluids tortuous path and the associated pressure drop away from the borehole.

In this laboratory study the flow through three types of fracture surfaces (smooth, rough, and natural) has been measured as a function of the normal stress across the fracture. Photographs of actual surfaces can be viewed in Section 4.2.

Figures 5.5 through 5.26 show the effect of normal stress on fracture permeability and equivalent fracture aperture for each type of fracture. Each sample is first loaded then unloaded and finally reloaded without interrupting the flow. Arrows on the curve show the loading path. Each data point represents the average of all readings at each normal stress. Tables 5.9 through 5.19 contain test data.

The greatest reduction in flow occurs at low normal stress on the first loading cycle, presumably due to initial surface mating and the closing of microfractures, or due to a change in the geometry of the pore spaces. Also evident is an irreversible decrease in permeability after the first loading/unloading cycle. Some hysteresis occurs due to the permanent deformation of asperities and the resulting better mated fracture surfaces.

As the fracture surfaces come closer together and surface asperities deform the fracture aperture decreases. The aperture never regains its former width on subsequent loading/unloading cycles. These

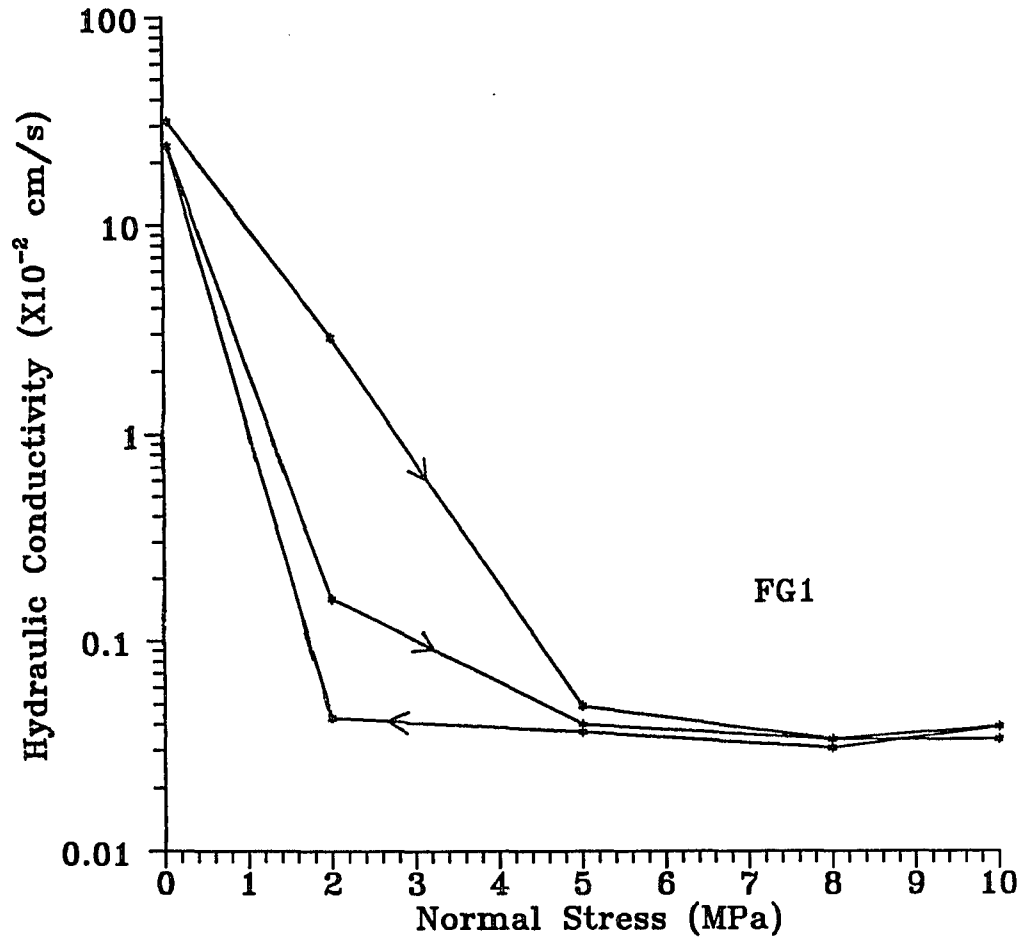


Figure 5.5 Hydraulic conductivity as a function of normal stress for sample AP21-3-6-FG1 (Tension induced fracture). Arrows indicate the loading sequence.

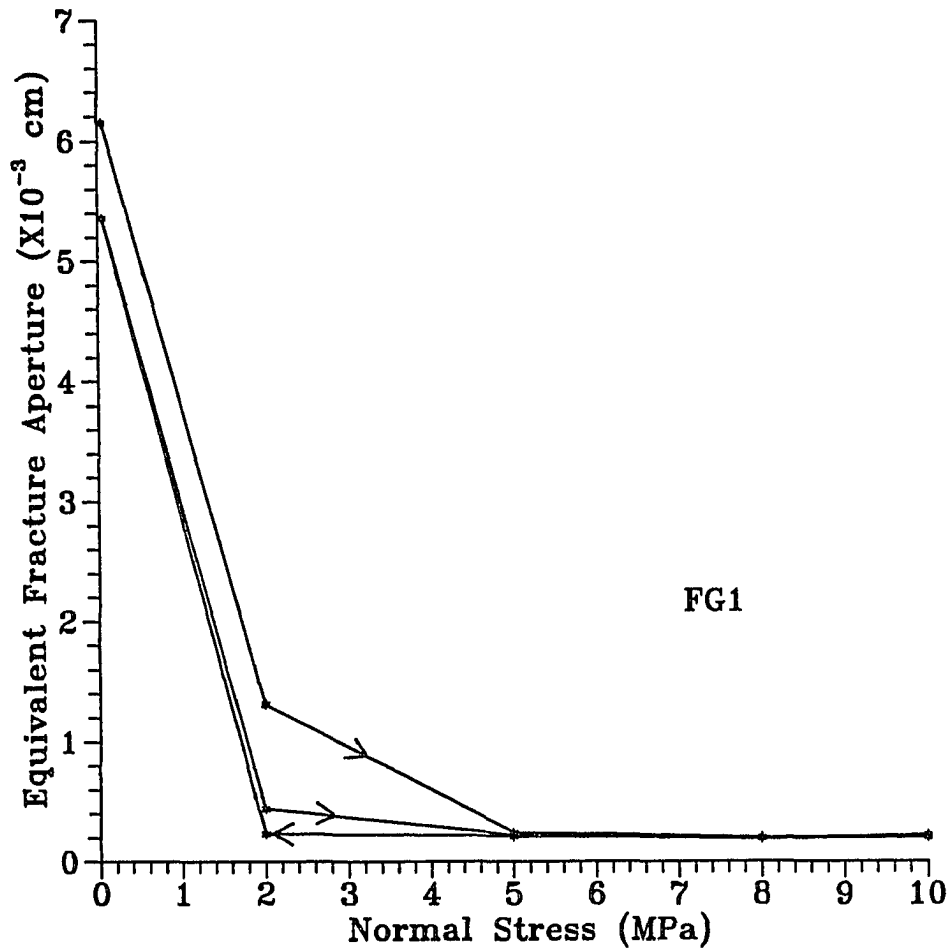


Figure 5.6 Equivalent fracture aperture as a function of normal stress for sample AP21-3-6-FG1 (Tension induced fracture). Arrows indicate the loading sequence.

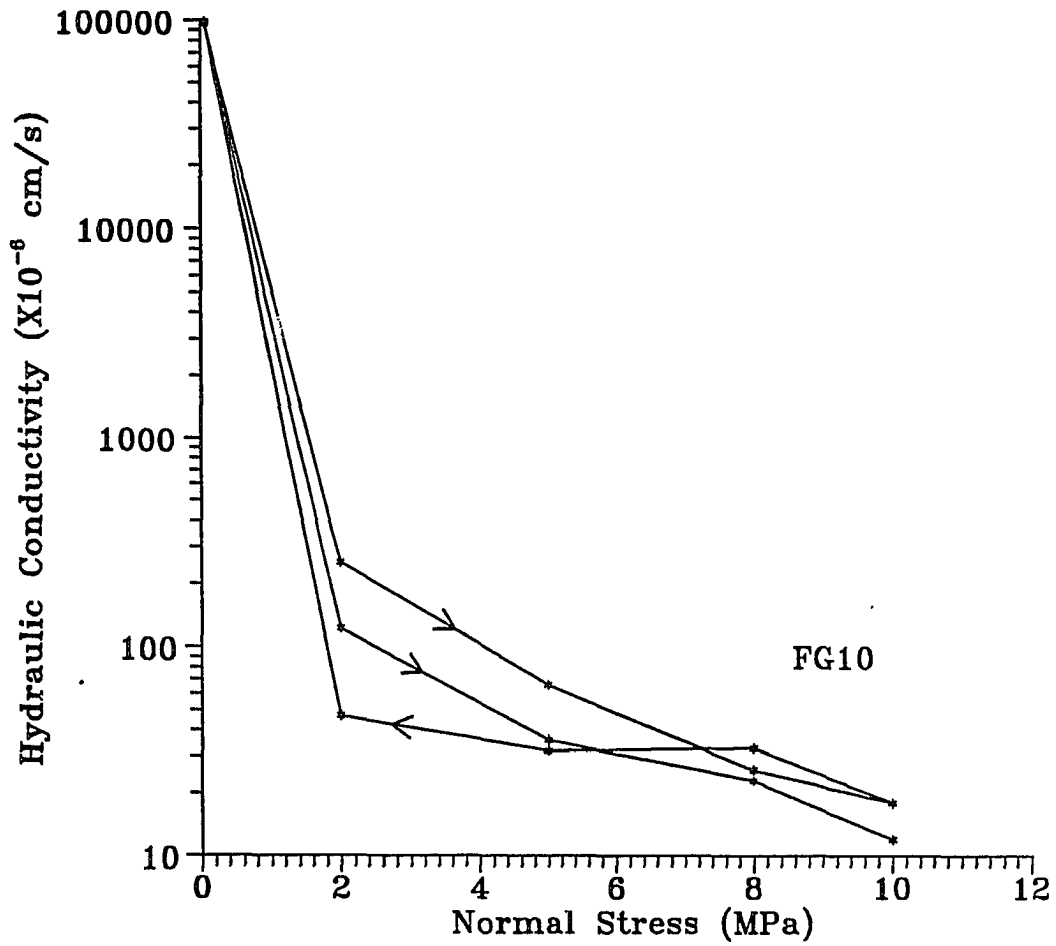


Figure 5.7 Hydraulic conductivity as a function of normal stress for sample AP30-2-6-FG10 (Tension induced fracture). Arrows indicate the loading sequence.

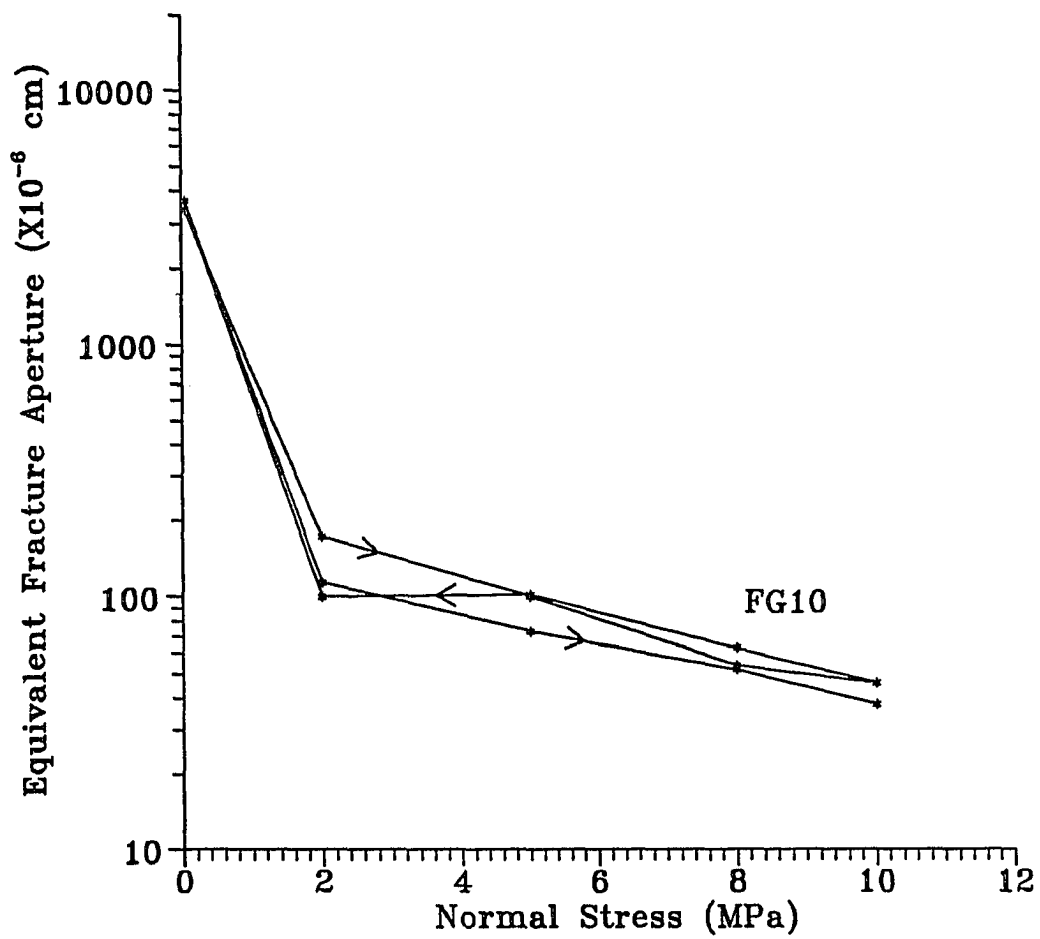


Figure 5.8 Equivalent fracture aperture as a function of normal stress for sample AP30-2-6-FG10 (Tension induced fracture). Arrows indicate the loading sequence.

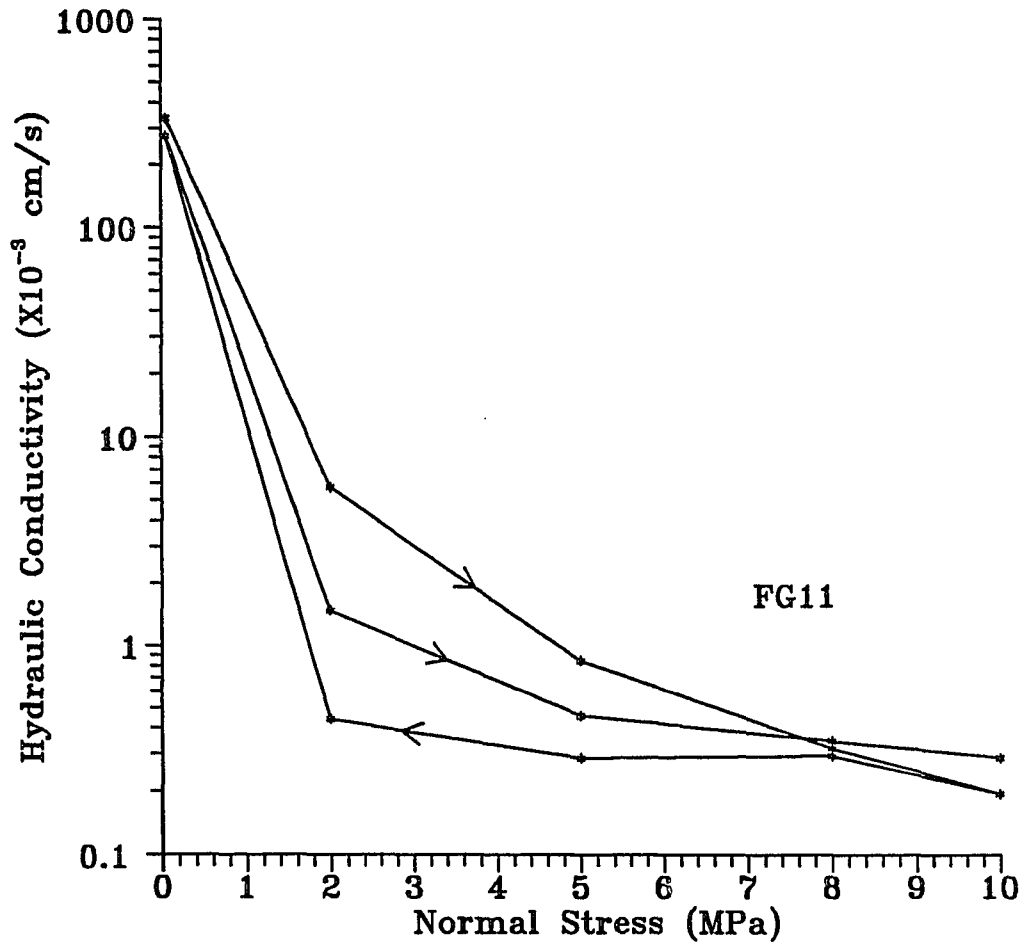


Figure 5.9 Hydraulic conductivity as a function of normal stress for sample AP30-1-6-FG11 (Tension induced fracture). Arrows indicate the loading sequence.

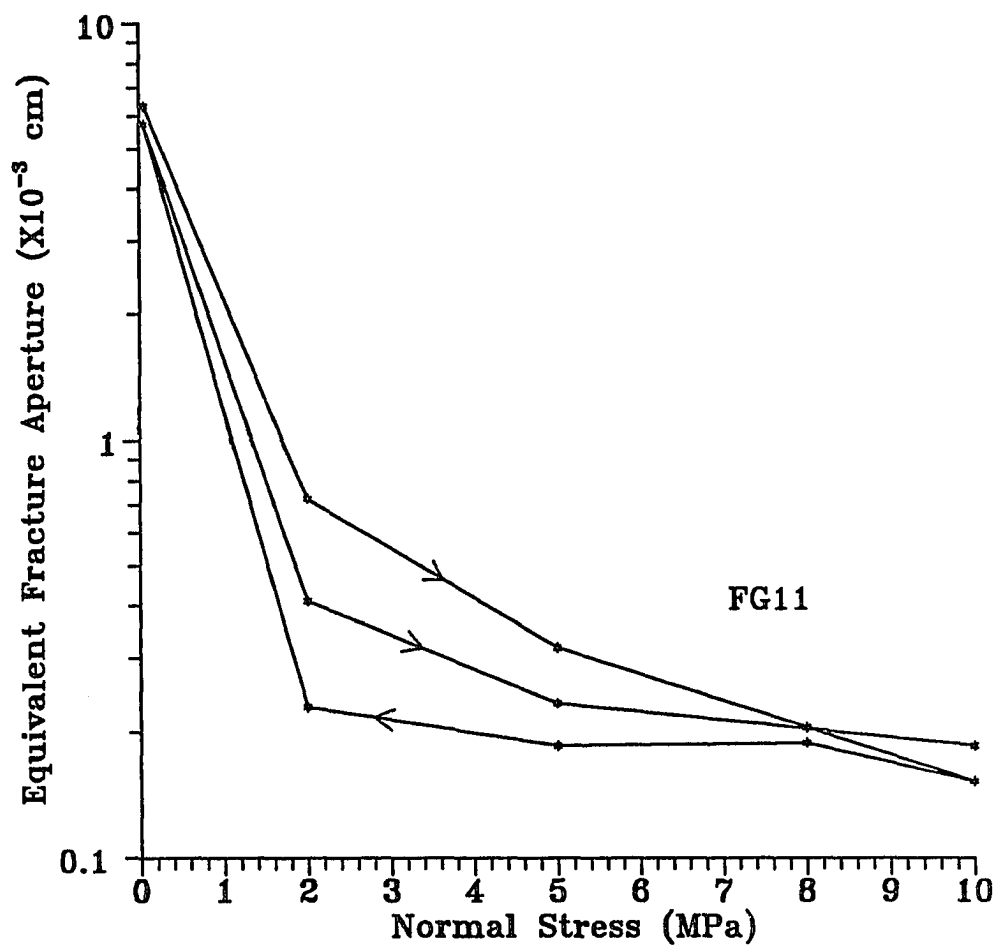


Figure 5.10 Equivalent fracture aperture as a function of normal stress for sample AP30-1-6-FG11 (Tension induced fracture). Arrows indicate the loading sequence.

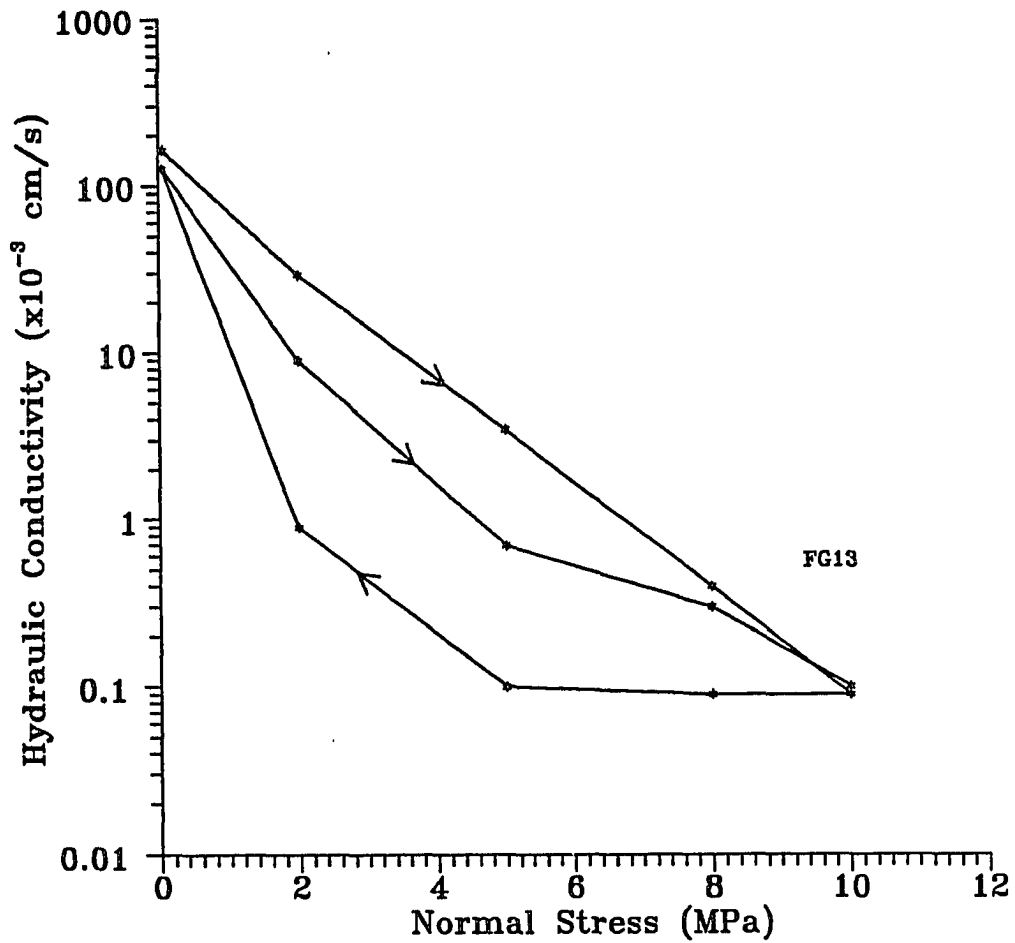


Figure 5.11 Hydraulic conductivity as a function of normal stress for sample AP36-1-6-FG13 (Tension induced fracture). Arrows indicate the loading sequence.

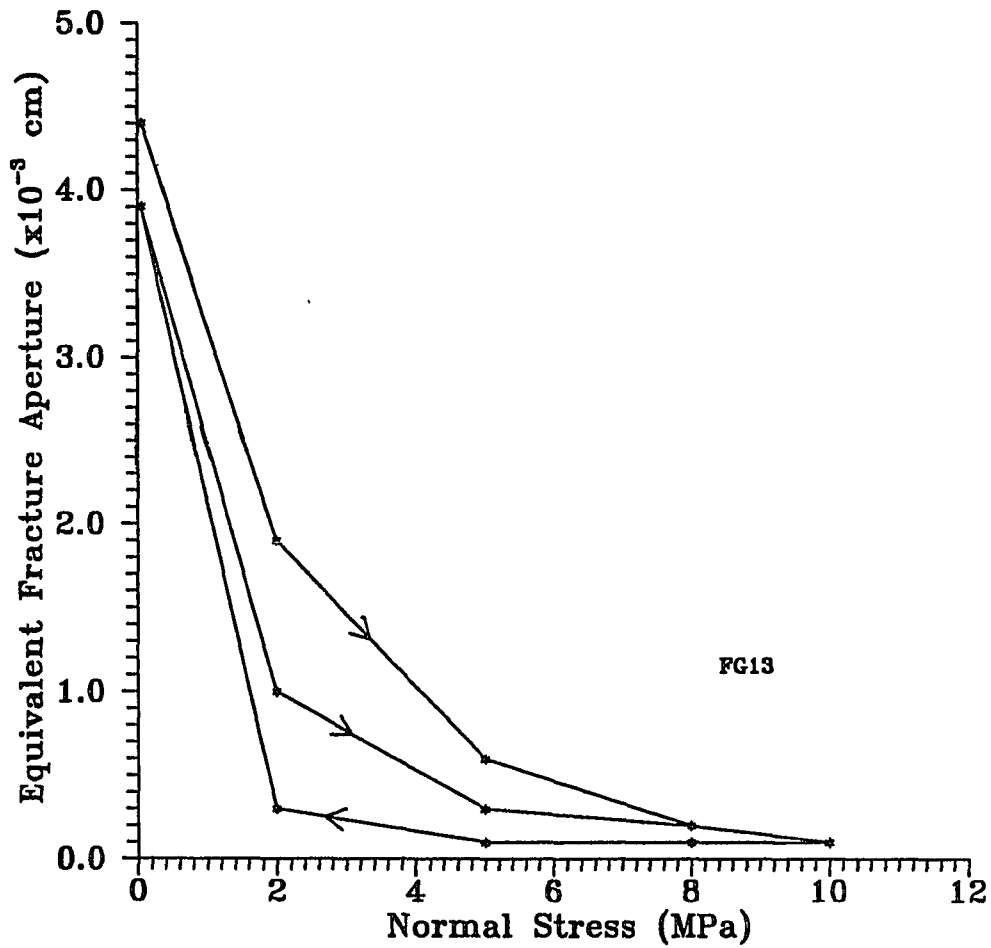


Figure 5.12 Equivalent fracture aperture as a function of normal stress for sample AP36-1-6-FG13 (Tension induced fracture). Arrows indicate the loading sequence.

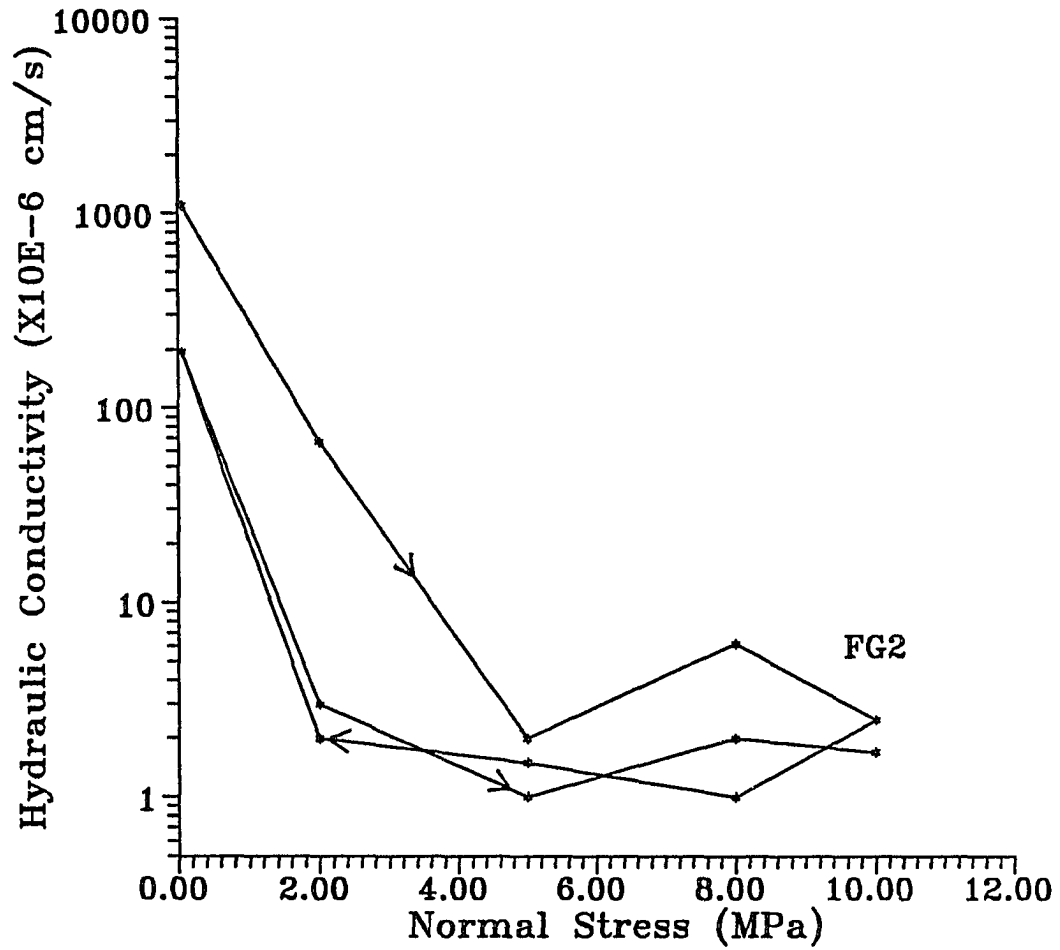


Figure 5.13 Hydraulic conductivity as a function of normal stress for sample AP4-1-6-FG2 (Sawcut). Arrows indicate the loading sequence.

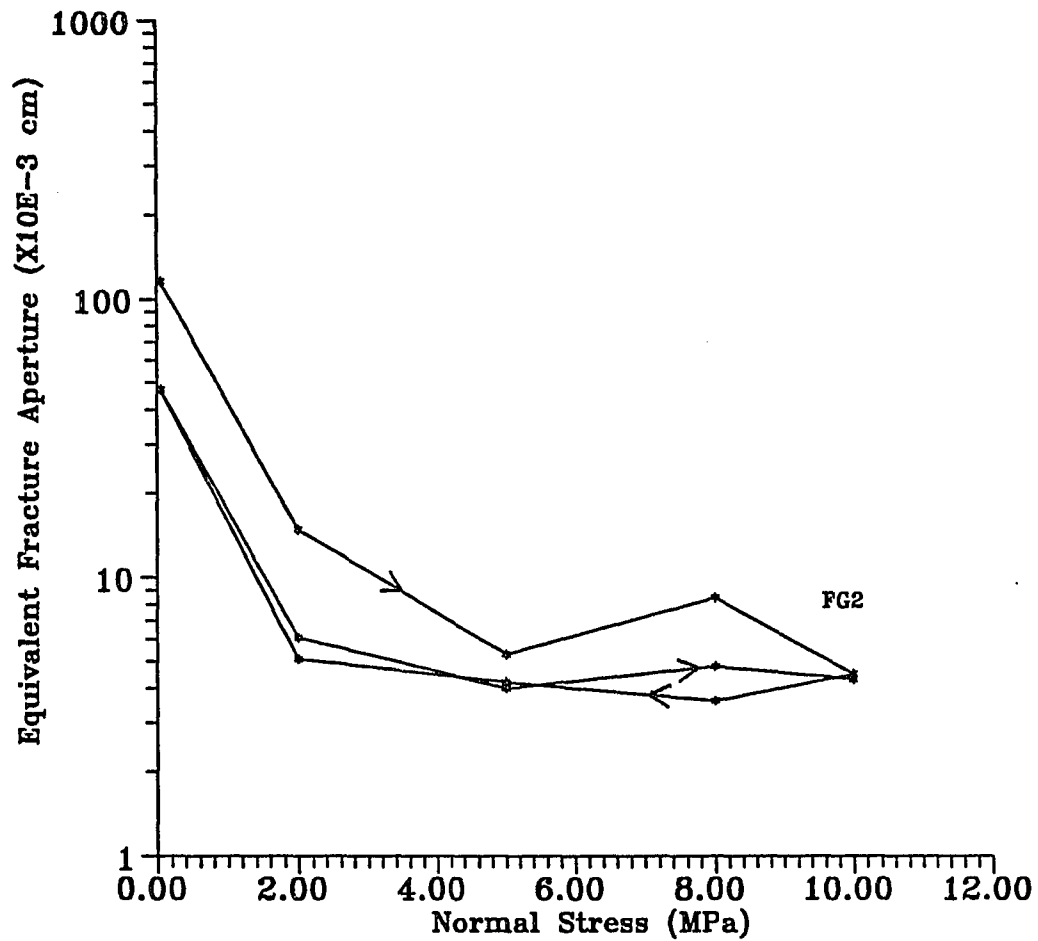


Figure 5.14 Equivalent fracture aperture as a function of normal stress for sample AP4-1-6-FG2 (Sawcut). Arrows indicate the loading sequence.

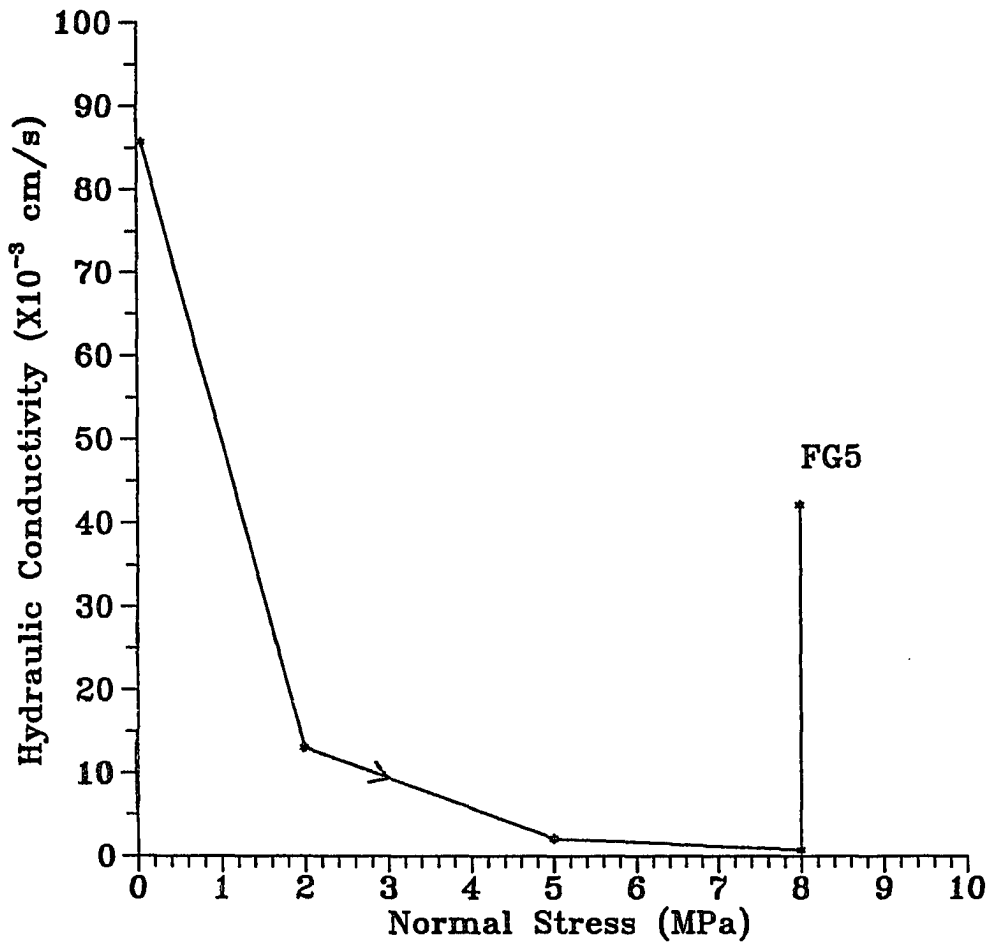


Figure 5.15 Hydraulic conductivity as a function of normal stress for sample AP7-2-6-FG5 (Sawcut). Arrows indicate the loading sequence. The increase in permeability at 8 MPa normal stress is due to the development of a vertical fracture.

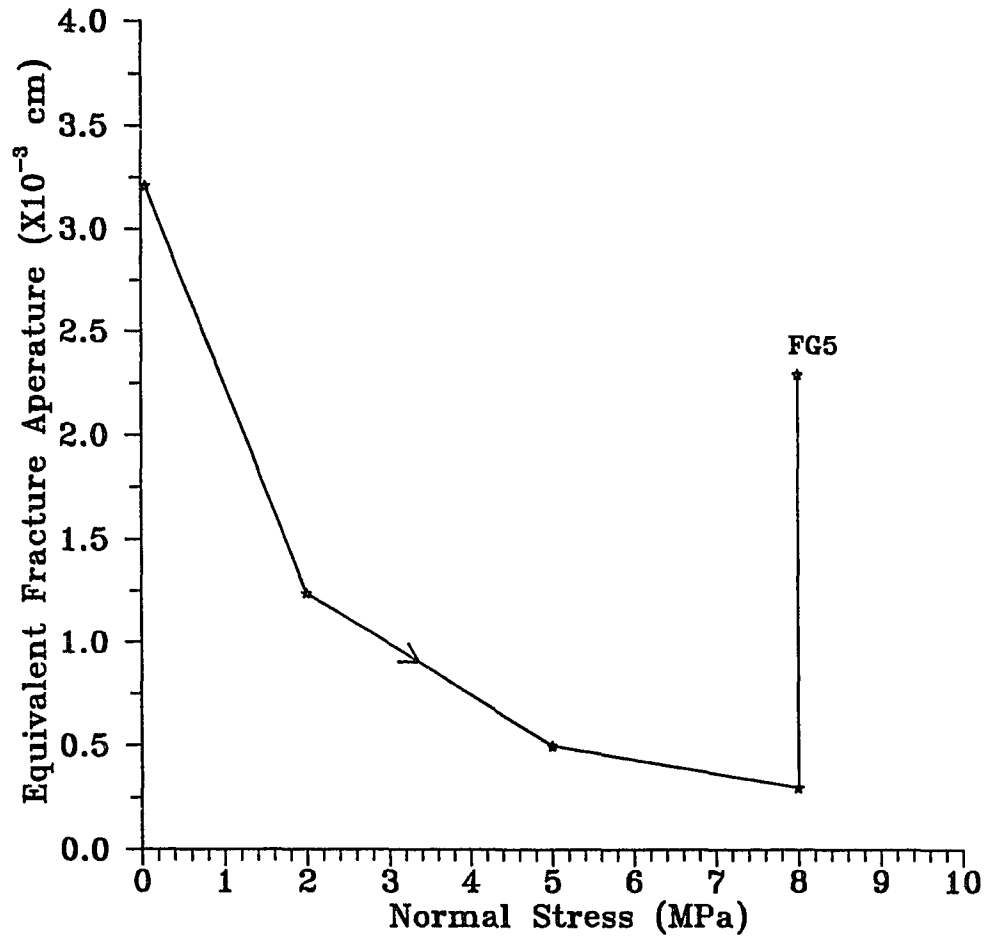


Figure 5.16 Equivalent fracture aperture as a function of normal stress for sample AP7-2-6-FG5 (Sawcut). Arrows indicate the loading sequence. The increase in the equivalent fracture aperture at 8 MPa normal stress is due to the development of a vertical fracture.

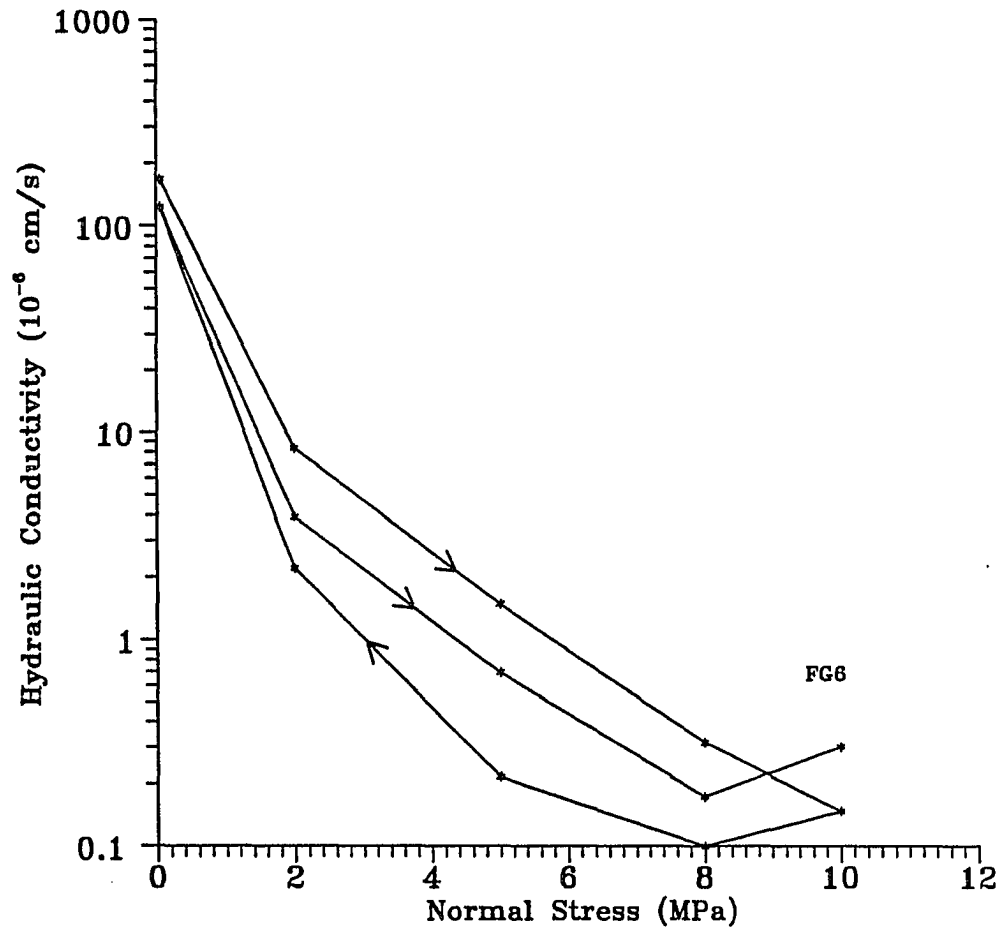


Figure 5.17 Hydraulic conductivity as a function of normal stress for sample AP3-1-6-FG6 (Sawcut). Arrows indicate the loading sequence.

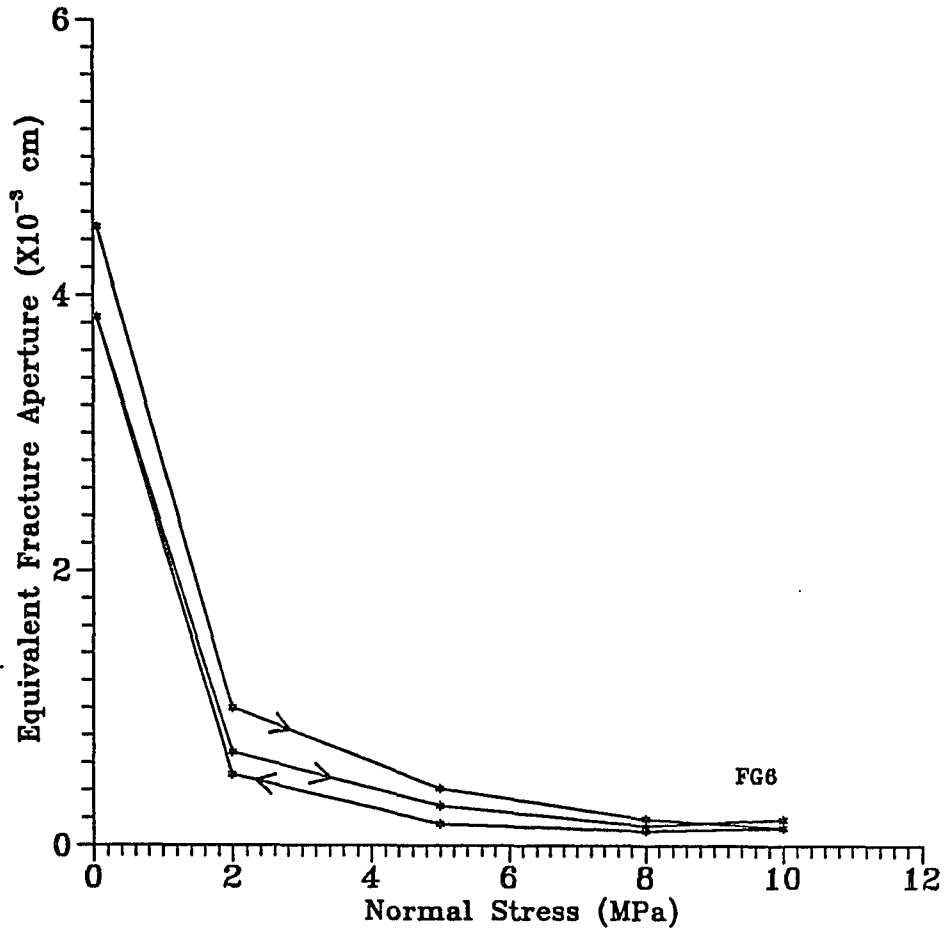


Figure 5.18 Equivalent fracture aperture as a function of normal stress for sample AP3-1-6-FG6 (Sawcut). Arrows indicate the loading sequence.

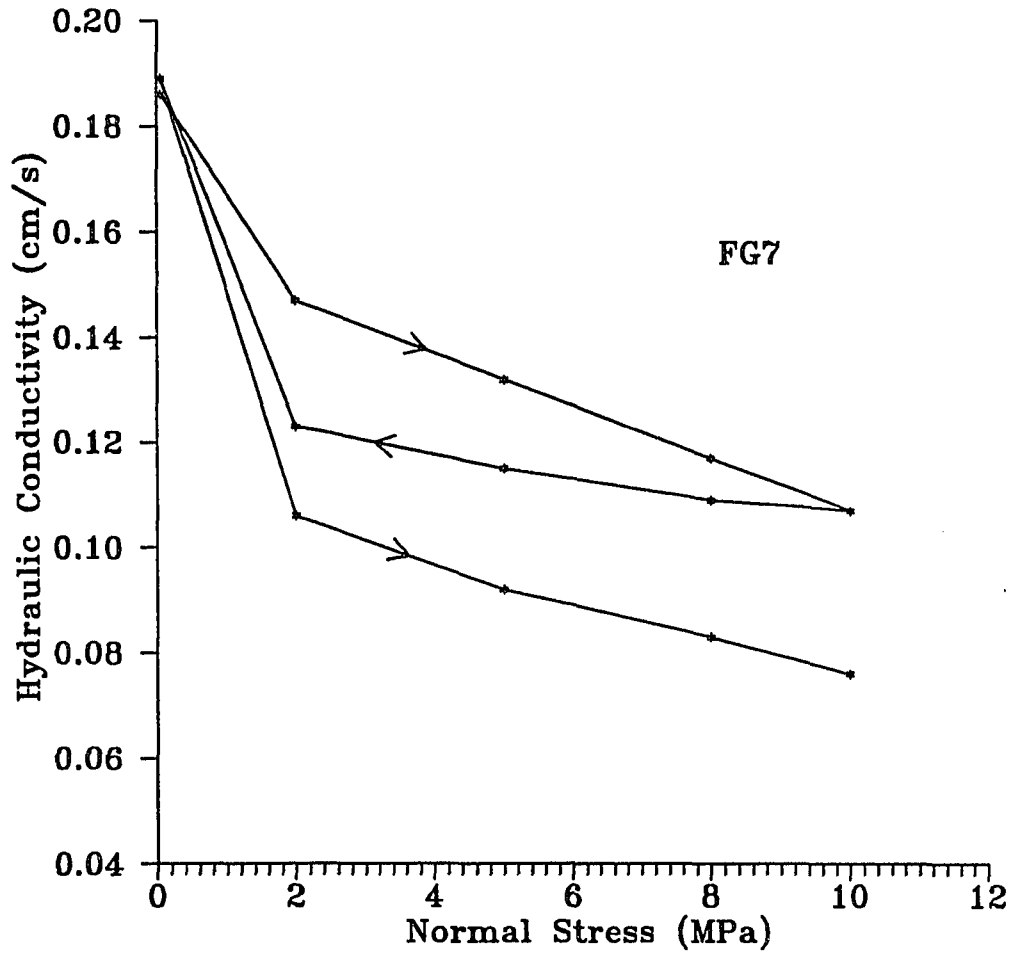


Figure 5.19 Hydraulic conductivity as a function of normal stress for sample AP2-1-6-FG7 (Natural fracture). Arrows indicate the loading sequence.

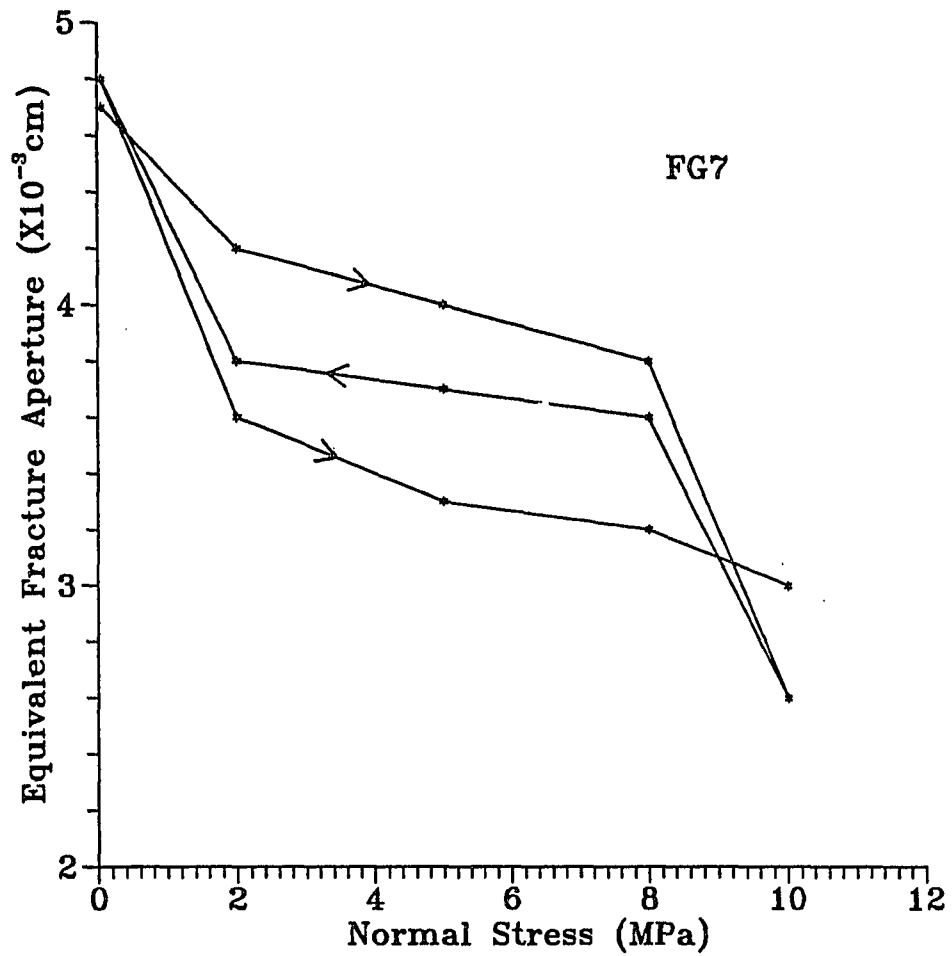


Figure 5.20 Equivalent fracture aperture as a function of normal stress for sample AP2-1-6-FG7 (Natural fracture). Arrows indicate the loading sequence.

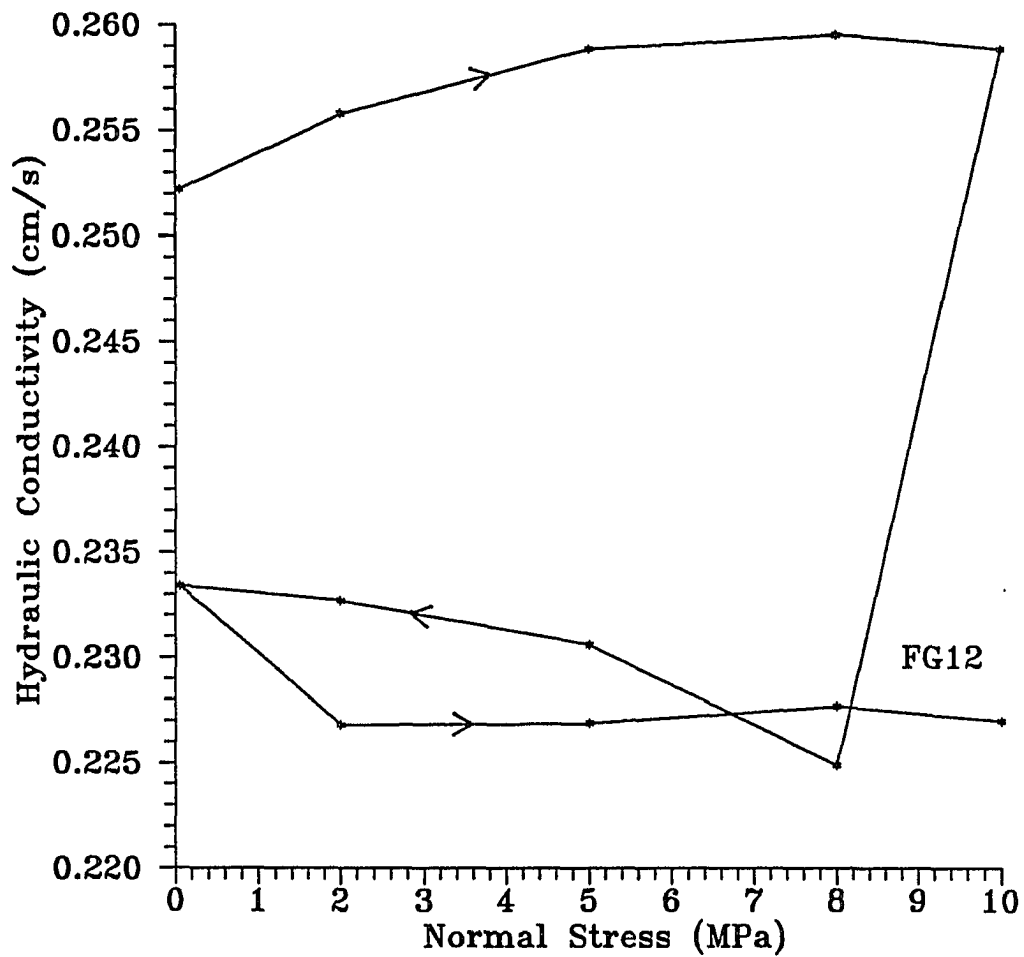


Figure 5.21 Hydraulic conductivity as a function of normal stress for sample AP56-5-6-FG12 (Natural fracture). Arrows indicate the loading sequence.

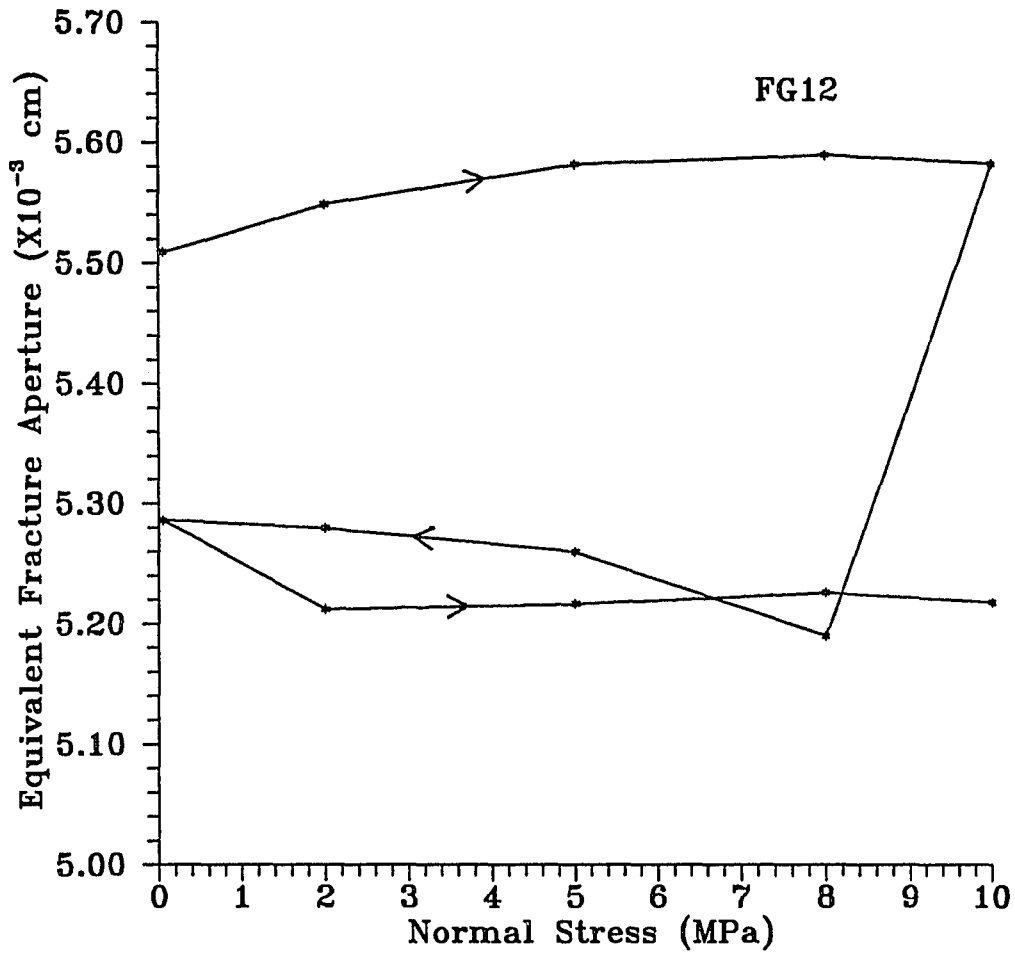


Figure 5.22 Equivalent fracture aperture as a function of normal stress for sample AP56-5-6-FG12 (Natural fracture). Arrows indicate the loading sequence.

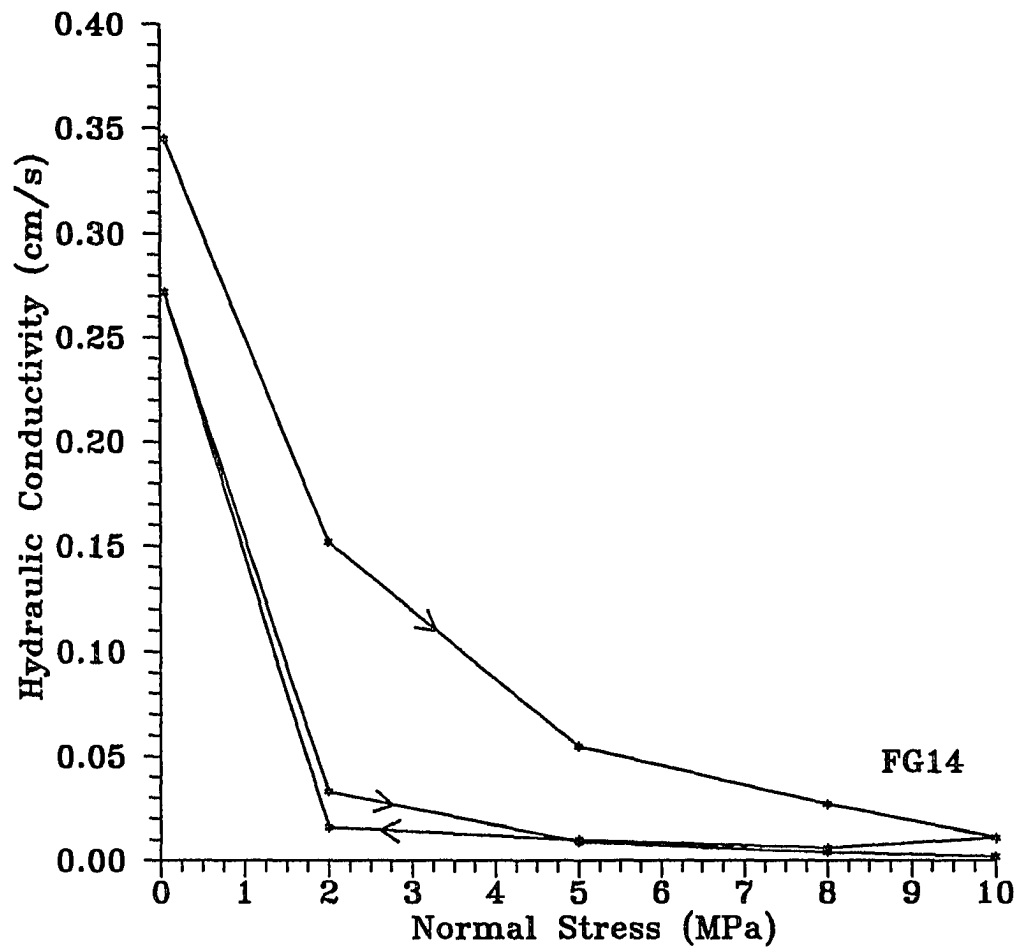


Figure 5.23 Hydraulic conductivity as a function of normal stress for sample AP56-2-6-FG14 (Natural fracture). Arrows indicate the loading sequence.

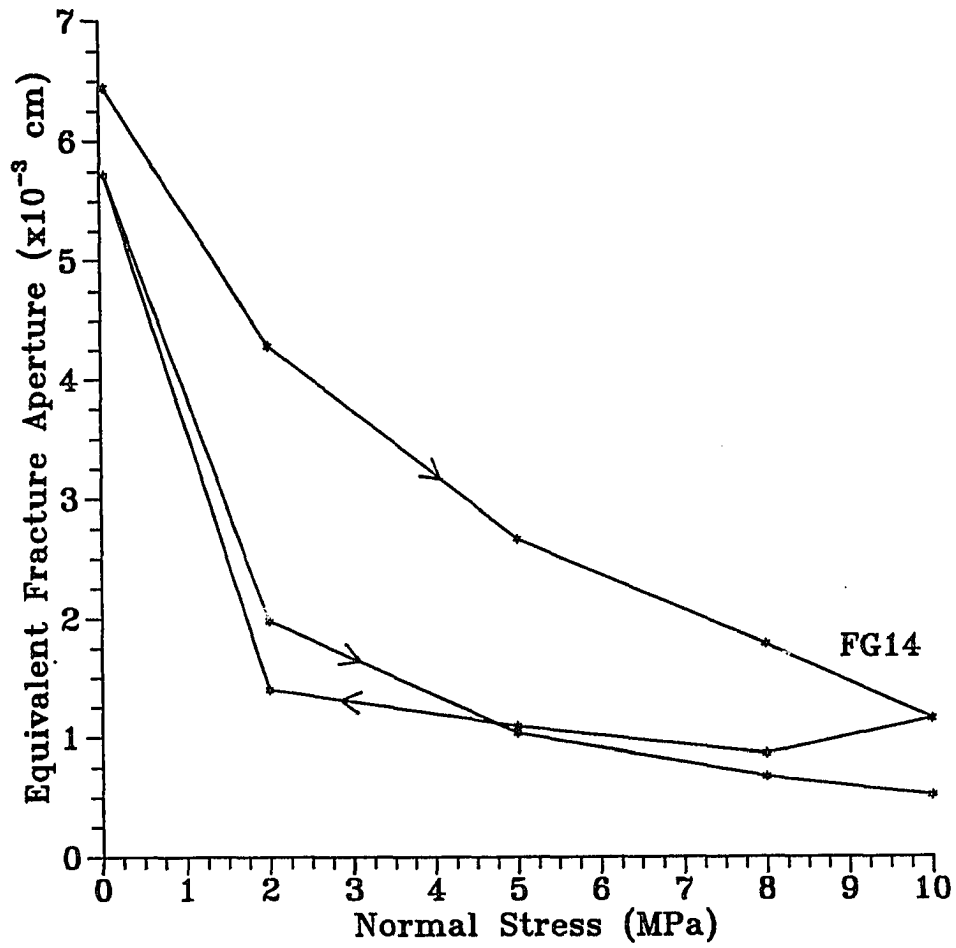


Figure 5.24 Equivalent fracture aperture as a function of normal stress for sample AP56-2-6-FG14 (Natural fracture). Arrows indicate the loading sequence.

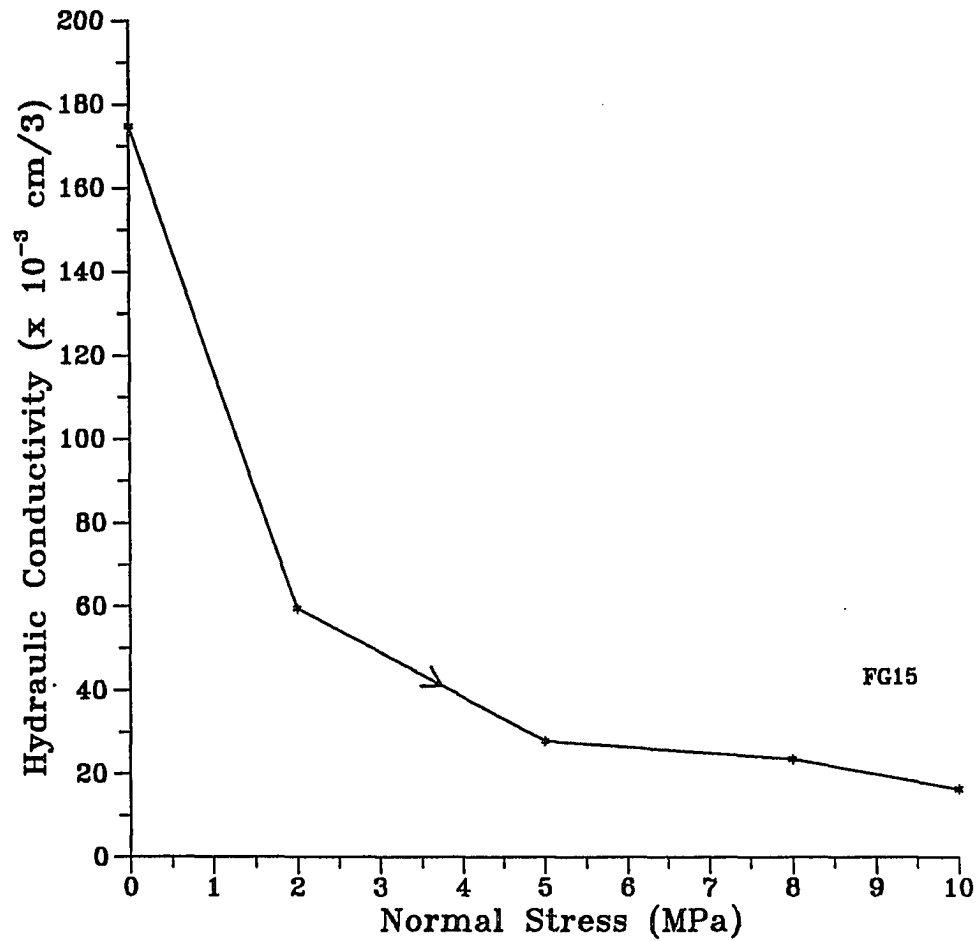


Figure 5.25 Hydraulic conductivity as a function of normal stress for sample AP56-3-6-FG15 (Natural fracture). Arrows indicate the loading sequence.

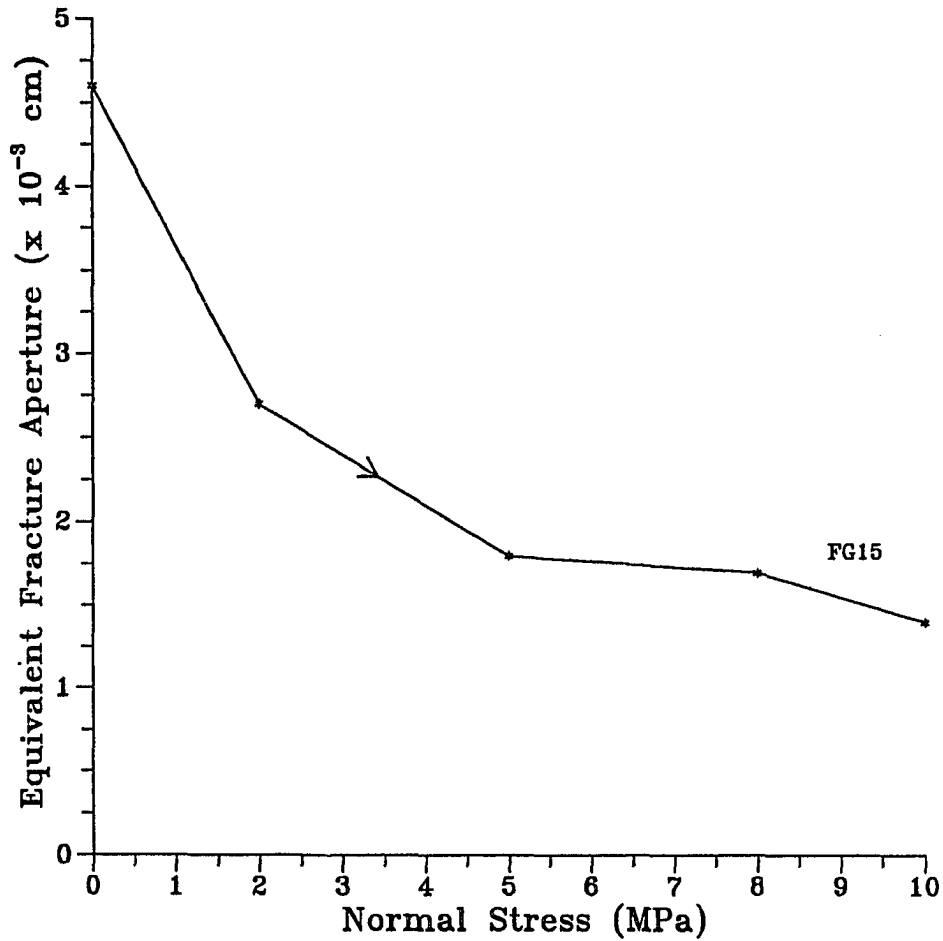


Figure 5.26 Equivalent fracture aperture as a function of normal stress for sample AP56-3-6-FG15 (Natural fracture). Arrows indicate the loading sequence.

Table 5.9 Parameters involved in the Determination of Fracture Permeability and Equivalent Fracture Aperture for Sample AP21-3-6-FG1 with a Tension Induced Fracture.

Number of Readings	σ_N (MPa)	K_j ($\times 10^{-3}$ cm/s)	e ($\times 10^{-3}$ cm)	h_o (cm)	h_f (cm)	SD($k_j \times 10^{-6}$)	SD($e \times 10^{-6}$)
3	0.05	315	6.15	183	131	0	0
44	2	29	1.31	183	131	16000	700
6	5	0.49	0.24	183	131	93	23
4	8	0.34	0.20	183	131	10	2.7
3	10	0.39	0.22	183	131	17	4.6
3	8	0.31	0.19	183	131	62	20
3	5	0.37	0.21	183	131	18	4.9
3	2	0.43	0.23	183	131	6.8	21
3	0.05	239	5.36	183	131	0	0
5	2	1.6	0.44	183	131	300	42
4	5	0.4	0.22	183	131	13	3.5
4	8	0.34	0.20	183	131	21	6.1
4	10	0.34	0.20	183	131	7.6	2.2

σ_N = normal stress
 K_j = fracture permeability (mean)
 e = equivalent fracture aperture (mean)
 h_o = starting height in falling head pipette
 h_f = water head difference used in falling head permeameter test.
SD(K_j) = standard deviation about mean
SD(e) = standard deviation about mean

Table 5.10 Parameters involved in the Determination of Fracture Permeability and Equivalent Fracture Aperture for Sample AP30-2-6-FG10 with a Tension Induced Fracture.

Number of Readings	σ_N (MPa)	K_j ($\times 10^{-3}$ cm/s)	e ($\times 10^{-3}$ cm)	P_i (MPa)	Δh (cm)	SD($k_j \times 10^{-6}$)	SD($e \times 10^{-6}$)
6	0.05	96178	3402	0.5	5002	990	18
5	2	254	173	0.5	5003	21	0
4	5	66	100	0.5	5005	7	0
3	8	26	54	0.5	5006	9	9
4	10	18	46	0.5	5007	7	11
3	8	33	63	0.5	5007	8	8
3	5	32	102	0.5	5007	14	13
3	2	47	100	0.5	5001	2	13
3	0.05	98090	3683	0.5	5004	4781	83
3	2	123	114	0.5	5001	67	24
3	5	36	73	0.5	5001	13	24
2	8	23	52	0.5	5001	5	6
2	10	12	38	0.5	5001	2.2	9

σ_N = normal stress
 K_j = fracture permeability (mean)
 e = equivalent fracture aperture (mean)
 P_i = injection pressure
 Δh = water head difference used in falling head permeameter test.
 ($P_i / \gamma_w - h_o$)
 SD(K_j) = standard deviation about mean
 SD(e) = standard deviation about mean

Table 5.11 Parameters involved in the Determination of Fracture Permeability and Equivalent Fracture Aperture for Sample AP30-1-6-FG11 with a Tension Induced Fracture.

Number of Readings	σ_N (MPa)	K_j ($\times 10^{-6}$ cm/s)	e ($\times 10^{-6}$ cm)	h_o (cm)	h_f (cm)	SD($k_j \times 10^{-6}$)	SD($e \times 10^{-6}$)
18	0.05	335800	6357	170	131	6700	64
20	2	5767	727	173	137	3500	260
9	5	850	319	130	119	140	130
6	8	320	206	129	127	55	16
3	10	194	153	129	128	22	8.5
4	8	294	189	128	127	12	3.3
6	5	287	186	128	126	25	7.9
4	2	441	230	129	127	47	12
10	0.05	275000	5750	180	131	0	0
7	2	1477	412	178	144	19	3.4
3	5	458	235	130	128	28	7.6
4	8	347	205	127	126	22	6.5
3	10	288	186	129	120	27	8.7

σ_N = normal stress
 K_j = fracture permeability (mean)
 e = equivalent fracture aperture (mean)
 h_o = starting height in falling head pipette
 h_f = water head difference used in falling head permeameter test.
SD(K_j) = standard deviation about mean
SD(e) = standard deviation about mean

Table 5.12 Parameters involved in the Determination of Fracture Permeability and Equivalent Fracture Aperture for Sample AP36-1-6-FG13 with a Tension Induced Fracture.

Number of Readings	σ_N (MPa)	K_j ($\times 10^{-3}$ cm/s)	e ($\times 10^{-6}$ cm)	h_o (cm)	h_f (cm)	SD($k_j \times 10^{-6}$)	SD($e \times 10^{-6}$)
3	0.05	163.70	4439	0.1	998	101.8	1.4
4	2	29.40	1879	1.0	10013	2357.1	75.2
4	5	3.50	646	1.0	10012	1011.1	93.5
5	8	0.40	217.6	1.0	10018	70.7	19.5
4	10	0.09	102.8	1.0	10018	28.7	15.7
5	8	0.09	102.9	1.0	10019	1.7	1.0
4	5	0.13	127.4	1.0	10019	1.7	0.8
4	2	0.90	327.6	1.0	10019	179.2	32.3
4	0.05	126.45	3901.2	0.1	10016	1023.6	15.8
3	2	8.98	1039.5	1.0	10013	73.0	4.2
3	5	0.66	280.1	1.0	10011	154.9	31.6
3	8	0.29	187.1	1.0	10011	38.5	12.2
4	10	0.15	132.7	1.0	10011	17.1	7.8

- σ_N = normal stress
 K_j = fracture permeability (mean)
 e = equivalent fracture aperture (mean)
 P_i = injection pressure
 Δh = water head difference used in falling head permeameter test.
 ($P_i/\gamma_w - h_o$)
 SD(k_j) = standard deviation about mean
 SD(e) = standard deviation about mean

Table 5.13 Parameters involved in the Determination of Fracture Permeability and Equivalent Fracture Aperture for Sample AP4-1-6-FG2 with a Tension Induced Fracture.

Number of Readings	σ_N (MPa)	K_j ($\times 10^{-6}$ cm/s)	e ($\times 10^{-6}$ cm)	P_i (MPa)	Δh (cm)	SD($k_j \times 10^{-6}$)	SD($e \times 10^{-6}$)
4	0.05	51583.3	2496.5	0.5	5003	1103.0	26.5
3	2	898.5	320.4	0.5	5008	523.0	94.1
2	5	107.9	114.2	0.5	5008	7.2	3.8
2	8	276.9	182.9	0.5	5008	1.4	0.5
3	10	77.3	96.6	0.5	5008	5.1	3.2
2	8	49.2	76.9	0.5	5008	9.3	7.3
2	5	69.0	90.7	0.5	5008	23.2	15.4
2	2	99.6	109.5	0.5	5008	18.5	10.2
5	0.05	5100.7	784.1	0.5	4999	577.2	44.1
3	2	143.2	131.6	0.5	5004	2.6	1.2
3	5	61.8	86.4	0.5	5005	5.1	3.6
3	8	95.4	102.1	0.5	5005	76.9	40.8
3	10	69.7	91.4	0.5	5006	14.6	9.9

σ_N = normal stress

K_j = fracture permeability (mean)

e = equivalent fracture aperture (mean)

P_i = injection pressure

Δh = water head difference used in falling head permeameter test.
($P_i/\gamma_w - h_o$)

SD(K_j) = standard deviation about mean

SD(e) = standard deviation about mean

Table 5.14 Parameters involved in the Determination of Fracture Permeability and Equivalent Fracture Aperture for Sample AP7-2-6-FG5 with a Tension Induced Fracture.

Number of Readings	σ_N (MPa)	K_j ($\times 10^{-3}$ cm/s)	e ($\times 10^{-3}$ cm)	P_i (MPa)	Δh (cm)	SD($k_j \times 10^{-6}$)	SD($e \times 10^{-6}$)
4	0.05	85.7	3.2	1.0	10016	7.7	0.1
8	2	13.1	1.2	1.0	10015	4210.3	194.1
4	5	2.1	0.5	1.0	10015	732.0	86.9
3	8	0.7	0.3	1.0	10015	97.0	20.4
3	8	42.2	2.3	0.1	10020	1736.0	46.5

- σ_N = normal stress
- K_j = fracture permeability (mean)
- e = equivalent fracture aperture (mean)
- P_i = injection pressure
- Δh = water head difference used in falling head permeameter test.
($P_i / \gamma_w - h_o$)
- SD(K_j) = standard deviation about mean
- SD(e) = standard deviation about mean

Table 5.15 Parameters involved in the Determination of Fracture Permeability and Equivalent Fracture Aperture for Sample AP3-1-6-FG6 with Sawcut Surfaces.

Number of Readings	σ_N (MPa)	K_j ($\times 10^{-3}$ cm/s)	e ($\times 10^{-3}$ cm)	P_i (MPa)	Δh (cm)	SD($k_j \times 10^{-6}$)	SD($e \times 10^{-6}$)
3	0.05	168.0	4.49	0.1	999	760	10
3	2	8.40	1.00	1.0	10012	1400	860
5	5	1.50	0.42	1.0	10012	660	98
4	8	0.32	0.20	1.0	10012	58	18
3	10	0.02	0.13	1.0	10012	37	17
3	8	0.10	0.11	1.0	10012	3.9	2.1
4	5	0.22	0.16	1.0	10012	92	35
4	2	2.22	0.52	1.0	10017	240	28
3	0.05	123	3.84	0.1	996	3900	60
3	2	3.93	0.68	1.0	10011	1700	150
3	5	0.70	0.29	1.0	10010	150	30
4	8	0.17	0.14	1.0	10013	72	30
3	10	0.31	0.19	1.0	10016	62	19

σ_N = normal stress
 K_j = fracture permeability (mean)
 e = equivalent fracture aperture (mean)
 P_i = injection pressure
 Δh = water head difference used in falling head permeameter test.
 $(P_i/\gamma_w - h_o)$
SD(K_j) = standard deviation about mean
SD(e) = standard deviation about mean

Table 5.16 Parameters involved in the Determination of Fracture Permeability and Equivalent Fracture Aperture for Sample AP2-1-6-FG7 with a Natural Fracture.

Number of Readings	σ_N (MPa)	K_j ($\times 10^{-3}$ cm/s)	e ($\times 10^{-3}$ cm)	h_o (cm)	h_f (cm)	SD($k_j \times 10^{-6}$)	SD($e \times 10^{-6}$)
3	0.05	186	4.7	155	129	0	0
3	2	147	4.2	155	129	0	0
3	5	132	4.0	155	129	1000	20
3	8	117	3.8	155	129	0	0
3	10	107	2.6	155	129	1000	10
3	8	109	3.6	155	129	580	5.8
4	5	115	3.7	155	129	1700	31
4	2	123	3.8	155	129	820	13
5	0.05	189	4.8	155	129	4500	54
4	2	106	3.6	155	129	2200	39
3	5	92	3.3	155	129	580	10
3	8	83	3.2	155	129	1000	23
3	10	76	3.0	155	129	1500	31

σ_N = normal stress
 K_j = fracture permeability (mean)
 e = equivalent fracture aperture (mean)
 h_o = starting height in falling head pipette
 h_f = water head difference used in falling head pipette.
SD(K_j) = standard deviation about mean
SD(e) = standard deviation about mean

Table 5.17 Parameters Involved in the Determination of Fracture Permeability and Equivalent Fracture Aperture for Sample AP56-5-6-FG12 with a Natural Fracture.

Number of Readings	σ_N (MPa)	K_j ($\times 10^{-3}$ cm/s)	e ($\times 10^{-3}$ cm)	P_i (MPa)	Δh (cm)	SD($k_j \times 10^{-3}$)	SD($e \times 10^{-6}$)
5	0.05	252.2	5.51	0.05	495	4.2	45.4
5	2	255.8	5.55	.05	492	6.3	68.7
4	5	258.9	5.58	.05	494	1.1	11.4
4	8	259.6	5.59	.05	492	0.79	8.5
3	10	258.9	5.58	.05	494	1.40	4.0
6	8	224.9	5.19	.05	743	32.2	381.0
7	5	230.6	5.26	.05	707	28.3	326.7
6	2	232.7	5.28	.05	743	35.0	398.7
6	0.05	233.4	5.29	.05	743	37.6	427.7
6	2	226.8	5.21	.05	745	34.9	403.2
6	5	226.9	5.22	.05	743	30.2	348.6
6	8	227.7	5.23	.05	745	29.5	339.2
6	10	227.0	5.22	.05	741	29.1	337.8

σ_N = normal stress
 K_j = fracture permeability (mean)
 e = equivalent fracture aperture (mean)
 P_i = injection pressure
 Δh = water head difference used in falling head permeameter test.
 ($P_i/\gamma_w - h_o$)
 SD(K_j) = standard deviation about mean
 SD(e) = standard deviation about mean

Table 5.18 Parameters involved in the Determination of Fracture Permeability and Equivalent Fracture Aperture for Sample AP56-2-6-FG14 with a Natural Fracture.

Number of Readings	σ_N (MPa)	K_j ($\times 10^{-3}$ cm/s)	e ($\times 10^{-3}$ cm)	h_o (cm)	h_f (cm)	SD($k_j \times 10^{-6}$)	SD($e \times 10^{-6}$)
8	0.05	345.38	6.45	180	131	10529.5	98.4
8	2	152.89	4.29	180	131	3256.1	45.9
14	5	59.52	2.67	175	131	10211.5	232.5
4	8	26.55	1.79	180	131	2470.1	83.4
3	10	11.18	1.15	180	138	4971.1	168.5
4	8	6.29	0.86	170	153	1991.7	144.5
5	5	10.00	1.09	180	155	2763.8	154.5
3	2	16.41	1.40	180	145	3230.6	137.6
7	0.05	271.65	5.72	180	131	1842.2	19.4
4	2	32.60	1.98	180	131	1220.5	37.2
4	5	8.95	1.04	180	161	1422.7	81.7
4	8	3.75	0.67	177	170	490.3	44.9
3	10	2.20	0.51	175	172	75.3	8.8

σ_N = normal stress
 K_j = fracture permeability (mean)
 e = equivalent fracture aperture (mean)
 h_o = starting height in falling head pipette
 h_f = water head difference used in falling head permeameter test.
SD(K_j) = standard deviation about mean
SD(e) = standard deviation about mean

Table 5.19 Parameters involved in the Determination of Fracture Permeability and Equivalent Fracture Aperture for Sample AP56-3-6-FG15 with a Natural Fracture.

Number of Readings	σ_N (MPa)	K_j ($\times 10^{-3}$ cm/s)	e ($\times 10^{-3}$ cm)	P_i (MPa)	Δh (cm)	SD($k_j \times 10^{-3}$)	SD($e \times 10^{-6}$)
4	0.05	174.8	4.6	0.1	999	2.7	36.0
4	2	59.6	2.7	0.1	997	7.9	176.9
4	5	27.9	1.8	0.1	999	2.4	77.7
4	8	23.6	1.7	0.1	999	1.7	60.3
4	10	16.4	1.4	0.1	997	3.5	150.0

σ_N = normal stress
 K_j = fracture permeability (mean)
 e = equivalent fracture aperture (mean)
 P_i = injection pressure
 Δh = water head difference used in falling head permeameter test.
 ($P_i/\gamma_w - h_o$)
 SD(K_j) = standard deviation about mean
 SD(e) = standard deviation about mean

trends of irreversible reductions in fracture permeability and equivalent fracture aperture agree with many results, e.g. Schaffer and Daemen (1987), Iwai (1976), Johnson (1983).

The first type of surface tested is a tension induced fracture. This type of fracture is created by diametrically point loading a cylindrical tuff core to failure. The resulting surfaces are generally planar and horizontal with surface asperities seemingly evenly distributed on both surfaces. When placed back together these fractures are easily mated at their original position. Fracture permeabilities for these samples range from 1×10^{-3} cm/s at 0.05 MPa to 1×10^{-5} cm/s at 10MPa normal stress. Tables 5.9 - 5.12 show the permeability parameters, including injection pressures and hydraulic gradient.

The second type of surface tested was produced by saw cutting a tuff cylinder perpendicular to the core axis midway through the sample. The resulting surfaces are smooth to the touch and more closely match those assumptions made in calculating hydraulic conductivity, such as smooth parallel plates, horizontally positioned. These sawcut surfaces match together at any rotation with little chance of surface mismatch. The lack of surface asperities lessens the possibility of their apertures being propped open, which would have resulted in abnormally high permeabilities. Permeability testing of this type of fracture resulted in hydraulic conductivity values ranging from 1×10^{-1} cm/s at 0.05 MPa to 1×10^{-6} cm/s at 10 MPa normal stress. Tables 5.13 through 5.15 show permeability parameters including injection pressures and hydraulic gradients.

Figure 5.15 shows the higher permeability of a sawcut sample (FG5) due to the presence of an initially unobserved natural fracture and the eventual failure of the sample due to the applied injection pressure.

The final type of surface tested are natural fractures. Tuff blocks containing a single natural fracture were collected in the field and pryed apart (because of their great weight) and put back together in the laboratory. The only sample to deviate from this description was sample AP2-1-6-FG7 whose fracture was left intact and has a complex nonplanar geometry. These natural fracture surfaces are discolored, presumably due mineral staining. They are generally clean, with little gouge present.

Fracture permeabilities for natural fractures range from 1×10^{-1} cm/s at 0.05 MPa to 2×10^{-3} cm/s at 10 MPa normal stress. Tables 5.16 through 5.19 show permeability parameters including applied injection pressures and hydraulic gradient. In an attempt to speed up testing for natural fracture sample AP56-3-6-FG15 (Figure 5.25) permeability measurements were taken only during the final loading cycle after the sample had been loaded in the usual sequence.

Of the three types of surfaces tested natural fractures show the greatest hydraulic conductivities and equivalent fracture apertures at all stress levels. This is due to the greater area available for flow created by surface shearing and weathering in its geologic history. For all types of fracture surfaces tested permeabilities were within three orders of magnitude at any one stress level. Even at high normal stress distinct areas on these surfaces make contact thus not allowing the fracture to close completely. Increasing the load only serves to increase the stress at these contacts while not contributing to the reduction of overall area available for flow.

The second greatest flow rates were observed in tension induced fractures. Initially it was expected that this type of fracture would have the lowest permeability due to the surfaces tight interlocking closing nature and surface roughness requiring longer flow paths as well as the pressure drop along the fluids tortuous path.

Sawcut surfaces had the lowest permeability overall which is presumably due to the very smooth and parallel surfaces created by the circular diamond saw. These surfaces have high contact area (low effective flow area) even at low normal stress. As the stress levels are increased the surfaces deform together to create an even tighter interface. It is highly unlikely that this type of fracture surface would occur in nature. Even if a fracture were clean and slickensided the surfaces would not be truly parallel leaving preferential paths available for flow.

Comparison of permeability results may indicate that the significance of surface roughness is very secondary in influencing the flow rate through fractures with laminar flow conditions. If the surface of the fractures were held apart just out of contact the effect of surface roughness would probably be more significant when comparing smooth and rough joints. Surface roughness may be more important in terms of grouting due to the properties of the grout slurry having viscosity as well as cohesion.

5.3 Fracture Compression

Fracture permeability has been found to depend on the width of the fracture's aperture, which is dependent on the applied normal stress and stress history.

Fracture compression or closure has been measured as a function of the applied normal stress under cyclic loading.

Figure 5.27 shows the effect of normal stress on fracture compression for sample AP36-1-6-FG13. Each new loading cycle causes new surface deformation accompanied by some hysteresis. Two very distinct stiffness regions are observed, with remarkable repeatability for both, and a well defined transition stress between the two. The greatest changes occur at low normal stress (<1 MPa).

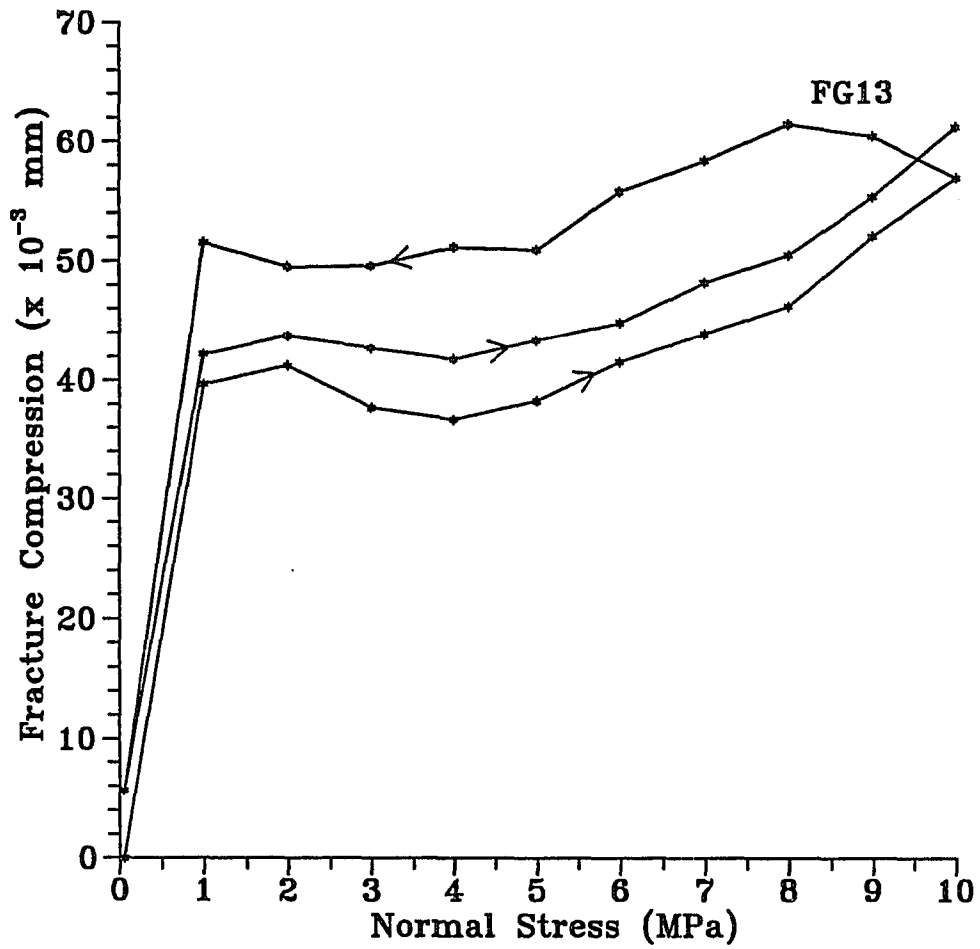


Figure 5.27 The effect of normal stress on fracture closure for Sample AP36-1-6-FG13. Arrows indicate loading and unloading paths.

Measurement of fracture compression only provides information as to how the aperture changes. An actual value of the fracture's aperture can not be obtained.

Figure 5.28 shows the fracture closure of sample AP36-1-6-FG13 (last loading cycle) as a function of normal stress in terms of calculated equivalent fracture aperture and measured fracture compression. It is clear that the two different regions of stiffness are observed both in compression testing and in flow testing. However, the behavior deviates substantially at the higher normal stresses, where the fracture appears to be much stiffer during flow testing than during compression testing.

5.4 Surface Characterization

Fracture surfaces are characterized by their roughness or height of asperities, surface waviness, orientation, and contact area or flow paths of high resistance.

The scope of this paper only allows the use of this surface characterization to be used for a visual understanding of the undulating and tortuous path that flow must traverse. Roko et al (1991) present a method where by this data base may be used to predict general flow trends. Knowledge of these potential flow paths may allow calculations of actual flow lengths and the associated pressure drops away from the borehole.

Figure 5.29 shows the exaggerated roughness of sample AP21-3-6-FG1 looking from an 80 degree tilt off the Z-axis. Figure 5.30 shows this same sample looking from a 30 degree tilt off the Z-axis.

Figures 5.31 and 5.32 show topographic plots of the top and bottom fracture surfaces of sample AP21-3-6-FG1 respectively.

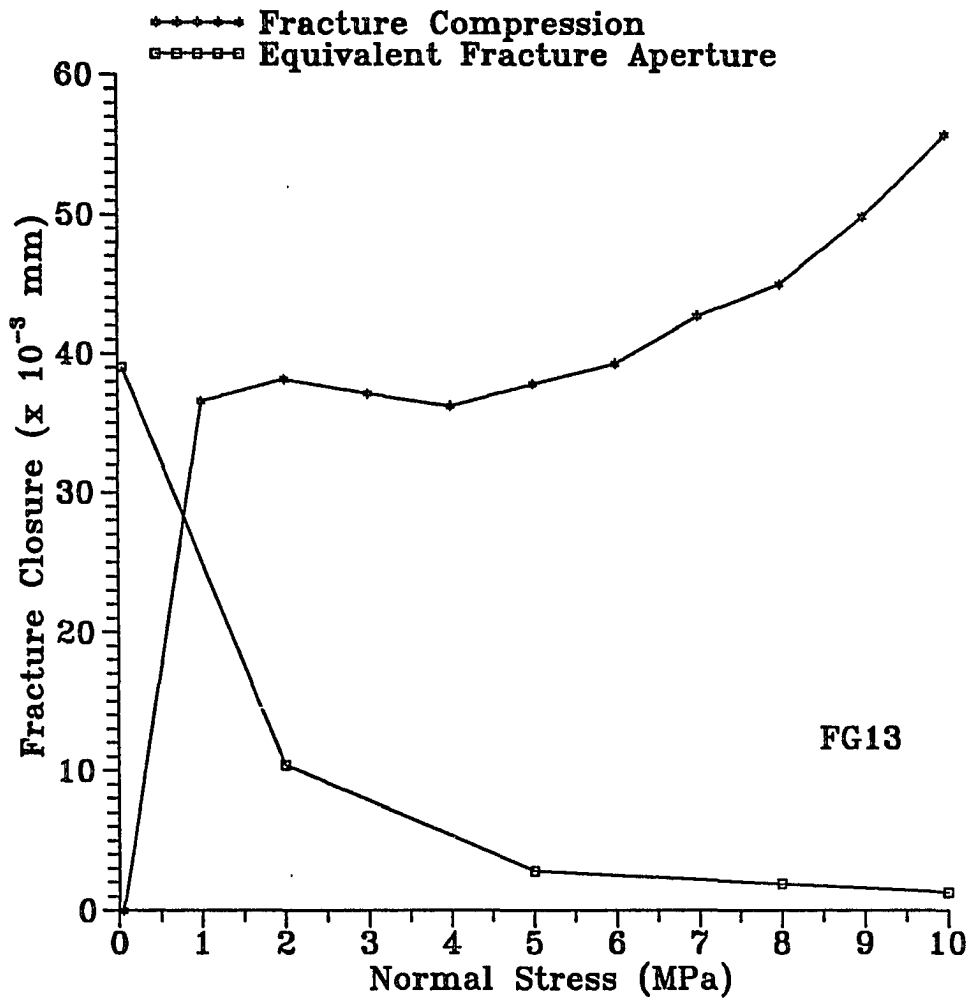


Figure 5.28 Comparison between fracture compression and equivalent fracture aperture for final loading cycle of Sample AP36-1-6-FG13.

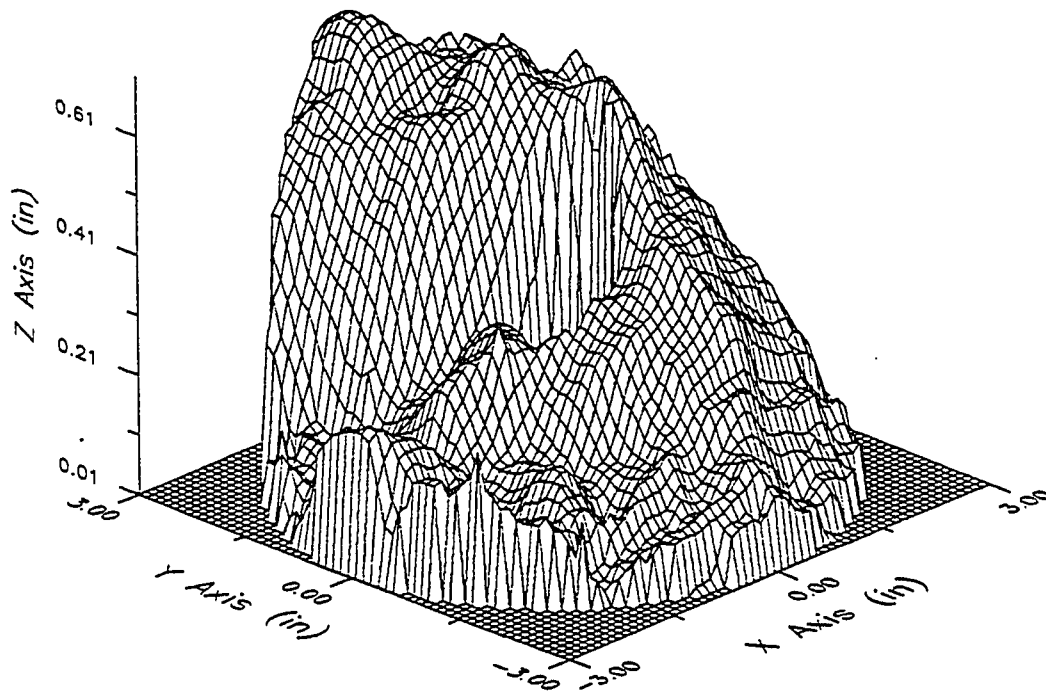


Figure 5.29 Three-dimensional image of the surface roughness of Sample AP21-3-6-FG1 (80 degree tilt off of the z-axis). Vertical scale is exaggerated.

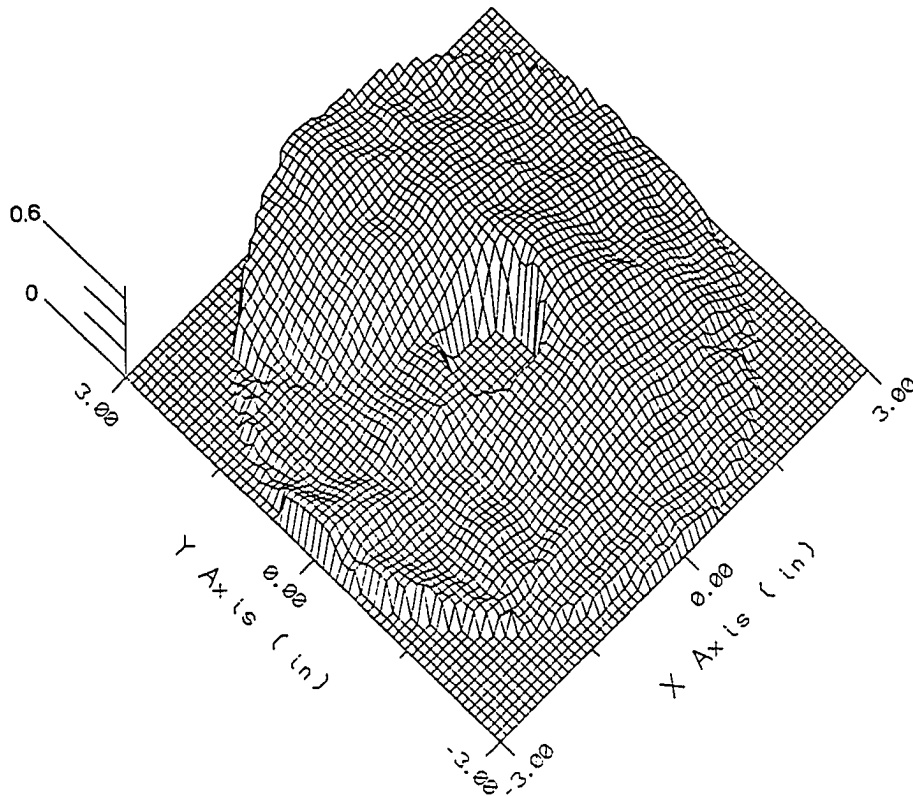


Figure 5.30 Three-dimensional image of the surface roughness of Sample AP21-3-6-FG1 (30 degree tilt off of the z-axis). Vertical scale is exaggerated.

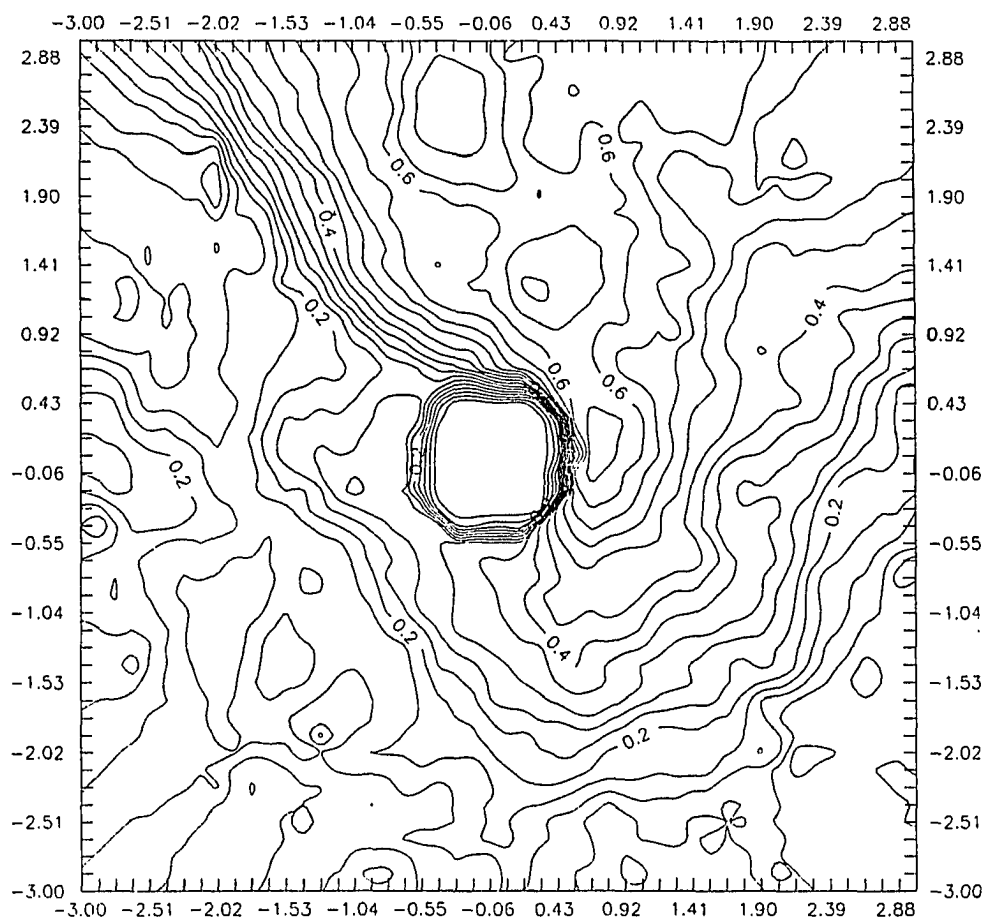


Figure 5.31 Topographic plot of the surface roughness of sample AP21-3-6-FG1 (top fracture surface). Contour lines represent points of constant surface roughness.

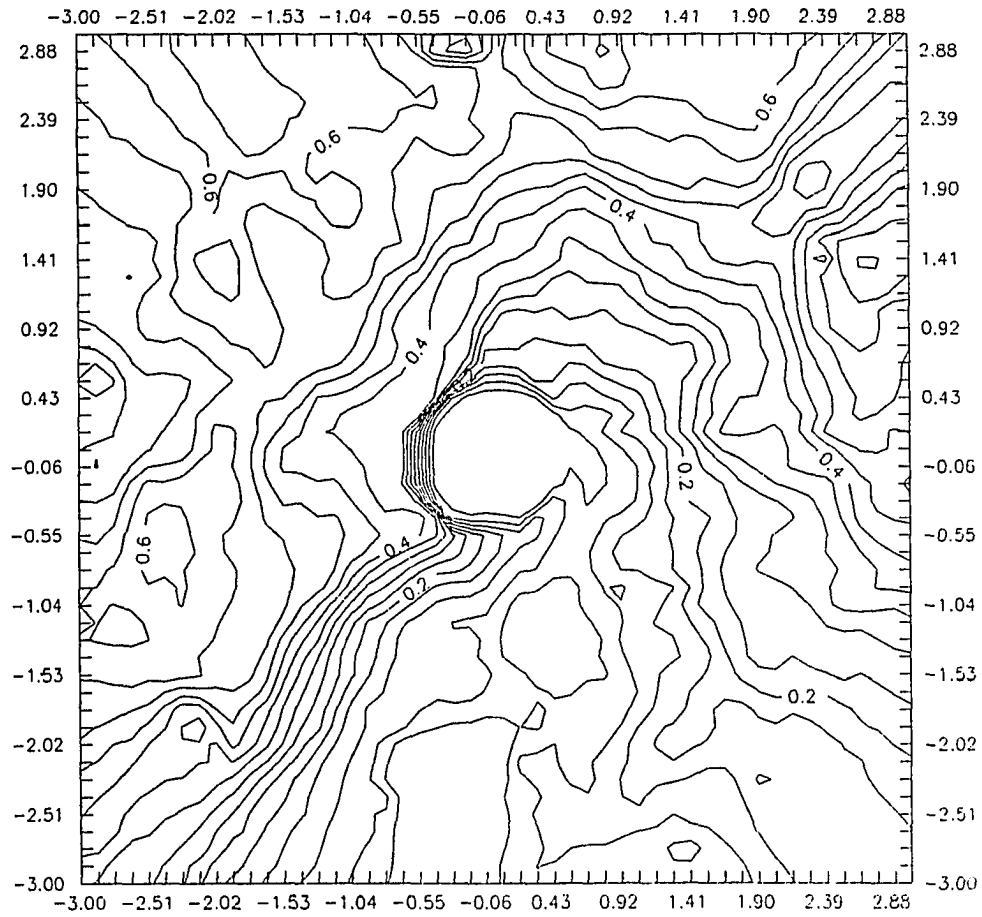


Figure 5.32 Topographic plot of the surface roughness of sample AP21-3-6-FG1 (bottom fracture surface). Contour lines represent points of constant surface roughness.

5.5 Grout Characterization

Rheologic properties, strength, and stability are important parameters in defining a grout's behavior during pumping and its useful lifetime.

Cementitious grout characterization includes the determination of uniaxial compressive strength, density, viscosity, cohesion, Marsh flow time, and stability.

Uniaxial Compressive Strength

Table 5.20 contains results of 7, 8, and 28 day strength testing. Cylindrical grout specimens have a length to diameter ratio > 2.0 . Mixing procedures can be found in section 4.4. Curing conditions can be found in section 4.5.

Fann viscosity and Cohesion

Table 5.21 contains results of viscosity measurements as a function of rotor speed. Comparisons between grout formulations are difficult due to varying water to cement ratios as well as bentonite content. Section 4.5 describes test procedure. Figure 5.33 shows the effects of rotor speed on viscosity readings for all grout formulations. Table 5.22 contains results of plastic viscosity and cohesion calculations. Section 4.5 contains the method of calculation.

Marsh funnel viscosity and stability

Table 5.23 contains Marsh funnel viscosities and bleed capacities for various grout formulations. Testing procedures can be found in section 4.5.

5.6 Grouting Effectiveness

Sample AP21-3-6-FG1:

Test 1

Grouting of the tension induced fracture in sample AP21-3-6-FG1 was conducted at an injection pressure of 5.0 MPa and a normal stress of 2.0 MPa. Due to the tight nature of a tension induced fracture it was

Table 5.20 Results of Strength Testing Grout Formulations

# OF TESTS	MIX TYPE	7-DAY STRENGTH [#] /SD (MPa)	8-DAY STRENGTH [#] /SD (MPa)	28-DAY STRENGTH [#] /SD	W/C RATIO	O/O BENTONITE	FLUID DENSITY (g/cc)
5	MIX 1+	-	21.15/0.61	22.99/1.47	0.6	2	1.77
5	MIX 2+	-	14.33/0.52	14.91/1.62	0.7	3	1.70
4	MIX 3+	-	7.86/0.33	11.47/0.16	0.9	5	1.58
3	MIX 4+	-	20.62/1.03	33.72/0.99	0.45	0	1.90
3	MC-500*	23.96/1.52	-	30.51/1.73	1.0	0	1.22

Uniaxial compression strength
 * 1% Napthalene Sulphonate (NS-200)
 + 1% Dispersant (D65)
 SD = Standard Deviation

Table 5.21 Results of Fann Viscosities for Different Grout Formulations.

# OF TESTS	ROTOR SPEED (rpm)	READING INTERVAL AFTER MIXING	VISCOSITY READINGS					
			MIX 1	MIX 2	MIX 3	MIX 4	MIX 5	MC-500
3	300	60	50.2*	42.4*	39.8*	28.5*	5.0*	17.5*
3	200	80	38.6	33.1	30.9	19.6	3.0	13.5
3	100	100	22.5	22.7	22.7	10.6	1.9	8.9
3	6	120	11.2	10.6	14.0	1.1	0.6	2.9
3	3	140	10.6	10.1	13.8	0.9	0.63	2.5
w/c Ratio			0.6	0.7	0.9	0.45	1.33	1.0
o/o Bentonite			2	3	5	0	2	0

* Newtonian Viscosities (cp)

Table 5.22 Plastic Viscosity and Yield Value of Grout Formulations.

# OF TESTS	MIX NUMBER	PLASTIC VISCOSITY (cp)	YIELD VALUE (N/m ²)
3	1	41.5	4.2
3	2	29.6	6.1
3	3	25.7	6.8
3	4	26.9	0.8
3	5*	4.7	16.8
3	MC-500	12.9	2.2

* Unstable mix

Table 5.23 Marsh Funnel Viscosity and Bleed Capacity

MARSH FUNNEL VISCOSITY (SEC)							
TEST NUMBER	MIX 1	MIX 2	MIX 3	MIX 4	MIX 5	MC-500	WATER
1	35	34	36	37	28	29	26
2	34	34	35	38	28	29	26
3	35	34	34	37	28	29	26
w/c Ratio	0.6	0.7	0.9	0.45	1.33	1.0	-
o/o Bentonite	2	3	5	0	2	0	-
Bleed capacity	<1	<1	<1	0	>10	10	-

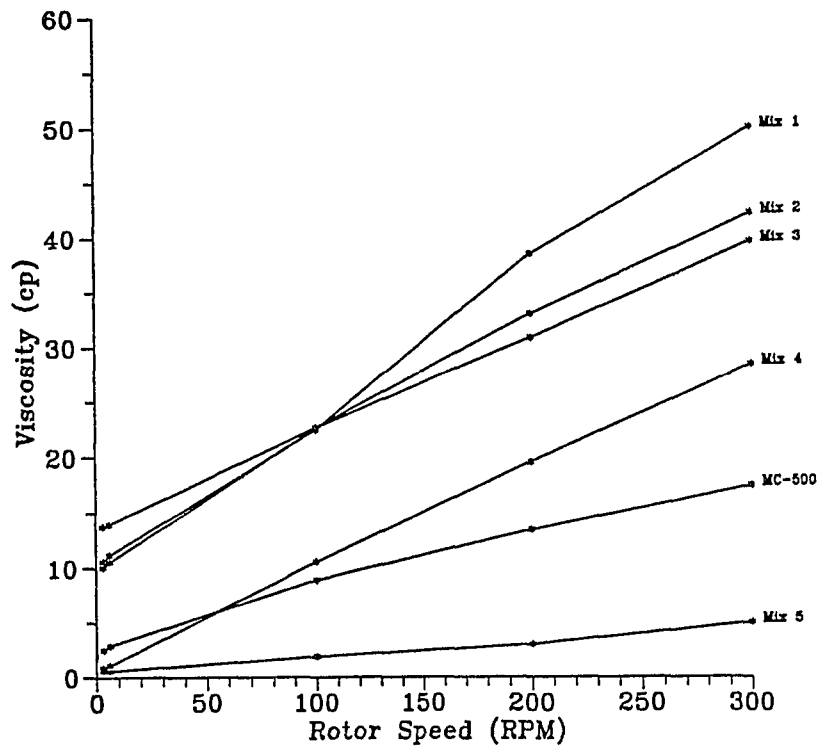


Figure 5.33 Fann viscosity readings as a function of rotor speed for various grout formulations.

decided to use mix formulation three (the thinnest O.P.C. grout used in this study), which has a water to cement ratio of 0.9 with 5 percent bentonite. After ten minutes under pressure no grout flow was evident. It was not known if any grout was emplaced in the fracture. Water flow testing was conducted after a curing period of two days. Further permeability testing was done to find the overall reduction in flow resulting from grouting. Results are shown in Figure 5.34. The last reloading cycle of the ungrouted sample is shown for comparison. After testing, the sample was separated. Filter blockage at the periphery of the injection borehole resulted in a misleading reduction in flow. Figure 5.35 shows this blockage and the small amount of grout emplaced around the periphery of the one inch borehole. This blockage results in a reduction in apparent permeability that is not indicative of the true surrounding permeability. Cement bonding around the periphery of the borehole was not strong and was easily broken away with the hand.

Test 2

Grouting of tension induced fracture, sample AP21-3-6-FG1 with MC-500 cement was conducted at a normal stress of 1.5 MPa and an injection pressure of 0.62 MPa. Grout flowed from the fracture. After two days of curing, permeability measurements showed an increase in flow through the fracture. This increase in flow is possibly attributed to a misalignment of the fracture prior to grouting or perhaps a rock particle nesting on the fracture surface propping open the fracture. Why this new fracture orientation was not sealed by the grout is unknown. Figure 5.36 shows the fracture permeability before and after grouting. Figure 5.37 shows sample FG1 being grouted. Figure 5.38 shows the fracture surfaces after curing and testing.

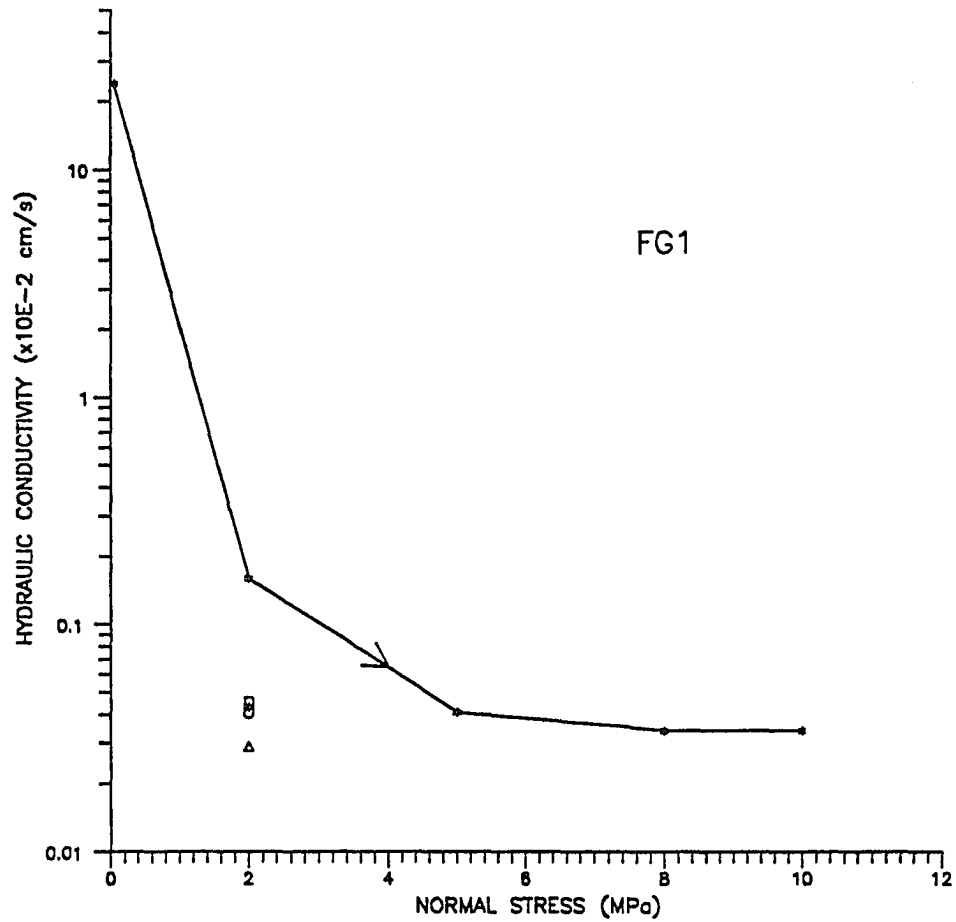


Figure 5.34 Hydraulic conductivity of Sample AP21-3-6-FG1 as a function of normal stress. Curve depicts last reloading cycle of ungrouted sample. Points under curve represent permeability after grouting (o : 2 days of curing; Δ : 6 days of curing; □ : 7 days of curing; + : 8 days of curing).



Figure 5.35 Filter blockage of sample AP21-3-6-FG1 showing the small amount of grout emplaced around the periphery of the one inch borehole.

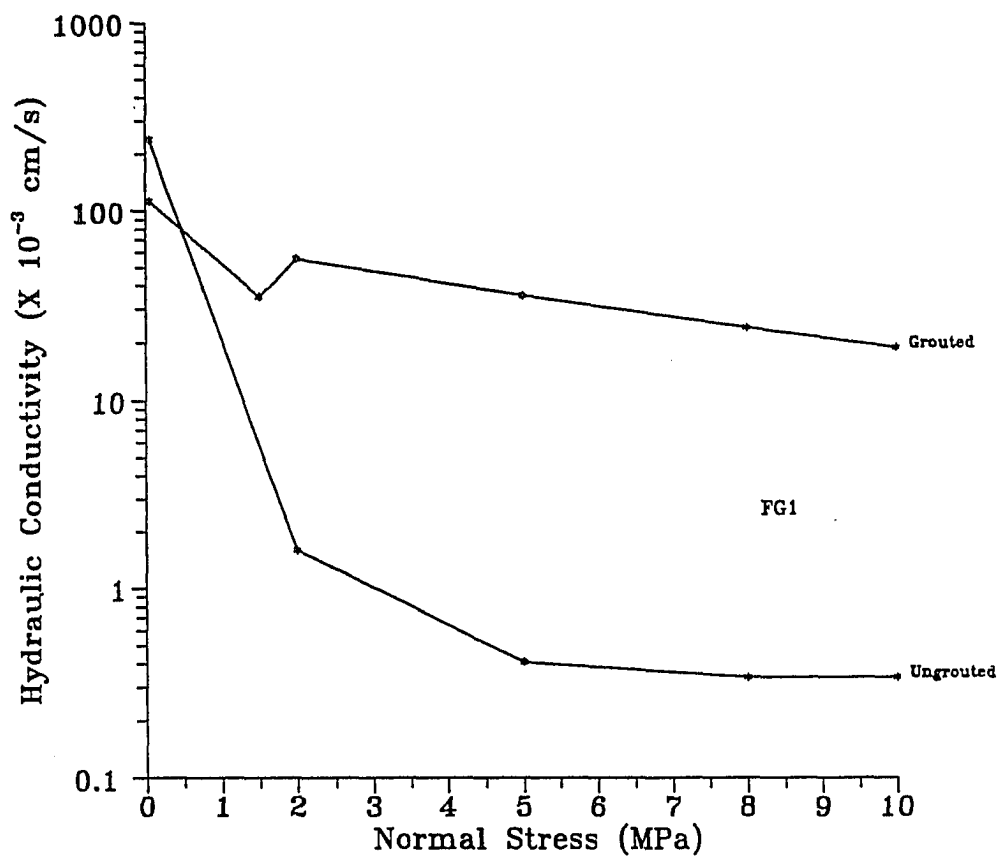


Figure 5.36 Hydraulic conductivity of Sample AP21-3-6-FG1 before and after grouting.

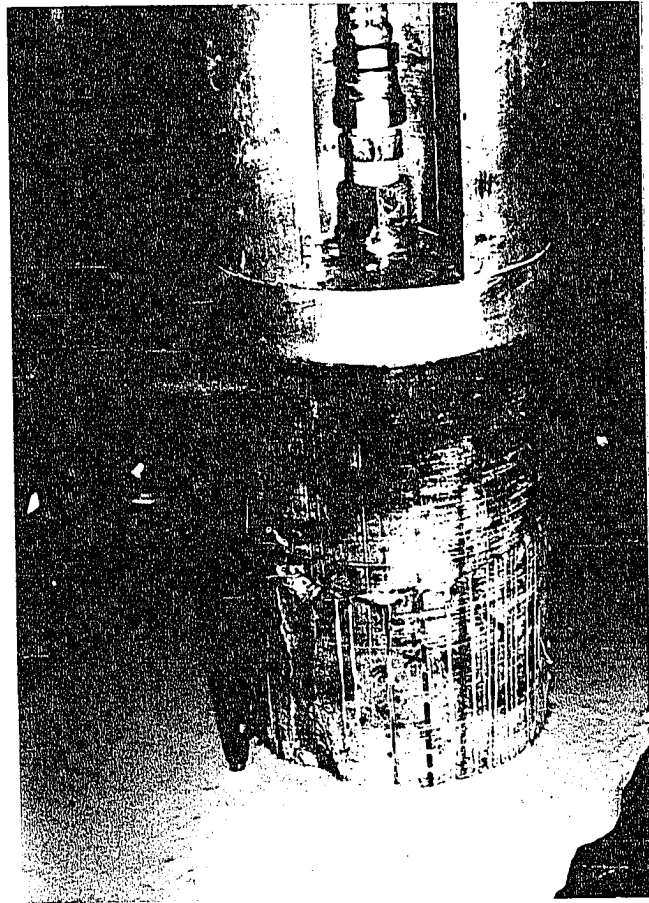


Figure 5.37 MC-500 grout flowing from the fracture of Sample AP21-3-6-FG1.

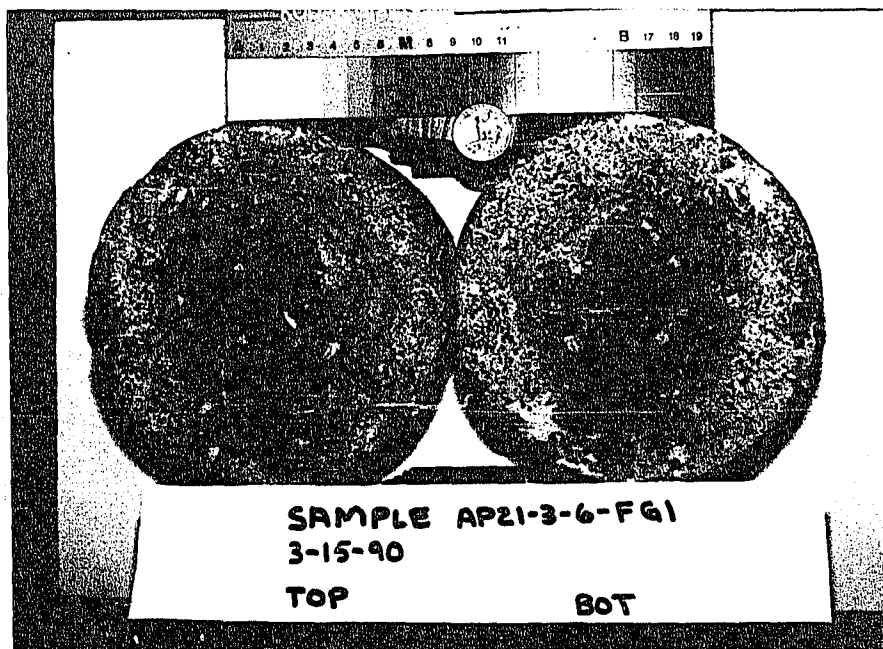


Figure 5.38 Surfaces of Sample AP21-3-6-FG1 after grouting, curing and permeability testing.

Sample AP30-2-6-FG10:

Tests 1 and 2

Two attempts to grout sample AP30-2-6-FG10 (tension induced fracture) have been performed using MC-500 grout. The first attempt was performed at a normal stress of 1 MPa and at an injection pressure greater than 2 MPa. The exact injection pressure was unknown because cement clogged the tube leading to the pressure gauge. Immediately after borehole washing and inspection this sample was found to have filter blockage (Figure 5.39a). No grout was emplaced on the fracture surfaces. The second attempt to grout sample FG10 was performed at 1 MPa normal stress but at an injection pressure of 4.1 MPa. Filter blockage was evident. Figure 5.39b shows this filter blockage.

Test 3

In an attempt to increase the aperture of sample AP30-2-6-FG10, six shims were placed 60 degrees apart around the fracture's surface. Shims had a thickness of 25.4 μm . Grouting was performed at 0.5 MPa normal stress and 4.1 MPa injection pressure. No grout could be seen exiting the fracture and after inspection filter blockage was evident with no grout emplaced in the fracture. Figure 5.40 shows this filter blockage. Figure 5.41 shows the apparent decrease in permeability due to filter blockage.

Sample AP4-1-6-FG2:

Sample AP4-1-6-FG2 (sawcut) was held in place with a normal stress of 2.0 MPa and grouted at an injection pressure of 4.5 MPa with mix formulation one. After ten minutes under pressure clear water could be seen dribbling out around the periphery of the sample. No grout could be seen exiting the sample. After separation and inspection of the sample it could be seen to have its one inch bore hole clogged with

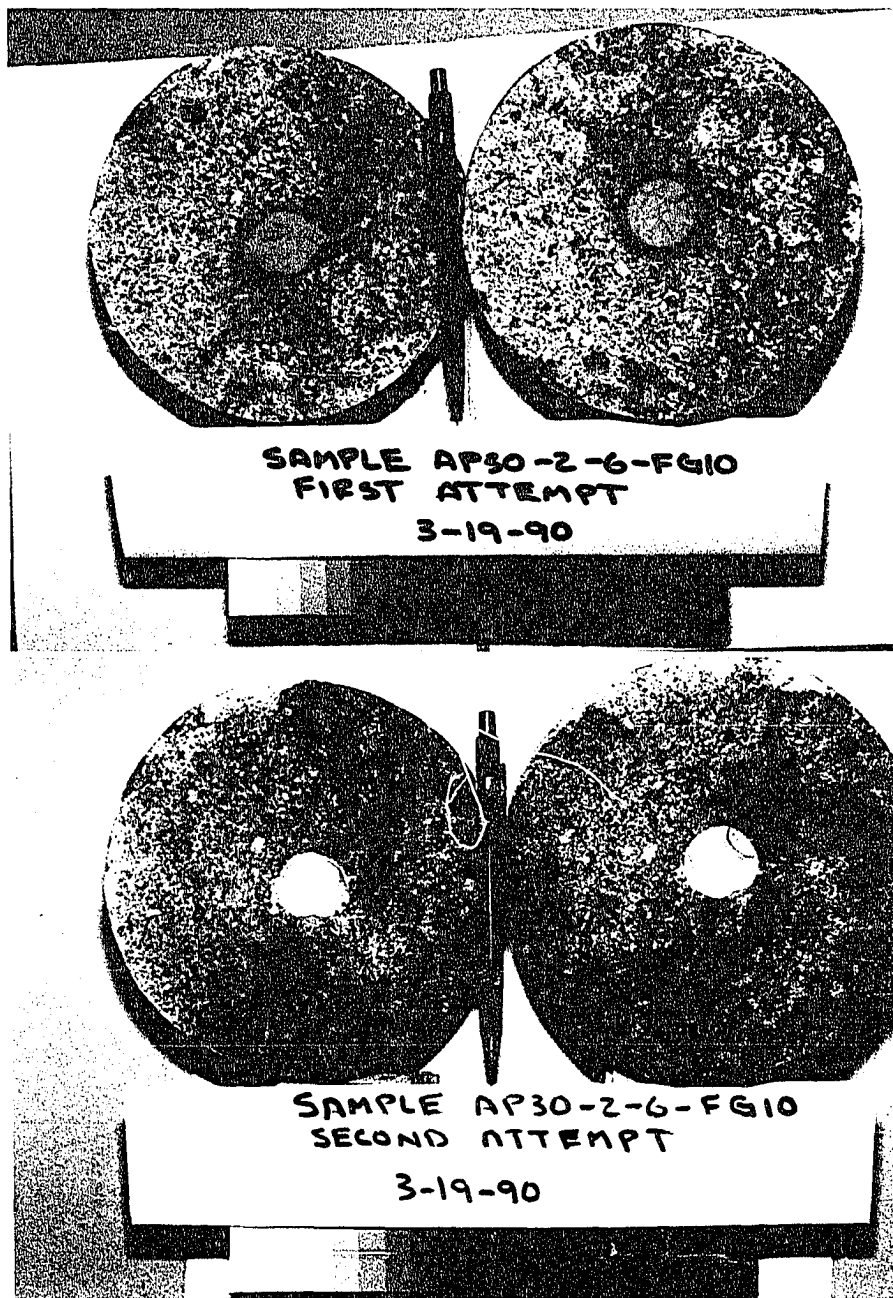


Figure 5.39a (top) and b (bottom) Filter blockage of Sample AP30-2-6-FG10.

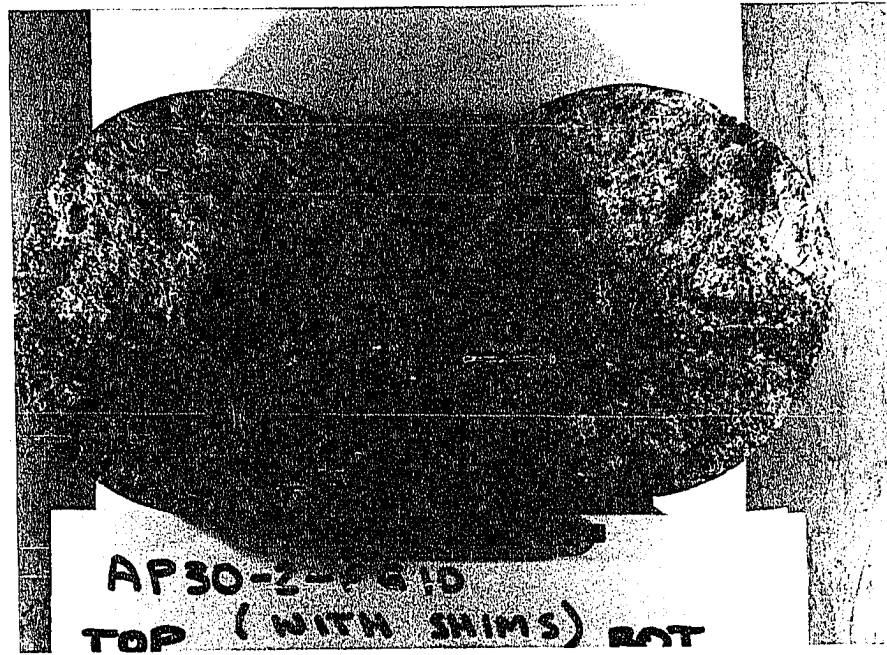


Figure 5.40 Filter blockage of shimmed sample AP30-2-FG10.

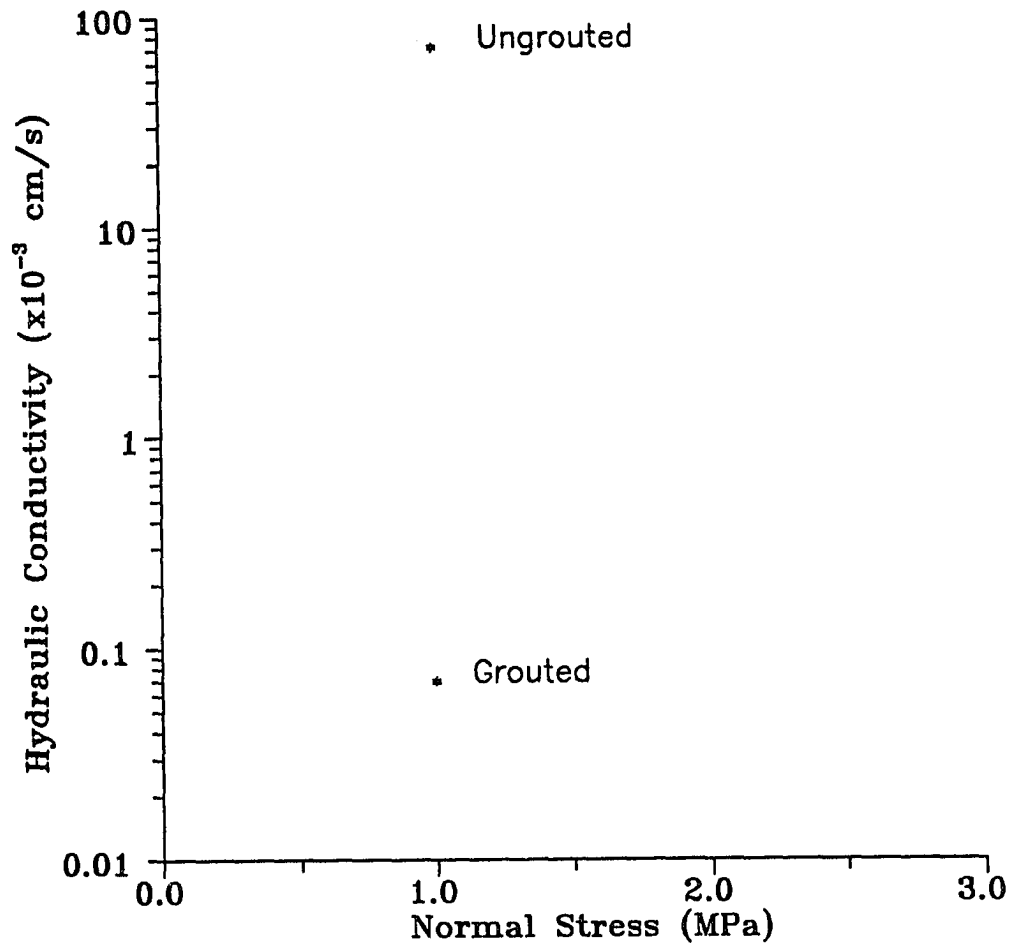


Figure 5.41 Decrease in hydraulic conductivity of shimmed sample AP30-2-6-FG10 due to filter blockage.

grout at this port. No grout is emplaced on the sawcut surfaces. Figure 5.48 shows that no grout has entered the sawcut. This sample did not have its borehole washed after grouting.

Sample AP3-1-6-FG6

Tests 1 and 2

Sample AP3-1-6-FG6 (sawcut) was held in place with a normal stress of 0.43 MPa and grouted at an injection pressure of 4.0 MPa with mix formulation two. Again after ten minutes under this injection pressure no flow was evident. Inspection of the sample showed filter blockage of the one inch bore hole, with no further grout travel along the sawcut surface. A second attempt to grout sample FG6 was made after the sample was washed to remove any grout remaining in the borehole. Grouting progressed at an injection pressure of 3.5 MPa and normal stress of 0.23 MPa. Mix formulation 3 was used and was mixed for an additional two minutes to ensure thorough mixing. As before, clogging of the borehole occurred, with no grout entering the sawcut. The ring of cement causing filter blockage can be seen in Figure 5.43. In the first grouting attempt of sample FG6, clear water could be seen exiting the sawcut fracture. It was not known whether this water originated from washing the borehole surfaces prior to grouting or was the result of bleed water filtering through the cement ring causing filter blockage. For the second grouting attempt, no washing of the borehole was performed so that any water leaving the system would have to come from the slurry. Figure 5.44a shows the second grouting of sample FG6. Figure 5.44b shows the clear bleed water filtering out of the sample through the cement ring. This test raises questions of the extent of grout travel in fine fissures and the possibility that only bleed water from the slurry is traveling through the fracture system. The apparent grout take during grouting may not be indicative of the actual volume of grout being emplaced. Schaffer and Daemen (1987, p. 70) also had difficulty

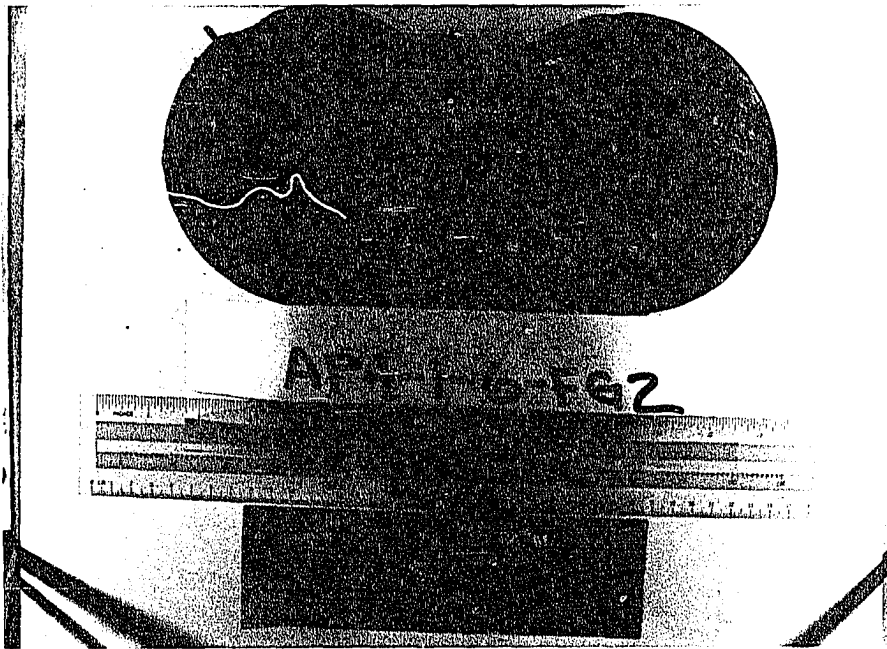


Figure 5.42 Clogging of one inch borehole of sawcut sample AP4-1-6-FG2.

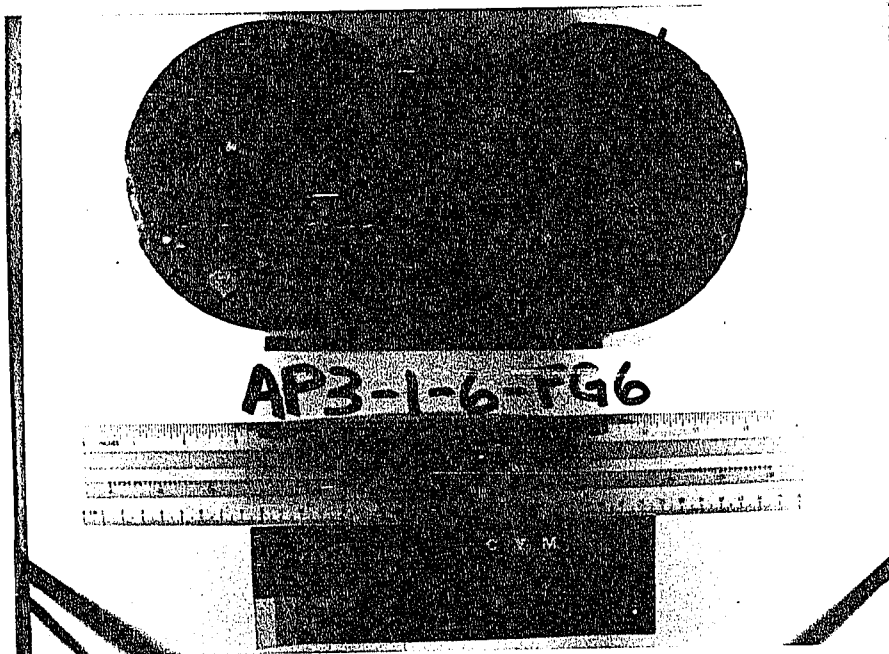


Figure 5.43 Ring of cement causing filter blockage of sample AP3-1-6-FG6.

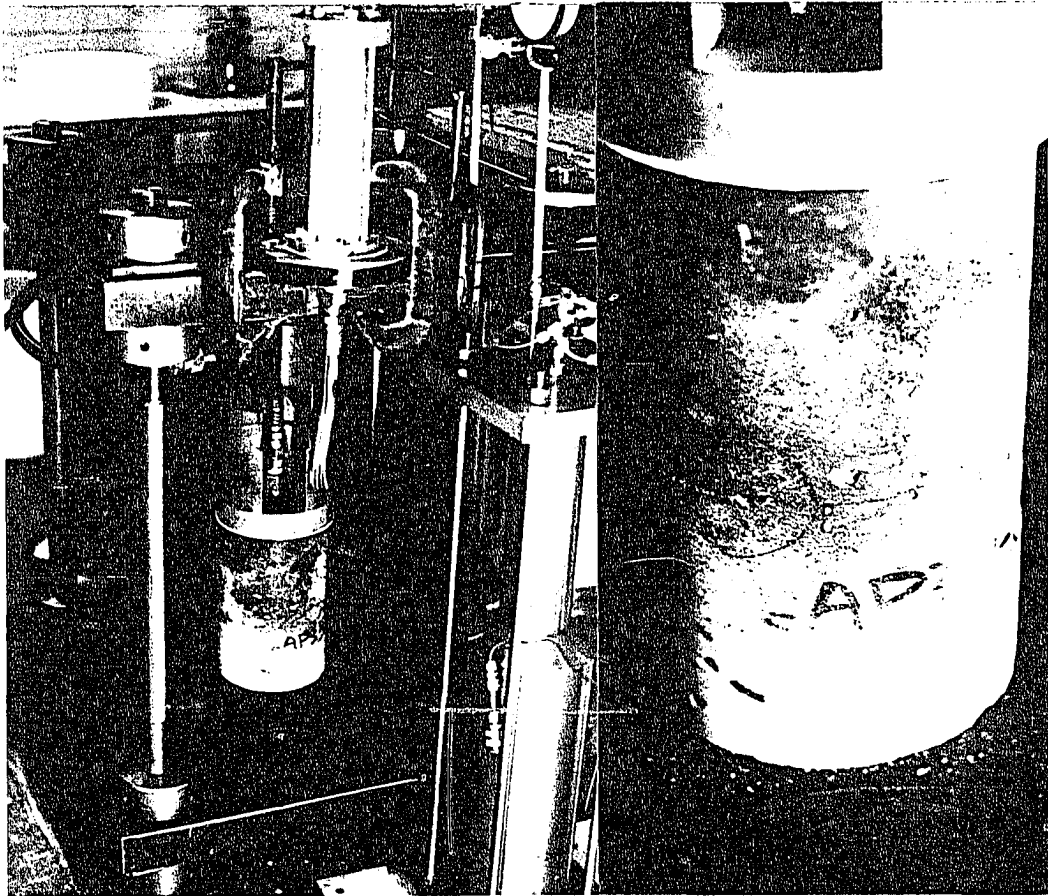


Figure 5.44a (left) and b (right). (a) Grouting of sawcut sample AP3-1-6-FG6. (b) Bleed water being squeezed out of sample AP3-1-6-FG6 during grouting.

with grouting sawcut fractures with this type of cement and report similar borehole clogging and the formation of a cement ring at the entrances of the fracture as well as an apparent reduction in permeability.

Sample AP-SHAFT6-FG16:

Sawcut sample AP-SHAFT6-FG16 was grouted at a normal stress of 1 MPa and 2.1 MPa injection pressure with MC-500 grout. 25.4 μm thick shims were used to prop open the aperture. Figure 5.45 shows these shims prior to grouting. Figure 5.46 shows the grouted surfaces of this sample. Note the flow channels where grout has been washed away. These channels are presumably created by bleed water filtering through the grout film. Also note the poor bonding on the top half of the sample. This poor bonding is probably a result of the high water content of the grout. The bleed water rises to the top of the grout film not allowing grout to come in contact with the upper surface. Figure 5.47 shows the decrease in permeability due to grouting.

Sample AP56-2-6-FG14:

Grouting of natural fracture sample AP56-2-6-FG14 emplaced little grout in the horizontal fracture. This sample was grouted at a final injection pressure of 6 MPa under 5 MPa normal stress. Grout formulation one containing 2 percent bentonite was used. Because of the high injection pressure used to force grout flow, a vertical crack developed in the top half of the sample. Grout penetration along the horizontal fracture ranged from 0.5 to 1.5 cm. Bonding appeared good as well as durable between both top and bottom surfaces of the fracture. Grout was visible in the vertical fracture but apparently did not seal it. Figure 5.48 shows the increase in permeability due to the development of this fracture by hydrofracturing. This is a good example of how over pressurizing a borehole can do more harm than good in

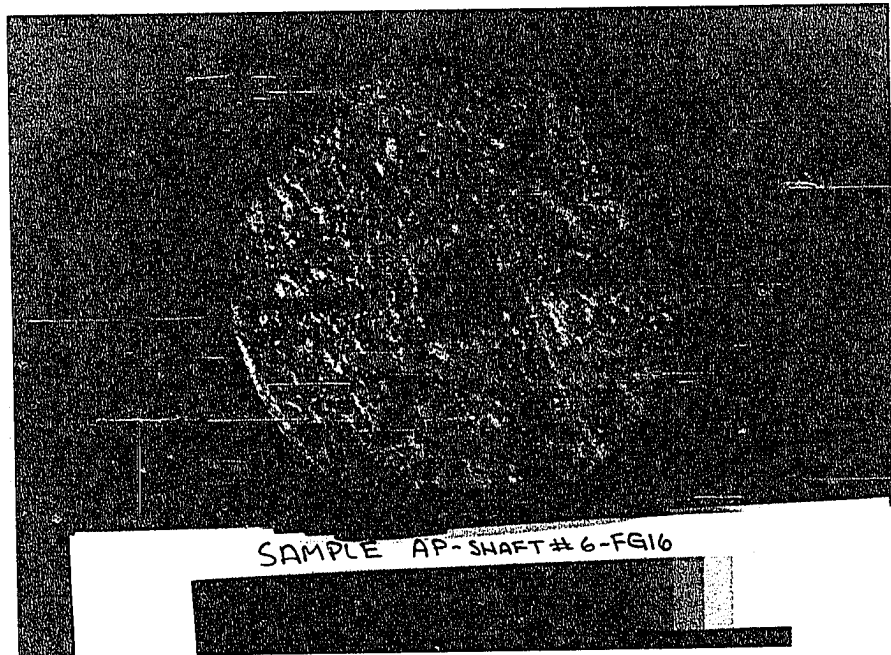


Figure 5.45 Shims used to prop open the aperture of sawcut sample AP-SHAFT6-FG16.

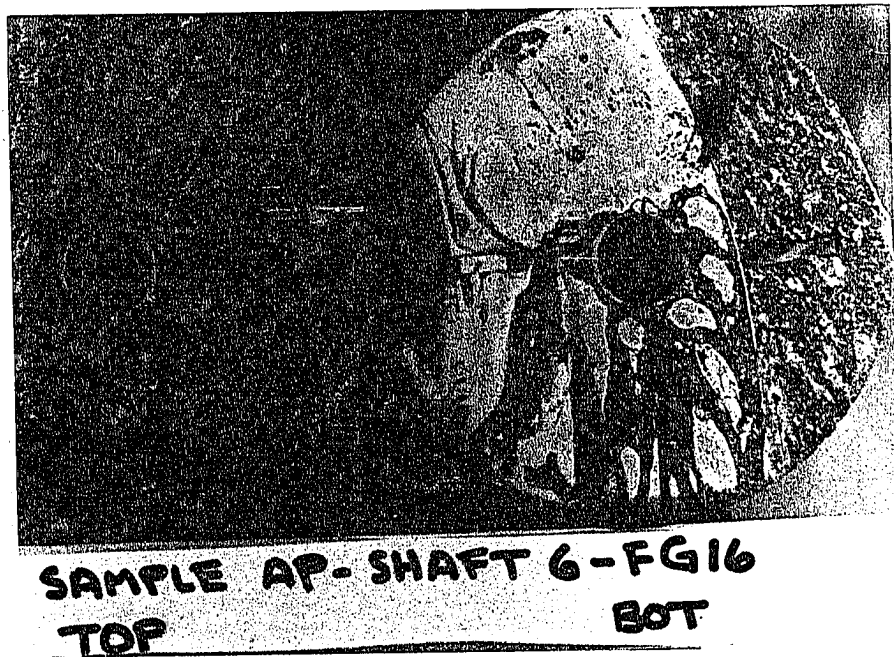


Figure 5.46 Grouted surfaces of shimmed sample AP-SHAFT6-FG16.

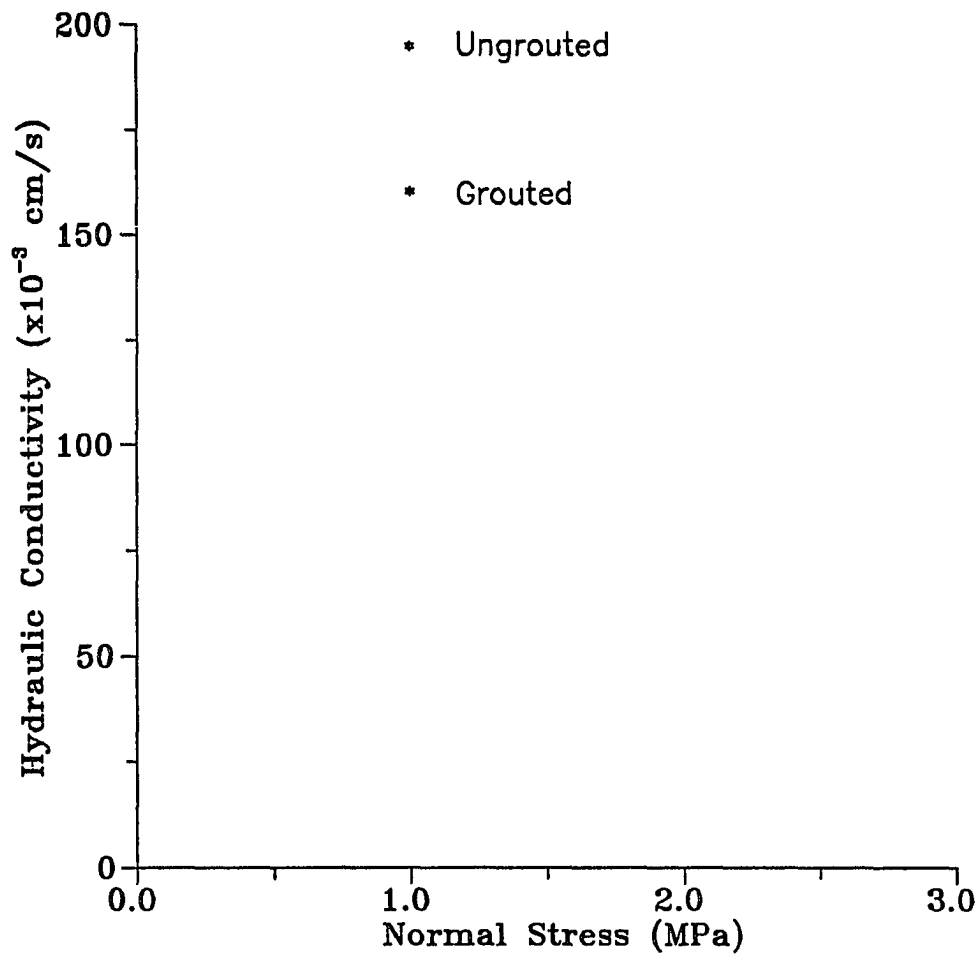


Figure 5.47 Reduction in permeability resulting from grouting sawcut sample AP-SHAFT6-FG16 (shimmed).

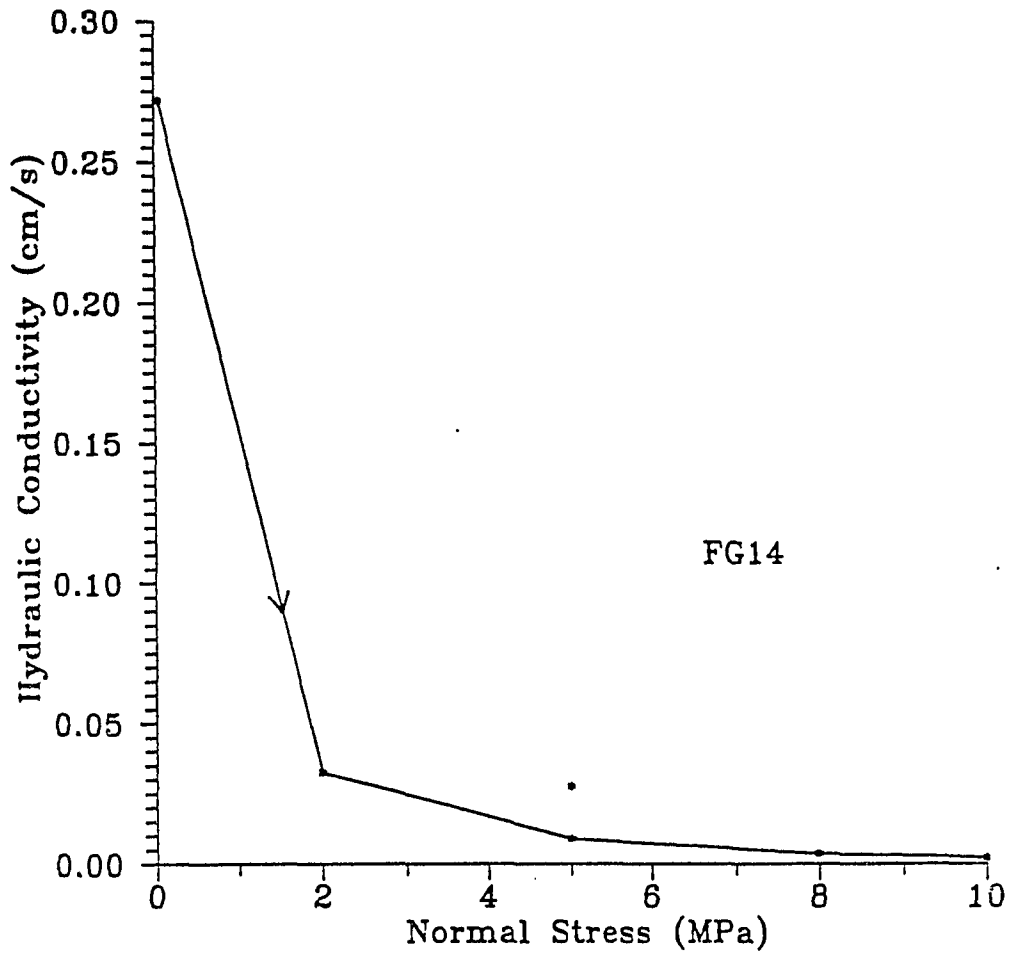


Figure 5.48 Hydraulic conductivity vs. normal stress for sample AP56-2-6-FG14. Apparent increase in permeability at 5 MPa due to hydrofracturing.

regards to reducing rock mass permeability. Figure 5.49a shows the grout penetration of this sample. Figure 5.49b shows the vertical crack caused by hydrofracturing.

Sample AP56-3-6-FG15:

Test 1

Sample AP56-3-6-FG15 containing a single natural fracture was grouted with MC-500 grout at an injection pressure of 2.8 MPa under 1 MPa normal stress. No grout flow was evident. After separation of sample halves filter blockage was present with no grout emplaced along the fracture.

Test 2

The second attempt to grout sample AP56-3-6-FG15 with MC-500 grout was conducted at 3.1 MPa under 0.5 MPa normal stress. After flow testing and inspection, small pockets of grout were evident on the fracture surfaces. Figure 5.50 shows the resulting emplaced grout. In the places where grout was present bonding appeared good between the top and bottom surfaces. Figure 5.51 shows the reduction in hydraulic conductivity resulting from grouting.

Table 5.24 shows the results of all grouting experiments as a function of injection pressure, equivalent fracture aperture and groutability ratio.

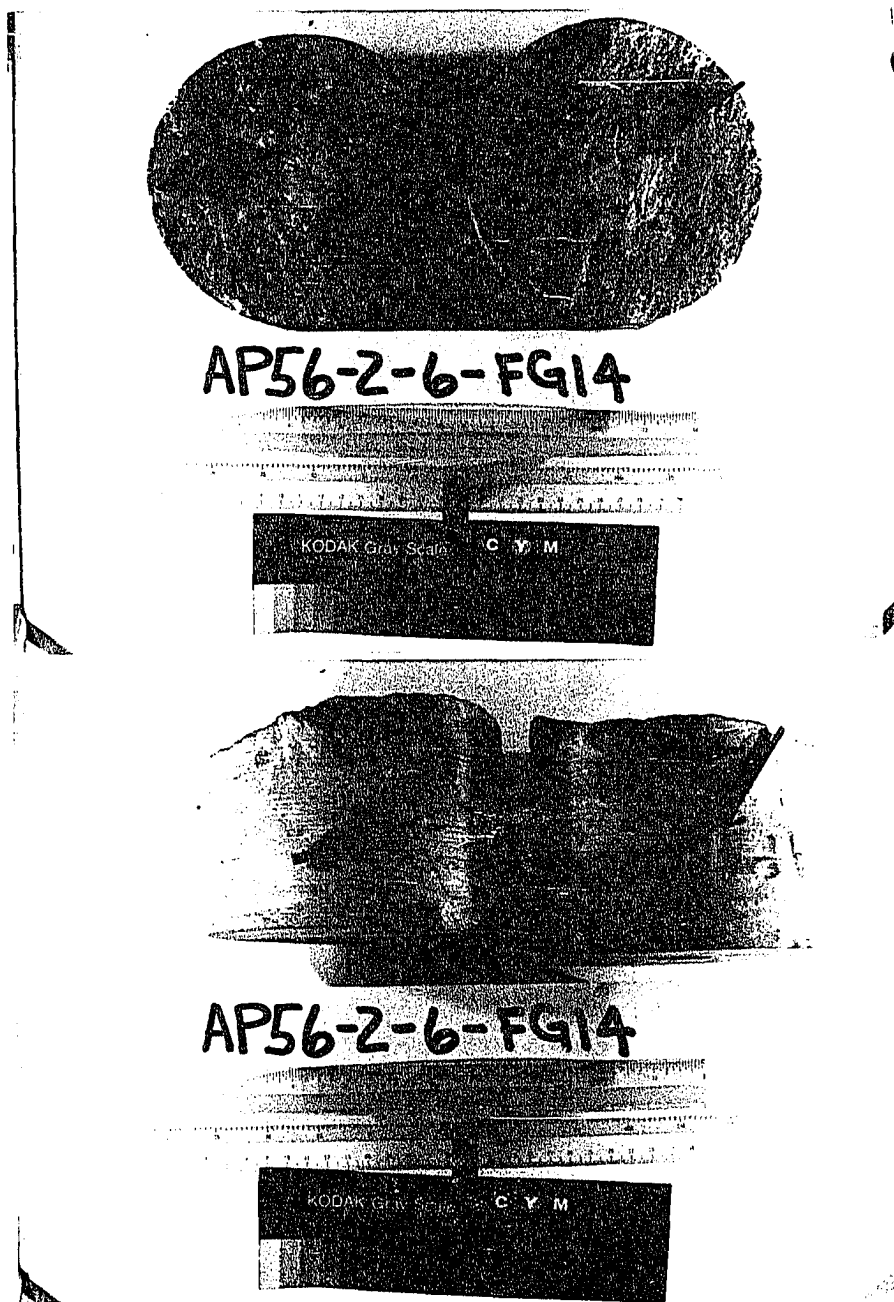


Figure 5.49a (top) and b (bottom). (a) Filter blockage of one inch borehole of sample AP56-2-6-FG14, a natural fracture. (b) Vertical fracture caused by overpressurizing borehole during pressure grouting.

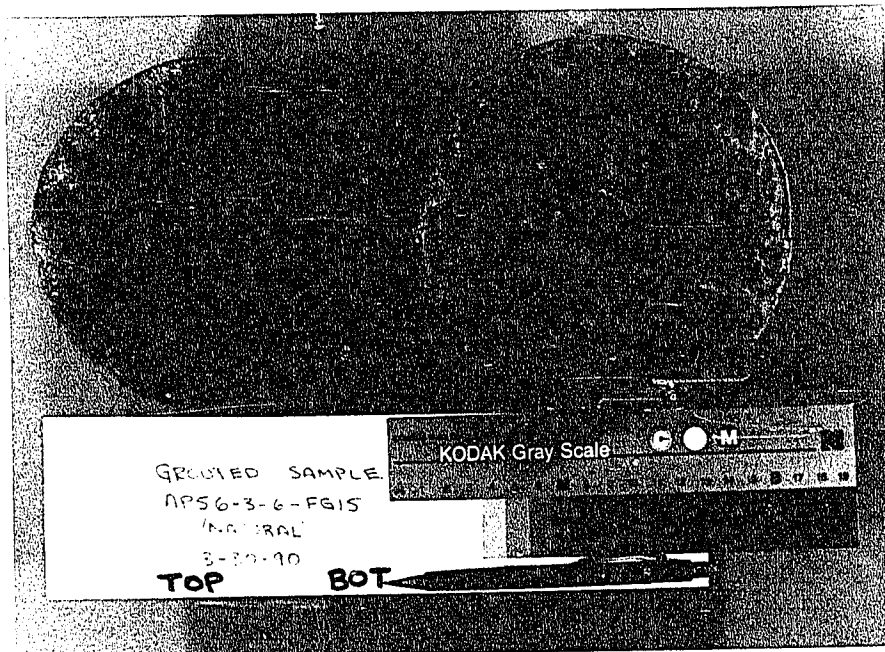


Figure 5.50 Pockets of emplaced grout in sample AP56-3-6-FG15.

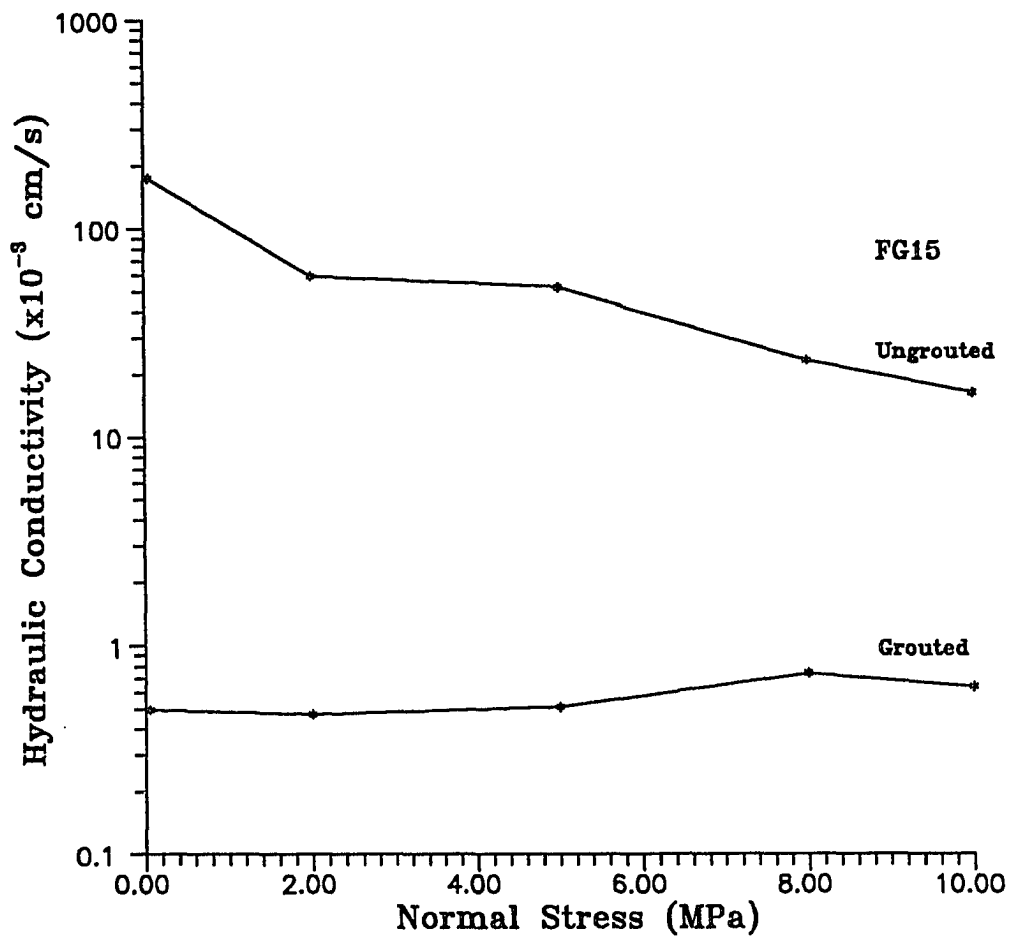


Figure 5.51 Reduction in hydraulic conductivity from grouting sample AP56-3-6-FG15 with MC-500 grout.

Table 5.24 Groutability Ratios Corresponding to Penetration.

SAMPLE NUMBER	NORMAL STRESS (MPa)	INJECTION PRESSURE (MPa)	EQUIVALENT FRACTURE APERTURE (μm)	CEMENT TYPE	GROUTABILITY RATIO	ACTUAL PENETRATION
FG1	2.0	5.0	4.4	OPC	0.04	NO
FG1	1.5	0.62	18.3	MC-500	1.83	YES ?
FG10	1.0	>2	6.5	MC-500	0.65	NO
FG10	1.0	4.1	6.5	MC-500	0.65	NO
FG10 W/SHIMS	0.5	4.1	41.9	MC-500	4.19	NO
FG14	5.0	6.0	10.4	OPC	0.10	SLIGHT
FG15	1.0	2.8	34.7	MC-500	3.47	NO
FG15	0.5	3.1	41.8	MC-500	4.18	YES
FG2	2.0	4.5	1.3	OPC	0.01	NO
FG6	0.43	4.0	32.0	OPC	0.32	NO
FG6	0.23	3.5	36.0	OPC	0.36	NO
FG6	2.0	0.34	6.8	MC-500	0.68	NO
FG16 W/SHIMS	1.0	2.1	79.0	MC-500	4.80	YES

CHAPTER 6

CONCLUSIONS AND RECOMMENDATIONS

Flow testing

Permeability testing of intact tuff samples showed a decrease in hydraulic conductivity with increasing normal stress. This decrease is presumably due to closing of pore spaces and pre-existing microfractures within the rock as the normal load increases. Intact rock permeabilities were several orders of magnitude lower than that of their fractures, even at high normal stress, and were therefore neglected.

Results of permeability testing indicate that fracture closure is dependent on the fractures stress history. Testing showed aperture reductions with each new loading cycles. This was presumably due to fracture deformation, although the maximum normal stress never exceeded 35 percent of the rock's uniaxial compressive strength.

Equivalent fracture apertures were calculated from the measured inflow through the application of the cubic law. A change in the degree of saturation could be responsible for the apparent reduction in equivalent fracture aperture. Future testing should include measurement of outflows as well as the degree of saturation.

Fracture closure was observed to be time dependent. This phenomenon was evident by the waiting time needed to allow permeability measurements to become quasi steady-state. Time dependence was observed to be most severe at each initial change in normal stress. Measurements of this time dependence were not obtained due to the initial interest in only the steady-state values. Further testing should include some measure of this phenomenon.

The greatest reduction in flow rates through fractures were observed at low normal stress. This behavior is presumably due to initial surface mating. This closing phenomenon was identical to

fracture compression results (Section 5.3) where two distinct stiffness region were observed, with remarkable repeatability for both, and a well defined transition stress between the two.

Grouting

Grouts with high water to cement (W/C) ratios suffered from excess bleed water which in turn affected bonding to the upper fracture surfaces. The use of ordinary portland cement (O.P.C) grouts with greater W/C ratios (up to 0.9) did not increase grout admittance.

The addition of Bentonite (2-5%) to O.P.C. grouts with increased W/C ratios (0.6 to 0.9) reduced bleed water to less than one percent but caused a marked decrease in uniaxial compressive strength. This decrease in strength is due to both the increase in bentonite content as well as the W/C ratio.

Comparisons between grout slurries rheologic properties is hardly possible due to differing W/C ratios and bentonite contents. Future testing should include characterization of grout properties at similar W/C ratios.

More work needs to be performed on the use of admixtures such as superplasticizers used to enhance penetration capabilities.

Results from over ten grouting tests confirm the extreme difficulty in emplacing O.P.C. grouts in tight fractures. Attempts at emplacing ultra fine grout (MG-500) fair somewhat better than O.P.C. grouts although filter blockage occurred with all grouting attempts when the groutability ratio was less than three.

Filter blockage was a prevailing problem with the formation of a characteristic ring of cement forming at the entrance to the fracture. Accompanied with the formation of this type of blockage was an apparent reduction in permeability not indicative of the surrounding permeability. In the field, post grouting core holes should be drilled to confirm the extent of grout travel.

Future laboratory grouting experiments should incorporate pulse or dynamic injection techniques (Pusch et al. 1988). Permeability, durability, and longevity testing should be performed to confirm the usefulness of cementitious grouts for nuclear waste repository sealing.

REFERENCES

- American Petroleum Institute, 1986, Specifications for Materials and Testing for Well Cements, Third Edition, American Petroleum Institute, Production Department, Dallas, Texas.
- ASTM C305-82, "Standard Method for Mechanics Mixing of Hydraulic Cement Pastes and Mortars of Plastic Consistency," Annual Book of ASTM Standards, Vol. 04-01, American Society for Testing and Materials, Philadelphia.
- Banks, D.C., 1972, "In Situ Measurements of Permeability in Basalt," Proceedings of the Symposium on Percolation Through Fissured Rock, Stuttgart.
- Bawden, W.F. and J.C. Roegiers, 1979, "Discussion and Interpretation of the Mathematics Governing Radial Flow in A Single Horizontal Rock Fracture", Prepared for Energy, Mines and Resources, Canada, Earth Physics Branch, Division of Seismology and Geothermal Studies, Ottawa, Ontario.
- Bear, J., 1979, "Hydraulics of Pumping and Recharging Wells," Hydraulics of Groundwater, McGraw-Hill Book Co., N.Y., pp. 300-307.
- Cambefort, H., 1977, "The Principles and Applications of Grouting," Quarterly Journal of Engineering Geology, Vol. 10, The Geological Society, London, pp. 57-95.
- Chapman, N.A. and I.G. McKinley, 1987, "The Geological Disposal of Nuclear Waste," John Wiley and Sons, New York.
- Cobb, S.L. and J.J.K. Daemen, 1982, "Polyaxial Testing of Borehole Plug Performance," Topical Report to the U.S. Nuclear Regulatory Commission, Contract No. NRC-04-78-271, prepared by the Department of Mining and Geological Engineering, University of Arizona, Tucson.
- Deere, D. and G. Lomardi, 1985, "Grout Slurries-Thick or Thin?," pp. 156-164, Issues in Dam Grouting, W.H. Baker, editor, American Society of Civil Engineers, New York.
- Deere, D.U., 1982, "Cement-Bentonite Grouting for Dams," Grouting in Geotechnical Engineering, W.H. Baker, editor, Proceedings of the conference on Feb. 10-12, New Orleans, LA, pp. 279-300. Published by the American Society of Civil Engineers, New York.
- Detournay, E., 1980, "Hydraulic Conductivity of Closed Rock Fracture: an Experiment and Analytical Study," pp. 168-173 of Underground Rock Engineering, 13th Canadian Rock Mechanics Symposium (The H.R. Rice Memorial Symposium), Toronto, Ontario, May 28-29. CIM Special Volume 22, The Canadian Institute of Mining and Metallurgy, Montreal, Quebec.
- Englman, R., Y. Gur and Z. Jaeger, 1983, "Fluid Flow Through a Crack Network in Rocks," Journal of Applied Mechanics, Vol. 50, pp. 707-711.
- Farmer, I.W., 1970, "Design of Cement Grouts," Research Report R.17/70, University of Newcastle upon Tyne, England, 69 pp.

- Fitzsimmons, A., 1987, Have Waste, Will Travel: An Examination of the Implications of High-Level Nuclear Waste Transportation, Institute of Behavioral Science, University of Colorado, Boulder, Colorado.
- Freeze, A. and J. Cherry, 1979, "Groundwater," Groundwater Resource Evaluation, Prentice-Hall Inc., N.J., pp. 335-339.
- Fuenkajorn, K. and J.J.K. Daemen, 1986, "Experimental Assessment of Borehole Wall Drilling Damage in Basaltic Rocks," Technical Report, Contract NRC-04-78-271, Prepared for U.S. Nuclear Regulatory Commission, Division of Radiation Programs and Earth Sciences by the Department of Mining and Geological Engineering, University of Arizona, Tucson.
- Fuenkajorn, K. and J.J.K. Daemen, 1990, "Mechanical Characterization of the Densely Welded Apache Leap Tuff" Technical Report, Contract NRC-04-86-113, Prepared for U.S. Nuclear Regulatory Commission, Division of Health, Siting and Waste Management, by the Department of Mining and Geological Engineering, University of Arizona, Tucson.
- Gale, J.E., A. Rouleau and L.C. Atkinson, 1985, "Hydraulic Properties of Fractures," pp. 1-16, Vol. 17, Part 1, Hydrogeology of Rocks of Low Permeability, Memoires, International Association of Hydrogeologists, Tucson, Arizona, Congress.
- Gnirk, P., 1988, "State-of-the-Art Evaluation of Repository Sealing Materials and Techniques," Materials Research Society Symposium, Proc. Vol. 112.
- Gupta, D.C., J.T. Buckley, 1989, "Technical Position on Postclosure Seals, Barriers, and Drainage System in an Unsaturated Medium," NUREG-1373. Prepared for the Division of High-Level Waste Management, Office of Nuclear Material Safety and Safeguards, Washington, D.C.
- Gyenge, M., 1980, "Nuclear Waste Vault Sealing," pp. 181-192, Underground Rock Engineering, 13th Canadian Rock Mechanics Symposium (The H.R. Rice Memorial Symposium), Toronto, Ontario, May 28-29. CIM Special Volume 22, The Canadian Institute of Mining and Metallurgy, Montreal, Quebec.
- Holtz, R.D. and W.D. Kovacs, 1981, "Geotechnical Engineering", Prentice-Hall, Inc., Englewood Cliffs, N.J.
- Houlsby, A.C., 1977, "Towards Appropriate Metric Units ofr Grouting", Ground Engineering, July.
- Houlsby, A.C. 1982a. "Cement Grouting for Dams". Proceedings of the Conference on Grouting in Geotechnical Engineering, New Orleans, Louisiana, pp. 1-34.
- Houlsby, A.C. 1982b. "Optimum Water-Cement Ratios for Rock Grouting". Proceedings of the Conference on Grouting in Geotechnical Engineering, New Orleans, Louisiana, pp. 317-331.
- Houlsby, A.C. 1985. "Cement Grouting: Water Minimizing Practices". Proceedings of the Session Sponsored by the A.S.C.E. Geotechnical Engineering Division on "Issues in Dam Grouting", Denver, Colorado, pp. 34-75.

- Hsieh, P.A. and S.P. Neuman, 1985, "Field Determination of the Three-Dimensional Hydraulic Conductivity Tensor of Anisotropic Media", *Water Resources Research*, Vol. 21, No. 11, Pages 1655-1665, November.
- Iwai, K., *Fundamental Studies of Fluid Through a Single Fracture*, Ph.D. thesis, 208 pp., Univ. of Calif., Berkeley, 1976.
- Jaeger, J.C. and N.G.W. Cook, 1984, *Fundamentals of Rock Mechanics*, Chapman and Hall Inc., New York, N.Y., 593 pp.
- Johnson, B., 1983, "Permeability of a Simulated-Fracture as a Function of Normal Stress," pp. 519-523, *Rock Mechanics - Theory - Experiment - Practice*, Proceedings of the 24th Symposium on Rock Mechanics, Texas A&M University, June. Published by the Association of Engineering Geologists.
- Karol, R.H., 1982, "Chemical Grouts and Their Properties," Proceedings of the Conference on Grouting in Geotechnical Engineering, American Society of Civil Engineers, New York, N.Y., pp. 359-377.
- Karol, R.H., 1985, "Grout Penetrability," American Society of Civil Engineers, 345 E. 47th St., New York.
- Kennedy, T.B., 1958, "Pressure Grouting Fine Fissures," *Journal of the Soil Mechanics and Foundations Division, ASCE*, Vol. 84, no. SM3, August 1958, Paper 1731.
- Lambe, T.W., 1951, "Soil Testing for Engineers," John Wiley and Sons, N.Y., 165 p.
- Littlejohn, G.S., 1982, "Design of Cement Based Grouts," Proceedings of the Conference on Grouting in Geotechnical Engineering, American Society of Civil Engineers, New York, N.Y., February 10-12.
- Lombardi, G., 1985, "The Role of Cohesion in Cement Grouting of Rock," pp. 253-261, Q. 58, R. 13, vol. 3, *Transactions, 15th Inter. Cong. on Large Dams, Lausanne, Switzerland, June*. Pub. by the Inter. Commission on Large Dams, Paris.
- Lomize, 1951, *Filtratsiya u Treshchinovatykh Porodakh* (Flow in fractured rock), Gosenergoizdat, Moscow.
- Londe, P., 1971 "The Flow of Water in Rock", University of Alberta, Edmonton.
- Louis, C., 1976, "Introduction A L'Hydraulique Des Roches" (Introduction to rock hydraulics), Ph.D Thesis, University of Pierre et Marie Curie, Paris.
- Louis, C. 1969. "A Study of Groudwater Flow in Jointed Rock and Its Influence on the Stability of Rock Masses". *Rock Mechanics Report No. 10*, Imperial College, University of London, England.
- Louis, C.L., 1974, "Rock Hydraulics", Bureau of Geology and Mining Research, National Geologic Service, Orleans, CEDEX.
- Lutze, W. and R.C. Ewing, 1988, "Radioactive Waste Forms for the Future", North-Holland Physics Publishing, New York, N.Y.

- Maini, Y.N.T., 1971, "In-situ Hydraulic Parameters in Jointed Rock-Their Measurement and Interpretation," Ph.D. Thesis, University of London, Imp. Coll. of Sci. and Technology.
- Mitchell, J.K., 1970, "In-Place Treatment of Foundation Soils," Journal of the Soil Mechanics and Foundations Division, Proceedings of the ASCE, Vol. 96, No. SM1.
- Mongan, C.E., 1985, "Validity of Darcy's Law Under Transient Conditions, U.S. Geological Survey, Paper 1331, United States Printing Office, Washington.
- Nonveiller, E., 1989, "Grouting Theory and Practice," Elsevier Science Publishing Company Inc., New York.
- Pusch, R., L. Borgesson, A. Fredrikson, I. Markstrom, M. Erlstrom, G. Ramqvist, M. Gray, W. Coon, 1988, Rock Sealing-Interim Report on the Rock Sealing Project (Stage 1), Stripa Project Report 88-11, Stockholm, Sweden.
- Roko, R.O., J.J.K. Daemen, and D.E. Myers, 1991, "Variogram Characterization of Joint Surface Morphology and Asperity Deformation During Shearing", Unpublished, University of Arizona, Tucson.
- Ruiz, M.D. and P.C. Leone, 1970, "The Importance of Grout Properties in Grouting Jointed Rock Masses," 1st International Congress of the International Association of Engineering Geology, September 8-11, Paris, Vol. 1, pp. 616-635.
- Sagar, B. and A. Runchal, 1982, "Permeability of Fractured Rock: Effect of Fracture Size and Data Uncertainties," Water Resources Research, Vol. 18, No. 2, pp. 266-274, April.
- Schaffer, A. and J.J.K. Daemen, 1987, "Experimental Assessment of the Sealing Effectiveness of Rock Fracture Grouting," NUREG/CR-4541, prepared for the U.S. Nuclear Regulatory Commission, by the Dept. of Mining and Geological Engineering, University of Arizona, Tucson.
- Shames, I.R., 1982, "Mechanics of Fluids", McGraw-Hill, New York.
- Shannon and Wilson, Inc., 1987, "Cement Grout Flow Behavior in Fractured Rock," for the Bureau of Reclamation, Denver, CO, and the Army Corps of Engineers, Omaha, NE.
- Sharp, J.C. and Y.N.T. Maini, 1972, "Fundamental Considerations on the Hydraulic Characteristics of Joints in Rock," Paper T1-F, Percolation Through Fissured Rock, Proceedings, Symposium, Stuttgart, 1972. Published by Deutsche Gesellschaft fuer Erdund Grundbau, Essen, with Prof. Dr. -Ing. Wittke.
- Shimoda, M. and H. Ohmori, 1982, "Ultra Fine Grouting Material," Grouting in Geotechnical Engineering, W.H. Baker, editor, proceedings of the conference on February 10-12, New Orleans, LA, Vol. 1, pp. 77-91. Published by ASCE, New York.
- Snow, D.T., 1965, A Parallel Plate Model of Fractured Permeable Media, Ph.D. thesis, Univ. of Calif., Berkeley.

- The Consulting Engineer, 1969, "Grouting Design and Practice," The Consulting Engineer, London, Vol. 33, No. 10, October, 40 p. insert.
- Tsang, Y.W. and P.A., Witherspoon, 1981, "Hydromechanical Behavior of A Deformable Rock Fracture Subject to Normal Stress" Journal of Geophysical Research Vol. 86, No. B10, pp. 9287-9298, October.
- Wallner, M. and W. Wittke, 1974, "Theory and Experiment of a New Grouting Procedure," Proc., 3rd Cong. of the Inter. Soc. of Rock Mechanics, Vol. II, p. 744-750, Denver, (In German).
- Wilson, C. R. and Witherspoon, P. A., 1970, an Investigation of Laminar Flow in Fractured Rocks, Geotechnical Report No. 70-7, University of California, Berkeley.
- Witherspoon, P.A., J.S.Y. Wang, K. Iwai and J.E. Gale, 1980, "Validity of the Cubic Law for Fluid Flow in a Deformable Rock Fracture," Water Resources Research, Vol. 16, No. 6, December pp. 1016-1024.
- Zeigler, T.W., 1976, "Determination of Rock Mass Permeability," U.S. Army Engr. Waterways Experiment Station, Technical Report S-76-2.